YU-ISSN 0352-5139
J.Serb.Chem.Soc. Vol. 66 No. 5 (2001)

CONTENTS

Organic Chemistry and Biochemistry

P. A. Hadžić and *N. S. Vukojević:* Selective desulfonylation in D-xylofuranose 3,5-disulfonates 289

B. Jovančićević, H. Wehner, G. Scheeder, D. Plećaš, M. Ercegovac and *D. Vitorović:* An organic geochemical correlation study of some Drmno depression crude oils (southern part of the Pannonian Basin, Yugoslavia) 297

D. Z. Marković: Photolysis of incorporated benzophenone derivatives inside compressed lipid monolayers 309

M. Petrićević, A. Inić, R. M. Jankov and *Lj. Dimitrijević:* Two new murine monoclonal antibodies raised against human IgG 323

Inorganic Chemistry

I. M. Hodžić and *S. R. Niketić:* Synthesis and characterization of a novel (glycinato-N,O) yttrium(III) complex (Short communication) 331

Materials

R. Petrović, Dj. Janaćković, B. Božović, S. Zec and *Lj. Kostić-Gvozdenović:* Densification and crystallization behaviour of colloidal cordierite-type gels 335

Electrochemistry

V. D. Jović and *B. M. Jović:* Underpotential deposition of cadmium onto Cu(111) and Cu(110) from chloride containing solutions 345

Published by the Serbian Chemical Society, Karnegijeva 4/III,
P.O. Box 35-08, YU-11001 Belgrade, Yugoslavia
Printed by the Faculty of Technology and Metallurgy, Karnegijeva 4,
P.O. Box 35-03, YU-11001 Belgrade, Yugoslavia

J.Serb.Chem.Soc. 66(5)289-295(2001) UDC 66.5.382
JSCS–2856 *Original scientific paper*

Selective desulfonylation in D-xylofuranose 3,5-disulfonates

PAVLE A. HADŽIĆ*# and NADA S.VUKOJEVIĆ

Institute of Chemistry, Faculty of Science, University of Novi Sad, trg Dositeja Obradovića 3, 21000 Novi Sad, Yugoslavia

(Received 4 December 2000)

A method for the preparation of D-xylofuranose derivatives with a free terminal (C5) alcohol function was developed, starting from monocyclohexylidene-3,5-disulfonyl- or 5-*O*-sulfonyl-3-*O*-methyl ester. The regioselective displacement of the C5 sulfonyl ester function with acetate ion in dimethylsulfoxide afforded the corresponding 5-*O*-acetyl-1,2-*O*-cyclohexylidene-3-*O*-sulfonyl or 5-*O*-acetyl-3-*O*-methyl- -D-xylofuranose. These esters could be readily hydrolysed into the desired 1,2,3-trisubstituted xylofuranose.

Keywords: D-xylofuranose, sulfonyl ester, nucleophilic substitution, desulfonylation.

INTRODUCTION

For the preparation of D-xylofuranuronic acid, xylofuranose derivatives with free terminal (C5) hydroxyl function were needed for oxidation. The easily accessible 1,2-*O*-cyclohexylidene-3,5-di-*O*-sulfonyl- -D-xylofuranose was seen as a convenient starting material.

Examples of the selective sulfonylation of hydroxyl groups in carbohydrates are numerous. The selective regeneration of the alcohol function from disulfonates (polysulfonates) seems to be a more complicated task.

In this paper, we report on the two step, high yield preparation of 1,2,3-trisubstituted -D-xylofuranose. The method consists in the regioselective displacement of the 5-sulfonylester group in 3,5-di-*O*-sulfonyl esters of 1,2-*O*-cyclohexylidene- -D-xylofuranose with the acetate ion in dimethylsulfoxide. Subsequent hydrolysis of the 5-*O*-acetyl group is readily achieved with sodium hydroxide in methanol, giving high yields of the desired products, Scheme 1.

RESULTS AND DISCUSSION

Sulfonates are labile and undergo substitution or elimination reactions very easily. Direct methods for the conversion of sulfonates to alcohols (regeniration of the

Serbian Chemical Society active member.

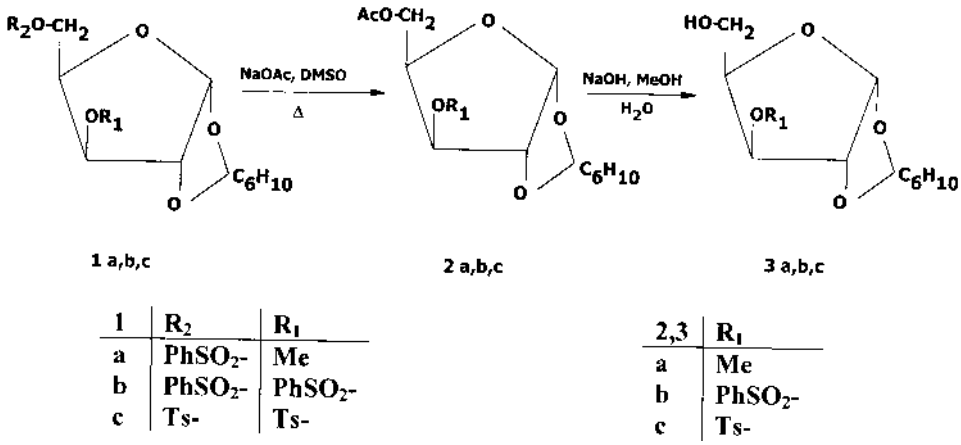

1	R_2	R_1
a	$PhSO_2$-	Me
b	$PhSO_2$-	$PhSO_2$-
c	Ts-	Ts-

2,3	R_1
a	Me
b	$PhSO_2$-
c	Ts-

Scheme 1. Formation of 1,2,3-trisubstituted derivatives of xylofuranose.

hydroxyl group), including reduction with sodium amalgam,[1] hydrogenolysis on nickel,[2] reduction with sodium in ammonia,[3] or the action of metal magnesium in methanol[4] are either too complicated for preparative work or are not appropriate for selective desulfonylation. Direct action of hydroxide ions on 3,5-disulfonyl esters of 1,2-alkylidene- -D-xylofuranose, particulary, is known to effect 3,5-anhydro ring closure[5] by an intramolecular nucleophilic C3 C5 attack.

On the other hand, highly regioselective substitution of primary 5-*O*-sulfonyl group in 3,5-disulfonyl esters of 1,2-*O*-cyclohexylidene- -D-xylofuranose with anionic nucleophiles (halogenes) was proven earlier in our laboratory,[6] pointing to the considerable difference in reactivity between a primary and a secondary sulfonyl ester group.

The method for the selective desulfonylation in xylofuranose-3,5-disulfonates was based on experimental observations in the preparation of the 5-*O*-acetyl-3-*O*-methyl derivative **1a**. Namely, it was found that when acetate ions are present in nonstoichiometric large amounts in dimethylsulfoxide, they quantitatively displace the primary sulfonyl ester group in **1a** in a short time on boiling the reaction mixture (Scheme 1). Simple workup of the reaction mixture gave 5-*O*-acetyl derivative **2a** in a high isolated yield.

On applying the same rigorous experimental conditions to 3,5-disulfonyl esters **1 b,c**, an unexpected outcome of the reaction was registered: the 3,5-disulfonyl esters **1 b,c** gave exclusively the 5-*O*-acetyl-3-*O*-sulfonates **2 b,c**. Analysis of the reaction mixture by TLC revealed that no 3,5-diacetate, 5-sulfonyl-3-*O*-acetate, nor 3,5-anhydro ring was formed, pointing to the high selectivity of the action of the acetate ion. It seems that key to the high reaction rate of the nucleophilic substitution, and the unespectedly short reaction times, lies in the ability of dimethylsulfoxide to solvate cationic species, which leads to the more nucleophilic acetate anion.[7]

On the other side, the high regioselectivity in the displacement of the primary sulfonyl group in the xylofuranose disulfonyl derivatives **1 b,c** could be understood in

line with the well known evidence relating to the inability of an anionic nucleophile to effect the displacement of certain secondary leaving groups attached to a furanose ring.[8]

The resulting acetyl derivatives **2a,b,c** are easily and selectively hydrolyzed in sodium hydroxide-methanol system at room temperature. On hydrolysis, they gave the 3-*O*-methyl derivative **3a**, or the 3-*O*-sulfonyl ester derivatives **3 b,c**, suitable for oxidation at their terminal C5 position.

The starting 5-*O*-sulfonyl-3-*O*-methyl derivative **1a** was prepared by selective C5 sulfonylation, followed by C3 methylation with MeI/silver(I) oxide, while the sulfonyl esters **1b,c** are prepared from 1,2-*O*-cyclohexylidene- -D-xylofuranose under the standard sulfonylation procedure (sulfonyl halide in pyridine).

EXPERIMENTAL

General methods

Melting points were determined on a Büchi SMP 50 apparatus and are not corrected. IR spectra were recorded on a Perkin-Elmer model 577 spectrometer. NMR spectra were taken on a Bruker AC250E apparatus in $CDCl_3$, using Me_4Si as an internal standard. The chemical shifts ( ) are expressed in ppm (*s*, *d*, *t* and *m* denote, respectively, singlet, dublet, triplet and multiplet form of the signal). The assignmats of the signals in the ^{1}H-NMR spectra are given after the description of the synthesis, while the assignments of the signals in the ^{13}C-NMR spectra are given in Table I. Mass spectra were recorded with a Finingen MAT311A spectrometer, the first number in the referring spectra denotes the *m*/*z* value, while the numbers in parenthesis correspond to the abundance of the mass peaks. Optical rotations were measured on an automatic polarimeter Polamat A (Karl Zeiss, Jena). TLC was performed on Silica gel alufolien (Merck 5333), with benzene–ethyl acetate 4:1 as mobile phase. Visualisation of the spots was achieved by spraying with 50 % sulphuric acid and subsequent heating to 150 ºC. All organic extracts were dried with anhydrous sodium sulphate.

*5-*O*-Benzenesulfonyl-1,2-cyclohexylidene-3-*O*-methyl-α-D-xylofuranose (**1a**)*

5-*O*-Benzenesulfonyl-1,2-cyclohexylidene-3- -D-xylofuranose (10.0 g, 27.7 mmol) and silver(I) oxide (30 g, 129.3 mmol) were refluxed in iodomethane (100 mL) for 20 h. After cooling to room temperature, chloroform (200 mL) was added to the reaction mixture upon which an insoluble material separated. Evaporation of the solvent under vacuo left a crude product, which on crystallysation from methanol gave crystalline **1a**, m.p. 111 ºC (10.34 g, 97 %), $_D^{20}$ = –24.42 (*c* 1.0, $CHCl_3$).

For $C_{18}H_{24}O_7S$, found: C 56.48, H 6.52, calculated: C 56.24, H 6.29.

Mass spectra: 384(M^+, 11), 341(14), 267(7), 233(40), 150(31), 55(31)

^{1}H-NMR: 1.32–1.73, *m*, 10H, from cyclohexylidene; 3.31, *s*, 3H, methyl; 3.73, *d*, 1H, H-3, $J_{3,4}$ = 3.1; 4.13, *dd*, 1H, H-5a, $J_{5a,4}$ = 5.8, $J_{5a,5b}$ = 9.4; 4.30, *dd*, 1H, H-5b, $J_{5b,4}$ = 5.9; 4.36, *m*, 1H, H-4; 4.53, *d*, 1H, H-2, $J_{1,2}$ = 3.7; 5.83, *d*, 1H, H-1; 7.52–7.98, group of signals, 5H, aromatic.

*5-*O*-acetyl-1,2-*O*-cyclohexylidene-3-*O*-methyl-α-D-xylofuranose (**2a**)*

5-*O*-Benzenesulfonyl-1,2-*O*-cyclohexylidene-3-*O*-methyl- -D-xylofuranose (1.15 g, 3 mmol), anhydrous sodium acetate (2.4 g, 29 mmol) and dimethylsulfoxide were mixed together in a 50 mL round-bottom, long neck reaction flask, and heated with an open flame and boiled for 10–15 s. After cooling to room temperature, the semi-solid reaction mixture was extracted with benzene–petroleum ether 1:1 (5 20 mL). The combined extracts were washed with concentrated aqueous sodium chloride (2 10 mL), dried, and decolourised with active carbon. Evaporation of solvent in vacuo and distillation at 150 ºC/0.02 mm Hg gave pure **2a** as an oil (800 mg, 92.7 %).

TABLE I. ˙C-NMR spectral parameters of compounds 1-3 (in ppm)

No.	C1	C2	C3	C4	C5	3’, 4’, 5’	2’, 6’	C1’	Aromatic	C=O	Me
1a	104.51	80.53	83.37	77.11	67.14	23.30, 23.61, 24.57	35.47, 36.21	112.44	127.70, 129.07, 133.71, 135.45 Cq		57.54
2a	104.75	80.94	84.34	77.97	62.42	23.51, 23.81, 24.81	35.65, 36.36	112.41		170.84	20.86 57.86
2b	104.24	82.52	81.66	76.21	60.61	23.24, 23.58, 24.55	35.44, 36.01	113.51	127.70, 129.35, 134.22, 135.56 Cq	170.04	20.45
2c	104.22	82.51	81.43	76.21	60.70	23.21, 23.56, 24.53	35.43, 36.00	113.07	127.72, 129.90, 132.49 Cq, 145.38 Cq	170.00	20.61 21.67
3a	104.42	81.13	85.28	79.90	60.59	23.43, 23.73, 24.73	35.65, 36.30	112.27			57.67
3b	104.16	82.82	81.93	79.25	59.50	23.39, 23.7, 24.68	35.67, 36.15	113.31	127.82, 129.51, 134.44, 135.54 Cq		
3c	104.06	82.73	81.62	79.18	59.42	23.28, 23.61, 24.58	35.58, 36.05	113.0	127.75, 130.01, 132.3 Cq, 145.58 Cq		21.56

For $C_{14}H_{22}O_6$, found: C 58.97, H 7.64, calculated: C 58.73, H 7.75.

Mass spectra: 286(M^+, 79), 255(12.5), 244(100), 170(36), 151(49).

^{1}H-NMR: 1.3–1.7, *m*, 10H, from cyclohexylidene; 2.08, *s*, 3H, acetyl methyl group; 3.39, *s*, 3H, methoxy methyl group; 3.74, *d*, 1H, H-3, $J_{3,4}$ = 3.1; 4.19, *dd*, 1H, H-5a, $J_{5a,5b}$ =12.6, $J_{4,5a}$=8.5; 4.32–4.40, *m*, 2H, H-5b and H-4; 4.56, *d*, 1H, H-2, $J_{1,2}$ = 3.8; 5.92, *d*, 1H, H-1.

5-O-*Acetyl-3*-O-*benzenesulfonyl-1,2*-O-*cyclohexylidene*-α-*D-xylofuranose* ***(2b)***

3,5-di-*O*-Benzenesulfonyl-1,2-*O*-cyclohexylidene- -D-xylofuranose (2.0 g, 3.92 mmol), anhydrous sodium acetate (4.0 g, 48.8 mmol) and dimethylsulfoxide (10 mL) were mixed together in a 50 mL round-bottom, long neck reaction flask and heated with an open flame and boiled for 10–15 s. On cooling, the reaction mixture formed a semi-solid mass, which was extracted with benzene–petroleum ether 1:1 (5 20 mL). The combined extracts were washed with concentrated aqueous sodium chloride (3 10 mL), dried, and the solvent evaporated. The remaining oil solidified on standing, and after crystallisation from methanol–ethyl acetate gave **2b**, m.p. 111–112 ºC (1.52 g, 94 %). $_D^{20}$ = –27.31 (*c* 0.997, $CHCl_3$).

For $C_{19}H_{24}O_8S$, found: C 55.22, H 5.58, calculated: C 55.32, H 5.86.

Mass spectra: 412(M^+, 65.1), 328(15.4), 371(85.9), 240(21.6), 150(81.7).

^{1}H-NMR: 1.33–1.72, *m*, 10H, from cyclohexylidene; 1.96, *s*, 3H, methyl; 4.03, *dd*, 1H, H-5a, $J_{5a,5b}$ = 11.65, $J_{5a,4}$ = 5.8; 4.15, *dd*, 1H, H-5b, $J_{5b,4}$ = 6.7; 4.41, *m*, 1H, $J_{3,4}$ = 2.9; 4.70, *d*, 1H, H-2, $J_{1,2}$ = 3.7; 4.91, *d*, 1H, H-3; 5.94, *d*, 1H, H-1; 7.54–7.98, 5H, aromatic.

5-O-*Acetyl-1,2*-O-*cyclohexylidene-3*-O-*tosyl*-α-*D-xylofuranose*[9] ***(2c)***

1,2-*O*-cyclohexylidene-3,5-di-*O*-tosyl- -D-xylofuranose[10] (2.0 g, 3.71 mmol), anhydrous sodium acetate (4.0 g, 48.8 mmol) and dimethyl sulfoxide (10 mL) were mixed together in a 50 mL round-bottom, long neck reaction flask and heated with an open flame and boiled for 10–15 s. On cooling, the reaction mixture formaed a semisolid mass, which after the described workup and crystallisation from methanol–ethyl acetate 9:1, gave **2c**, m.p. 136–138 ºC (1.37 g, 87 %), $_D^{20}$ = –27.17 (*c* 0.91, $CHCl_3$).

Mass spectra: 426(M^+, 65.1), 397(21.5), 382(71.2), 254(35.8), 169(54.8), 139(74.4).

^{1}H-NMR: 1.31–1.72, *m*, 10H, from cyclohexylidene; 1.96, *s*, 3H, acetyl methyl group; 2 methyl group; 4.04, *dd*, 1H, H-5a, $J_{5a,5b}$ = 11.6, $J_{5a,4}$ = 5.7; 4.15, *dd*, 1H, H-5b, $J_{5b,4}$ = 6.7; 4.41, *m*, 1H, H-4, $J_{3,4}$ = 2.9; 4.70, *d*, 1H, H-2, $J_{1,2}$ = 3.7; 4.88, *d*, 1H, H-3; 5.94, *d*, 1H, H-1; 7.37 and 7.81, 2*d*, 4H, aromatic.

1,2-O-*Cyclohexylidene-3*-O-*methyl*-α-*D-xylofuranose* ***(3a)***

The 5-*O*-acetyl-1,2-*O*-cyclohexylidene-3-*O*-methyl derivative **2a** (750 mg, 2.6 mmol) was added to sodium hydroxide (0.5 g) dissolved in methanol (5 mL), and left at room temperature. The end of reaction was established after 30 min (vide TLC). The reaction mixture was concentrated in an evaporator and chloroform (50 mL) added. The chloroform solution was washed with concentrated sodium chloride, dried and decolourised with active carbon. Evaporation of chloroform left **3a** as an oil (560 mg, 88 %). Analysis vide TLC revealed a single spot.

Mass spectra: 244(M^+, 30.12), 202(52.3), 139(36.5), 100(15.07), 55(39.17).

^{1}H-NMR: 1.33–1.74, *m*, 10H, from cyclohexylidene; 2.38, *bs*, 1H, O*H*; 3.43, *s*, 3H, methyl; 3.82, *d*, 1H, H-3, $J_{3,4}$ = 3.0; 3.85–3.96, *m*, 2H, 5-CH_2, $J_{5a,5b}$ = 11.9, $J_{5a,4}$ = 7.3, $J_{5b,4}$ = 5.2; 4.27, *m*, 1H, H-4; 4.58, *d*, 1H, H-2, $J_{1,2}$ = 3.7; 5.95, *d*, 1H, H-1.

3-O-*Benzenesulfonyl-1,2*-O-*cyclohexylidene*-α-*D-xylofuranose* ***(3b)***

The 5-*O*-acetyl-3-*O*-benzenesulfonyl derivative **2b** (4.12 g, 10 mmol) was added to a solution of sodium hydroxide (0.5 g) in mixture of methanol (80 mL) and water (20 mL) and left stirring at room temperature. After 10 min all the solid had dissolved and TLC revealed the end of reaction after 30 min. The reaction mixture was concentrated to approximately 15 mL, and chloroform (100 mL) added. Washing the chloroform layer with concentrated sodium chloride, drying and evaporation of the chloroform left **3b** as a colourless oil (3.40 g, 92 %), pure according to TLC.

Mass spectra: 370(M^+, 3.12), 327(2.8), 285(1.5), 139(4.19), 98(44.9), 69(39.2).

^{1}H-NMR: 1.2–1.9, *m*, 10H, from cyclohexylidene; 2.32, *t*, 1H, 5-OH, $J_{OH,5\text{-}CH_2}$ = 6.3; 3.60, *m*, 1H, H-5a, $J_{5a,5b}$ = 11.8, $J_{4,5a}$ = 6.1; 3.77, *m*, 1H, H-5b, $J_{4,5b}$ = 6.6; 4.33, *td*, 1H, H-4, $J_{3,4}$ = 2.5; 4.56, *d*, 1H, H-2, $J_{1,2}$ = 3.7; 4.92, *d*, 1H, H-3; 5.89, *d*, 1H, H-1; 7.53–7.99, *m*, 5H, aromatic.

1,2-O-*Cyclohexylidene-3*-O-*tosyl*-α-*D-xylofuranose*[11] ***(3c)***

5-*O*-Acetyl-1,2-*O*-cyclohexylidene-3-*O*-tosyl- -D-xylofuranose (**2c**) (4.26 g) was added to a solution of sodium hydroxide (0.5 g) in methanol (100 mL) and left stirring at room temperature. Thin-layer chromatography showed the complete disapearance of the starting material and the formation of a more polar product. The reaction mixture was then concentrated to about 20 mL and chloroform (100 mL) added. The chloroform solution was washed with concentrated sodium chloride (3 15 mL), decolourised with active carbon, dried and evaporated to leave an oil which crystallysed on standing. Recrystallisation from di-*iso*-propyl ehter– petrolether gave **3c**, m.p. 87 ºC (3.17 g, 83 %). $_D^{20}$ = –7.22 (*c* 0.97, $CHCl_3$).

For $C_{18}H_{24}O_7S$, found: C 56.40, H 6.13, S 8.23, calculated: C 56.23, H 6.29, S 8.33.

Mass spectra: 384(M^+, 100), 343(78.9), 267(14), 155(57), 139(84).

^{1}H-NMR: 1.27–1.8, *m*, 10H, from cyclohexylidene; 2.01, *t*, 1H, 5-O*H*, $J_{H5,OH}$ = 6.5; 2.48, *s*, 3H, CH_3; 3.65, *m*, 1H, H-5a, $J_{5a,5b}$ = 11.9, $J_{5a,4}$ = 6.4; 3.80, *m*, 1H, H-5b, $J_{5b,4}$ = 6.4; 4.36, *td*, 1H, H-4, $J_{3,4}$ = 2.8; 4.59, *d*, 1H, H-2, $J_{1,2}$ = 3.7; 4.92, *d*, 1H, H-3; 5.91, *d*, 1H, H-1.

Acknowledgment: Authors are indebted to Professor M. Popsavin for recording the NMR spectra and valuable discussion.

И З В О Д

СЕЛЕКТИВНО ДЕСУЛФОНОВАЊЕ 3,5-ДИСУЛФОНАТА D-КСИЛОФУРАНОЗЕ

ПАВЛЕ А. ХАЏИЋ* и НАДА С. ВУКОЈЕВИЋ

Институт за хемију, Природно-математички факултет, Универзитет у Новом Саду, Трг Д. Обрадовића 3, 21000 Нови Сад

Разрађена је метода за добијање деривата D-ксилофуранозе са слободном терминалном (C5) алкохолном групом. Поступак полази од лако доступних 3,5-дисулфонил естара моноциклохексилиден-D-ксилофуранозе и састоји се у селективној супституцији 5-сулфонилестарске групе ацетилном групом. Селективна супституција се врши ацетатним јоном из натријум-ацетата у диметилсулфоксиду, при чему настају одговарајући 5-ацетати. Ови се лако хидролизују натријум-хидроксидом у систему метанол–вода дајући високе приносе 1,2,3-трисупституисаних деривата D-ксилофуранозе.

(Примљено 4. децембра 2000)

REFERENCES

1. K. Freundenberg, F. Broums, *Chem. Ber.* **55** (1922) 3233
2. G. W. Kenner, M. A. Murray, *J. Chem. Soc.* (1949) 178
3. D. B. Denney, B. Goldstein, *J. Org. Chem.* **21** (1956) 429
4. M. Sridhar, B. Ashok Kumar, R. Nerender, *Tetrahedron Lett.* **39** (1998) 2487
5. B. Helferich, M. Burgdorf, *Tetrahedron* **3** (1958) 274
6. N. Vukojević, D. Miljković, M. Popsavin, *Collect. Czech. Chem. Commun.* **58** (1993) 902; N. Vukojević, M. Popsavin, E. Foro, D. Miljković, *J. Serb. Chem. Soc.* **57** (1992) 137
7. C. Reichardt, *Solvents and Solvent Effect in Organic Chemistry;* VCH, Weinheim (1988) 213-218
8. D. H. Ball, F. W. Parish, *Adv. Carbohydr. Chem.* **24** (1969) 139

9. D. Miljković, N. Vukojević, Lj. Milenković, *Bull. Chem. Soc. Belg.* **48** (1983) 303
10. V. F. Kazimirova, K. V. Levitskaya, *Zh. Obsch. Khim.* **30** (1960) 723
11. S. Petrović, E. Lončar, M. Popsavin, V. Popsavin, *J. Planar Chromatography* **10** (1997) 406.

J.Serb.Chem.Soc. 66(5)297–308(2001)
JSCS–2857

UDC 553.98
Original scientific paper

An organic geochemical correlation study of some Drmno depresssion crude oils (southern part of the Pannonian Basin, Yugoslavia)

B. JOVANČIĆEVIĆ[1,2#], H. WEHNER[3], G. SCHEEDER[3#], D. PLEĆAŠ[1], M. ERCEGOVAC[4] and D. VITOROVIĆ[2#] *

[1]Faculty of Chemistry, University of Belgrade, P.O. Box 158, YU-11001 Belgrade, [2]ICTM-Center of Chemistry, P.O. Box 815, YU-11001 Belgrade, [3]Federal Institute for Geosciences and Natural Resources, P.O. Box 510153, Hannover, Germany and [4]Faculty of Mining and Geology, University of Belgrade, Belgrade, Yugoslavia

(Received 8 January 2001)

The results of an investigation of crude oils originating from the Sirakovo and Bradarac-Maljurevac localities (southern part of the Pannonian Basin) are reported in this paper. The aim was to estimate the organic geochemical similarity of the crude oils from the Drmno (Kostolac) depression oil fields. The nine selected samples originated from reservoir rocks of various depths. Reliable source and organic geochemical maturation parameters served as the basis for the correlation studies. The similar origin of the investigated Drmno depression crude oils was corroborated, characterized by a significant participation of terrestrial precursor biomass. They were shown to be of relatively low maturity and to have been formed during the earlier stages of the diagenet- ic-catagenetic sequence of processes leading to the formation of crude oils, most probably in source rocks of Tertiary age, corresponding to vitrinite reflectances between R*o* = 0.70 % and R*o* = 0.80 %. The crude oils from Bradarac-Maljurevac seemed to be somewhat less homogeneous with respect to organic geochemical parameters compared to Sirakovo crude oils.

Keywords: crude oils, Drmno (Kostolac) depression, correlation parameters, source, maturation, age.

INTRODUCTION

The most recent organic geochemical investigations of Drmno (Kostolac) depression crude oils (the southern part of the Pannonian Basin, Yugoslavia) were aimed at correlating them with the crude oils from the Banat and North Bačka depressions. Thus, for example, based on a number of bulk and specific correlation parameters, the Drmno depression crude oils were shown to have a different origin compared to crude oils from three oil fields of the Banat depression and one field from the North Bačka depression.[1] The differences between the Drmno depression crude oils and the crude oils

Serbian Chemical Society active member.

* Corresponding author.

from the most important Banat depression oil fields Kikinda and Mokrin were corroborated on the basis of detailed gas chromatographic-mass spectrometric analysis of the corresponding sterane and terpane fractions.[2] Dissimilarities in the type of precursor organic material of the mentioned crude oils were also confirmed by carbon isotope analysis.[3] The Drmno depression crude oils are characterized by more negative $^{13}C_{PDB}$ values compared to Banat depression crude oils, *i.e.,* they contain a smaller amount of the heavier ^{13}C isotope. Lastly, a higher participation of terrestrial material in the precursor organic biomass of the crude oils from the Drmno depression was suggested compared to the Banat and North Bačka depression crude oils.[4]

Hence, the different origin of the Drmno depression crude oils compared to most other Yugoslav crude oils has been repeatedly emphasized. Nevertheless, sporadically, certain genetic resemblances were indicated between the Drmno depression crude oils and some crude oils from South Banat oil fields.[4]

On the other hand, concerning the Drmno depression oil fields and the corresponding crude oils themselves, one question, certainly of great interest for further exploration of this geological formation, has never been explicitly raised. This is the question of the organic geochemical similarity of the Drmno depression crude oils. Namely, it has never been clearly suggested that their origins and geological histories are quite the same. On the contrary, a certain heterogeneity in these crude oils was suspected.[1]

In order to contribute to the solution of this important problem, nine samples of Drmno depression crude oils, originating from Sirakovo and Bradarac-Maljurevac localities, were investigated. The samples were selected to represent reservoir rocks of diverse depths. To investigate the organic geochemical relationship of these crude oils, reliable source and maturation correlation parameters were used.

EXPERIMENTAL

Geological setting and samples

Drmno depression crude oils from Sirakovo (5 samples) and Bradarac-Maljurevac (4 samples) localities were investigated. A list of analyzed crude oils, including the basic geological data, is presented in Table I.

The geological column of the Drmno depression is characterized by the following lithostratigraphic units:[5,6]

1. Prebadenian units, which belong to highly heterogeneous clastic sediments. Within Prebadenian, "red formations", characterized by mixed subaquatic to continental development and varying lithofacies (predominantly marls, shales-sandstones, and sandstones) were found at depths of 2200–1900 m.

2. Ottnangian-Carpathian sediments (Upper Prebadenian), which in fact do represent the main object in the investigation of hydrocarbon deposits. These sediments belong to marine and brackish lake sediments with very complex lithological heterogeneity (predominantly sandstones and siltstones). They are situated at depths of 1700 to 1900 m (oil fields area) and 3250 to 3800 m (depocentre).

3. Badenian sediments, which belong to marine sediments formed during the Mediterranean development. The maximum depth of the Badenian in the depocentre (Drmno) may be 3250 m, and the maximum thickness is 1250 m. These sediments (sandstones, clayey sandstones, sandy claystones and clayey limestones) are characterized by frequent grain size changes, both laterally and vertically. The Drmno depression was formed either by the collapse of the basement along meridional faults at different periods and of different intensity, or by step-like sinking of the terrain along the faults. Faulting took place during and after the formation of Neogene deposits.

TABLE I. Geological data on the reservoirs of the sampled and analyzed oils

No.	Sample (Well)	Depth interval (m)	Age	Lithology
1	Sir-1	1782–1778	Ottnangian-Carpathian	Sandstone, aleurolite, breccia conglomerate
2	Sir-2	1704–1701	Ottnangian-Carpathian	Sandstone, aleurolite, breccia conglomerate
3	Sir-18	1548–1544	Ottnangian-Carpathian	Sandstone, marlstone, aleurolite, limestone
4	Sir-19	1436–1429	Ottnangian-Carpathian	Sandstone, marlstone, aleurolite, limestone
5	Sir-20	1444–1440	Ottnangian-Carpathian	Sandstone, marlstone, aleurolite, limestone
6	Bra-Malj-2	2307–2302	Ottnangian-Carpathian (partly "Red formation")	Crystalline rock
7	Bra-Malj-4	2170–2156	Prebadenian ("Red formation")	Marlstone, sandstone, breccia conglomerate
8	Bra-Malj-5	1989–1985	Badenian	Marlstone, sandstone, breccia conglomerate
9	Bra-Malj-10	1808–1804	Badenian	Sandstone, aleurolite, breccia conglomerate

Crude oil samples from boreholes Bra-Malj-2 and 4 (Table I) originated from "red formations" (Miocene) of the Prebadenian units. A large fault was discovered between these two boreholes during seismic investigation.

The boreholes Sirakovo-1,2 and 18 were located in one zone, *i.e.,* in the deeper, faulty zone, whereas the boreholes Sirakovo-19 and 20 were situated in another, shallower zone of the Ottnangian-Carpathian sediments (Upper Prebadenian).

Badednian oil deposits Bradarac-Maljurevac were found at depths of 1808-1804 m (Bra- Malj-10) and 1989-1985 m (Bra-Malj-5).

Analytical methods

Bulk correlation parameters, such as API density, contents of sulphur and asphaltenes, and group composition (proportion of alkanes, aromatics and NSO-compounds), were determined by standard organic geochemical methods, described elsewhere.[1,7]

The carbon isotope composition, $^{13}C_{PDB}$, of the aromatic fractions was determined using a mass spectrometer Delta Plus, Thermo Quest, Finnigan MAT, coupled with an Elemental Analyzer, Carlo Erba, NC 2500. Helium was used as a carrier gas (flow rate 120 cm^3/min).

n-Alkanes and the isoprenoid aliphatic alkanes pristane and phytane, as constituents of the saturated hydrocarbon fractions, were analyzed by gas chromatography (GC) using a Varian 3300 gas chromatograph (FID) fitted with a capillary column coated with BP-1. Hydrogen was used as the carrier gas at 1 cm^3/min flow rate.

Polycyclic alkanes of sterane and triterpane types were analyzed by gas chromatography with mass selective detector (GC-MSD), using the single ion monitoring (SIM) method. Steranes were identified from *m/z* 217 and triterpanes from *m/z* 191 fragmentograms. A Hewlett Packard 5890, Series II gas chromatograph was used fitted with a capillary column coated with HP-5MS and helium as a carrier gas (flow rate 1 cm^3/min), coupled to a Hewlett-Packard 5972 MSD operated at 70 eV.

RESULTS AND DISCUSSION

Bulk correlation parameters

The rationale for using crude oil bulk parameters in correlation studies was described elsewhere.[4] The observed bulk correlation parameters are shown in Table II.

TABLE II. Bulk parameters of the analyzed oil samples

No.	Sample	API°	Sulphur %	Asphaltenes %	Alkanes %	Aromatics %	NSO-compounds %	$^{13}C_{PDB}$ of aromatics ‰
1	Sir-1	46.71	0.21	0.04	59.5	3.4	37.1	–28.0
2	Sir-2	52.13	0.18	0.4	56.2	4.2	39.1	–28.0
3	Sir-18	46.86	0.19	0.4	70.3	7.7	21.5	–27.9
4	Sir-19	46.64	0.34	1.6	50.5	13.8	33.7	–28.0
5	Sir-20	46.13	0.32	0.1	56.5	4.4	38.9	–27.8
6	Bra-Malj-2	45.93	0.34	1.0	66.7	3.1	29.2	–28.0
7	Bra-Malj-4	37.92	0.35	0.2	59.9	10.9	29.0	–28.2
8	Bra-Malj-5	37.92	0.42	0.1	65.8	5.3	28.7	–27.9
9	Bra-Malj-10	41.52	0.19	0.3	61.1	11.1	27.3	–26.4

API densities of the nine investigated crude oils were apparently distributed in a relatively wide range (37.92–52.13°, Table II). Crude oils from Bradarac-Maljurevac seem to be somewhat heavier than Sirakovo oils. However, all these values were within the limits typical of light, paraffinic crude oils. This characteristic is generally considered as one of the first indications of substantial participation of terrestrial precursor material in the generation of an oil.[8,9]

The content of sulphur, a source parameter, was found to be relatively uniform (0.18–0.42 %, Table II). Since crude oils containing higher amounts of sulphur originated from higher saline marine environments, based on the observed values presented in Table II, such a characteristic could not be attributed to either of the nine crude oil samples investigated.

The observed contents of asphaltenes were not uniform (0.04–1.6 %, Table II). This relatively wide range might indicate a possible organic geochemical non-uniformity of the investigated crude oils, the amount of asphaltenes in crude oils generally depending on the length of migration and the degree of maturation.[8,9]

The group composition of all the examined oils was characterized by a dominance of the alkane fraction (over 50 %), and a noticeably low proportion of aromatics (3.1–13.8 %, Table II). The observed group compositions conformed with the API densities, *i.e.,* they corresponded to the indicated light crude oils type.

Eight out of the nine analyzed aromatic fractions had almost identical carbon isotope composition, $^{13}C_{PDB}$ (–27.8 to –28.2 ‰, Table II). The observed differences between these eight oils may be considered negligible, the experimental error of the used method being 0.2 ‰. Only the sample Bra-Malj-10 showed a less negative value of this parameter (– 26.4 ‰, Table II). The carbon isotope composition of any crude oil or its components depends mainly on its origin. Crude oils originating from precursor biomass with a higher participation of terrestrial material contain a higher proportion of the lighter isotope ^{12}C, resulting in more negative $^{13}C_{PDB}$ values.[10] Bitumens from mature ancient sediments and crude oils of dominantly terrestrial origin have 2–4 ‰ more negative values compared to bitumens and crude oils of marine origin.[8] Moreover, this

parameter is only slightly affected by the maturation processes, since the lighter carbon isotope, ^{12}C, forms weaker bonds compared with the heavier ^{13}C isotope.[9] Biodegradation, which presumably has affected the sample Bra-Malj-10 and which could have influenced the whole oil isotope ratio $^{13}C_{PDB}$,[11,12] should be excluded from consideration in this case, since aromatic fractions, known as relatively resistant towards microbiological decomposition,[13] were the investigated substrates.

Specific correlation parameters

Specific correlation parameters were based on GC analyses of the saturated hydrocarbons (*n*-alkanes and the isoprenoid aliphatic alkanes pristane and phytane), and GC-MSD analyses of the polycyclic alkanes (steranes, *m/z* 217; triterpanes, *m/z* 191).

The parameters calculated from gas chromatograms are shown in Table III.

TABLE III. Alkane molecular parameters of the analyzed oil samples

No.	Sample	Most abundant *n*-alkane	CPI	Pr/Phyt	Pr/*n*-C_{17}	Phyt/*n*-C_{18}
1	Sir-1	C_{19}	1.03	1.18	0.43	0.32
2	Sir-2	C_{19}	1.03	1.85	0.39	0.17
3	Sir-18	C_{19}	1.03	1.85	0.48	0.21
4	Sir-19	C_{21}	1.03	1.40	0.43	0.26
5	Sir-20	C_{21}	1.04	1.25	0.47	0.32
6	Bra-Malj-2	C_{21}	1.03	2.20	0.52	0.21
7	Bra-Malj-4	C_{25}	1.06	1.17	1.00	0.66
8	Bra-Malj-5	C_{21}	1.02	1.33	0.40	0.23
9	Bra-Malj-10	C_{23}	1.07	1.00	2.37	2.37

According to data shown in Table III, the investigated crude oils seem to be generally similar. Namely, all the chromatograms were characterized by the most abundant *n*-alkane located within the odd C_{19}–C_{25} carbon number range, by CPI values somewhat higher than 1 (CPI = 1.02–1.07), and by pristane dominating over phytane (with the single exception of the sample Bra-Malj-10, which contained equal amounts of pristane and phytane, Pr/Phyt = 1.00, Table III). These three parameters corroborated the above - mentioned statement that terrestrial type precursor biomass participated considerably in the generation of the crude oils from the Sirakovo and Bradarac-Maljurevac localities, a characteristic of Drmno depression crude oils revealed in earlier studies as well.[1–4]

Based on the Pr/*n*-C_{17} and Phyt/*n*-C_{18} parameters, most of the examined crude oils were not exposed to biodegradation (values below one, Table III). According to these parameters, again, the sample Bra-Malj-10 was the exception, the isoprenoid alkanes pristane and phytane being more abundant in this sample, compared to the corresponding *n*-alkanes C_{17} and C_{18}, respectively (Pr/*n*-C_{17} = 2.37; Phyt/*n*-C_{18} = 2.37, Table III), data suggesting minor biodegradation.[9] The Bra-Malj-4 sample also demonstrated somewhat higher values of these parameters compared to the other investigated crude oils (Pr/*n*-C_{17} =1.00; Phyt/*n*-C_{18} = 0.66, Table III).

As the observed bulk correlation parameters (Table II) and alkane correlation parameters (Table III) were relatively uniform (with the single clear exception of the sample Bra-Malj-10), similar fragmentograms of the polycyclic alkanes, *i.e.,* triterpanes and steranes, were also anticipated. However, surprisingly, the evidence obtained from the GC-MSD analyses was ambiguous. Fragmentograms typical of the analyzed oils are shown in Fig. 1. The calculated GC-MSD molecular source and maturation parameters are shown in Tables IV and V.

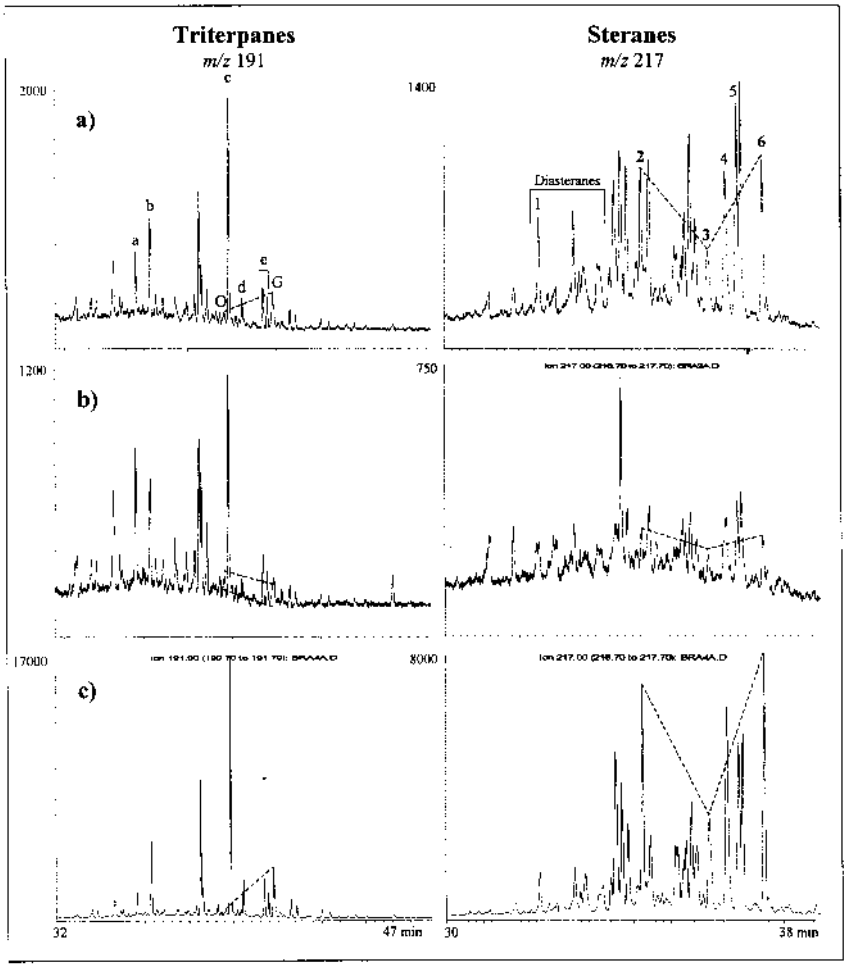

Fig. 1. Fragmentograms of triterpanes (*m/z* 191) and steranes (*m/z* 217) in Sir-18 (a), Bra-Malj-2 (b) and Bra-Malj-4 (c) alkane fractions, typical of all the investigated crude oils. a – C_{27}-18 (H)-22,29,30-trisnorneohopane (Ts); b – C_{27}-17 (H)-22,29,30-trisnorhopane (Tm); c – C_{30}-17 (H),21 (H) hopane; d – C_{30}-17 (H),21 (H) moretane; e – C_{31}-17 (H),21 (H) homohopanes (22*S* and 22*R*); O – oleanane; G – gammacerane; 1 – C_{27}-13 (H),17 (H) diasterane (20*S*); 2 – C_{27}-14 (H),17 (H) sterane (20*R*); 3 – C_{28}-14 (H),17 (H) sterane (20*R*); 4 – C_{29}-14 (H),17 (H) sterane (20*S*); 5 – C_{29}-14 (H),17 (H) sterane (20*R*); 6 – C_{29}-14 (H),17 (H) sterane (20*R*). (Detailed identification of the corresponding peaks was discussed in our previous papers).[2,3]

Firstly, in all *m/z* 217 mass chromatograms, the distribution of peaks originating from regular C_{27}–C_{29} *R* steranes was almost identical (C_{29}>C_{27}>C_{28}, Fig. 1; Table IV). This observation does not refer to the sample Bra-Malj-10, its corresponding distribution being somewhat different: the proportion of C_{29} being by far the highest and the abundance of C_{28} being higher than that of C_{27}. Hence, this reliable source correlation parameter gave one more proof of the similar or identical type of precursor biomass of all the investigated Drmno depression crude oils, except for the oil Bra-Malj-10.

TABLE IV. GC-MSD molecular source parameters of the analyzed oil samples

No.	Sample	*R* steranes			O/C_{30} hopane 100	G/C_{30} hopane 100
		% C_{27}	% C_{28}	% C_{29}		
1	Sir-1	35.1	19.1	45.8	7.4	6.7
2	Sir-2	33.0	20.4	46.6	7.6	5.9
3	Sir-18	32.7	18.4	48.9	5.7	15.4
4	Sir-19	36.1	19.6	44.3	6.8	16.2
5	Sir-20	34.5	19.5	46.0	6.0	16.5
6	Bra-Malj-2	32.8	26.6	40.6	12.8	10.3
7	Bra-Malj-4	37.0	16.5	46.5	1.9	18.8
8	Bra-Malj-5	33.0	18.2	48.9	5.7	21.1
9	Bra-Malj-10	20.0	28.2	51.8	3.0	9.8

O–oleanane; G–gammacerane.

However, the fragmentograms *m/z* 191, shown as examples in Fig. 1, as well as the calculated parameters O/C_{30} hopane 100 and G/C_{30} hopane 100 from Table IV, indicated different concentrations of oleanane and gammacerane in the crude oils. These pentacyclic triterpanes are considered to be reliable indicators either of the continental origin (oleanane), or proof of marine evaporite and/or higher salinity media origin (gammacerane).[8,9,14] The observed differences were particularly noticeable with the Bradarac-Maljurevac locality crude oils. Nevertheless, generally, the latter evidence does not contradict the conclusion on the predominantly continental origin of the investigated crude oils, all samples containing oleanane at least in small concentrations.

The values of some of the maturation parameters shown in Table V might also explain the non-uniformity in the distribution and abundance of triterpanes and steranes in the nine crude oils (Fig. 1). This refers in the first place to the parameters Ts/Ts+Tm and C_{27} dia/dia+ster (parameters 1 and 6, Table V). According to these parameters, the sample Bra-Malj-10 was once more unique, being characterized by much lower values. The observed differences might suggest differences in the thermal maturities of the oils. However, in contrast, the uniform values of the parameters 2–5 (Table V) indicate almost the same phase in the isomerization of triterpanes (moretane hopane, and 22*R* 22*S*) and steranes (, and 20*R* 20*S*), typical of maturation processes. Hence, it could be suggested that the differences in parameters 1 and 6 do not result from maturation processes, but rather from some other effects. For example, it is well known that isomerization processes Tm Ts (17 (H)-22,29,30-trisnorhopane 18 (H)-22,29,30-trisnorneohopane), as well as the isomerization of regular steranes

into diasteranes, are chiefly influenced by mineral catalysts of silicate type (acidic sites on clays), being constituents of source rocks.[15,16]

TABLE V. GC-MSD molecular maturation parameters of the analyzed oil samples

No.	Sample	Ts/Ts+Tm	22*S*/22*S* + 22*R* C_{31} hopanes	Moretane/Hopane C_{30}	/ + C_{29} steranes	20*S*/20*S* + 20*R* C_{29} steranes	C_{27} dia/dia + ster
1	Sir-1	0.47	0.59	0.12	0.57	0.48	0.21
2	Sir-2	0.49	0.61	0.13	0.56	0.54	0.62
3	Sir-18	0.46	0.61	0.11	0.56	0.46	0.19
4	Sir-19	0.40	0.60	0.13	0.60	0.50	0.22
5	Sir-20	0.41	0.61	0.11	0.58	0.47	0.19
6	Bra-Malj-2	0.54	0.62	0.11	0.63	0.55	0.59
7	Bra-Malj-4	0.24	0.61	0.13	0.39	0.44	0.04
8	Bra-Malj-5	0.43	0.60	0.11	0.59	0.48	0.20
9	Bra-Malj-10	0.10	0.60	0.11	0.57	0.45	0.13
	Equilibrium values	/	0.57–0.62	0.05–0.10–0.15	0.67–0.71	0.52–0.55	/
	Parameter	1	2	3	4	5	6

Ts – 18 (H)-22,29,30-trisnorneohopane; Tm – 17 (H)-22,29,30-trisnorhopane; Dia – C_{27} diasterane (20*S*); Ster – C_{27} sterane (20*R*)

Comparison of the parameters 2–5 from Table V with the known values characteristic of source rock bitumens and crude oils of high maturity, *i.e.,* equilibrium values corresponding to the related isomerization reactions (their ranges are also shown in Table V),[17] may serve as a basis for the estimation of the maturity degrees of the investigated samples, *i.e.,* their position in the diagenetic-catagenetic sequence of the processes leading to petroleum formation.

The values of parameter 22*S*/22*S*+22*R* (C_{31} hopanes) fitted into the equilibrium range of 0.57–0.62, suggesting that the equilibrium 22*R* = 22*S* (parameter 2, Table V) has already been attained in the investigated oils. However, it is known that this equilibrium in the isomerization reactions of polycyclic alkanes is established relatively quickly, already in the early oil-generative stages, and that subsequent maturation processes have no further influence on the 22*S*/22*S*+22*R* ratio. In most cases this stage is characterized by vitrinite reflectances R*o* = <0.60 %.[17,18] Therefore, based on this parameter, it is not possible to precisely define the position of the oil samples in the diagenetic-catagenetic sequence of processes leading to petroleum formation.

It is known that structural changes of moretane into hopane (17 (H), 21 (H) 17 (H), 21 (H)) lead to changes in the moretane/hopane (C_{30}) ratio from the "initial" 0.80 to even 0.05.[19] However, in addition to heat and geological time the isomerization reactions moretane hopane are influenced by source input and depositional environment as well.[17,20] Hence, in many source rock bitumens and crude oils of high maturity considerably higher values of this ratio were observed (0.10–0.15, and also up to 0.30). This means that the values of this parameter observed for the crude oils investigated do not exclude that the equilibrium = (moretane = hopane) has been established, *i.e.,* they might be the result of "later" stages in the sequence of reactions leading to crude

oil formation. However, they do not serve as an explicit proof for such a statement, since similar to the isomerization reactions 22*R* 22*S*, *i.e.,* to the establishment of the 22*R* = 22*S* equilibrium, the equilibrium = is also established in the earlier stage (vitrinite reflectance R*o* = 0.70 %).[17]

Sterane maturation parameters (parameters 4 and 5, Table V) may contribute to answering the question of the stage in which the Drmno depression crude oils were formed. Almost all the values of these parameters were found to be lower than those quoted in the literature as typical for the corresponding equilibria.[15] Equilibria 20*R* = 20*S* and = (steranes) are established in the stage known as the "oil generation peak" (R*o* = 0.80 % to 0.90 %).[17] The values observed in this paper indicate that the examined crude oils had not reached this phase. Hence, based on the maturation parameters 2–5 (Table V), the Drmno depression crude oils seem to have been formed in earlier phases of the diagenetic-catagenetic sequence of the petroleum formation processes, *i.e.,* those corresponding to vitrinite reflectances between R*o* = 0.70 % (terpanes' equilibria) and R*o* = 0.80 % (initial stages of sterane equilibria).

Maturation parameters 3 and 5 from Table V might also contribute to an indication of the age of the source rocks of the investigated oils. Namely, it was shown earlier that the isomerization reactions moretane hopane (parameter 3, Table V) and 20*R* 20*S* (parameter 5, Table V), in addition to heat, necessarily depended on geological time as well.[21] Investigations of a great number of crude oil samples have shown that samples originating from source rocks of the pre-Tertiary age had moretane/hopane parameter values lower than 0.10, and those of parameter 20*S*/20*S*+20*R* C_{29} steranes higher than 0.50. Parameters 3 and 5 from Table V, compared to boundary values, classified the examined Drmno depression crude oils into the group of oils originating from source rocks of Tertiary age.

Based on all observed group and specific correlation parameters (Tables II-V), the investigated crude oils from the Drmno depression seem to be relatively similar according to their origin and maturation degrees. Naturally, the similarity was not absolute with every examined parameter, but the most important ones indicated the same or similar precursor biomass for all the investigated samples (API, sulphur, alkanes and $^{13}C_{PDB}$, Table II; CPI and Pr/Phyt, Table III; regular steranes distribution and the presence of oleanane, Table IV), as well as similar maturity degrees, *i.e.*, originating from the same phase of the diagenetic-catagenetic sequence of processes leading to crude oil formation (parameters 2–5, Table V). Moreover, the examined crude oils from the Drmno depression may be supposed to have originated from Tertiary source rocks (parameters 3 and 5, Table V). According to certain parameters ($^{13}C_{PDB}$, Table II; partially Pr/Phyt, Pr/*n*-C_{17}, Phyt/*n*-C_{18}, Table III; regular steranes distribution, Table IV; parameters 1 and 6, Table V), the sample Bra-Malj-10, originating from the Bradarac-Maljurevac locality, differed from the other examined samples. Generally, the crude oils from this locality are characterized by a somewhat lower level of organic geochemical uniformity compared with crude oils from the Sirakovo locality.

Conclusions concerning the organic geochemical similarity of Drmno depression crude oils may be illustrated by comparing the values of the most important source and maturation correlation parameters from Tables IV and V with the corresponding parameters observed for crude oils from the major oil fields of the Banat and North

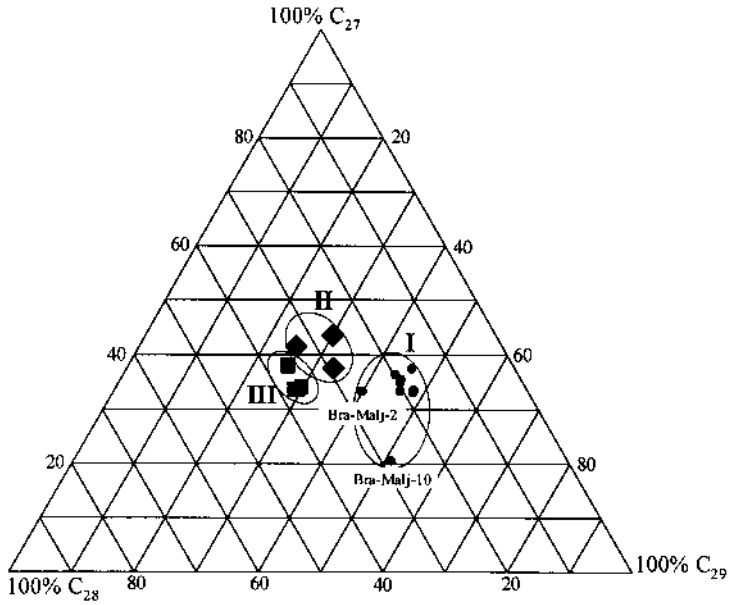

Fig. 2. Distribution of regular C_{27}–C_{29} *R* steranes in the Drmno depression (group I; ●), the Banat and North Bačka depressions' (groups II; ◆), and the West Drava, East Drava, Sava and Slavonija-Srem depressions' (group III; ■) crude oils.

Bačka depressions, as well as crude oils from the West Drava, East Drava, Sava, and Slavonija-Srem depressions.[1,22] According to source correlation parameters (Fig. 2), the investigated crude oils from the Drmno depression obviously differ from other crude oils from the southern parts of the Pannonian Basin. The triangular diagram also demonstrates the remarkable difference of the Bra-Malj-10 sample from the whole group of Drmno depression crude oils, and, to a certain degree, the diversity of the sample Bra-Malj-2 as well, corroborating the general statement concerning the crude oils from the Bradarac-Maljurevac locality and their geological setting. On the other hand, the maturation parameters calculated for the Drmno depression crude oils were similar to those of the Banat and North Bačka depression crude oils, but their maturation degrees were shown to be considerably higher compared to those of the West Drava, East Drava, Sava and Slavonija-Srem depression crude oils.

CONCLUSIONS

Based on source correlation parameters (primarily CPI, Pr/Phyt, distribution of regular steranes), the investigated crude oils from the Drmno depression were once more shown to be of similar origin, characterized by significant participation of terrestrial precursor biomass.

Based on terpane and sterane maturation correlation parameters, the investigated samples were shown to be of relatively low maturity and to have been formed during the earlier stages of the diagenetic-catagenetic sequence of processes leading to petroleum formation, corresponding to vitrinite reflectances of the source rocks between R*o* = 0.70 % (terpanes' equilibria) and R*o* = 0.80 % (initial phases of sterane equilibria).

Terpane and sterane correlation parameters, substantially influenced by geological time in addition to the influence of heat, suggested that the crude oils from the Drmno depression should be classified into the group of oils originating from source rocks of Tertiary age.

In spite of several common characteristics which were clearly observed with all the investigated crude oil samples, ideal organic geochemical uniformity of this group of oils cannot be suggested. Namely, according to some important correlation parameters (carbon isotope composition of the aromatic fraction, abundance of *n*-alkanes, distribution of regular steranes, ratio of some hopane isomers and ratio of diasteranes *vs*. steranes), the sample Bra-Malj-10 was found to be remarkably different from the other investigated crude oil samples. Generally, the crude oils from the Bradarac-Maljurevac locality were characterized by a somewhat lower level of organic geochemical uniformity than the crude oils from the Sirakovo locality.

Finally, based on the distribution of regular steranes, the origin of the Drmno depression crude oils seems to be different from the origin of the Banat and North Bačka depression crude oils, and also from the West Drava, East Drava, Sava and Slavonija-Srem depression crude oils. Consequently, the Drmno depression crude oils may be distinguished as a distinct crude oil genetic type among the crude oils from the southern part of the Pannonian Basin. On the other hand, their maturation parameters were similar to those of the Banat and North Bačka depression crude oils. In contrast, their maturity degrees were shown to be considerably higher compared to those of the West Drava, East Drava, Sava and Slavonija-Srem depression crude oils.

Acknowledgement. We thank the Alexander von Humboldt-Stiftung for supporting this research by giving a fellowship to the first author. We also thank Mrs. Angelika Hanisch and Mr. Michael Hiete (Federal Institute for Geosciences and Natural Resources, Hannover) for technical help with the GC-MSD analyses and the MS isotope analyses. Important help in sampling from Mr. Petar Ašanin and other colleagues from NIS-Jugopetrol, Belgrade, is greatly appreciated. This work was supported in part by the Research Fund of the Republic of Serbia.

И З В О Д

ОРГАНСКО-ГЕОХЕМИЈСКА КОРЕЛАЦИЈА НЕКИХ НАФТИ ДЕПРЕСИЈЕ ДРМНО (ЈУЖНИ ДЕО ПАНОНСКОГ БАСЕНА, ЈУГОСЛАВИЈА)

БРАНИМИР ЈОВАНЧИЋЕВИЋ[1,2], HERMANN WEHNER[3], GEORGE SCHEEDER[3], ДРАГАНА ПЛЕЋАШ[1], МАРКО ЕРЦЕГОВАЦ[4] и ДРАГОМИР ВИТОРОВИЋ[2]

[1]*Хемијски факултет, Универзитет у Београду, п. пр. 158, Београд,* [2]*Центар за хемију ИХТМ, Београд,* [3]*Federal Institute for Geosciences and Natural Resources, P.O. Box 510153, Hannover, Germany и* [4]*Рударско-геолошки факултет, Универзитет у Београду, Београд*

У овом раду испитивани су узорци сирових нафти депресије Дрмно (Костолац) са локалитета Сираково и Брадарац-Маљуревац. Циљ рада био је да се процени органско-геохемијска уједначеност нафти нафтних поља депресије Дрмно. Изабрани су узорци који потичу из резервоарских стена са различитих дубина и у њима су одређени групни и специфични изворни и матурациони органско-геохемијски параметри. Потврђено је да испитивани узорци депресије Дрмно имају слично порекло које карактерише већи удео терестријалне прекурсорске биомасе. Испитиване нафте су нешто нижег

степена матурисаности и настале су у ранијим фазама дијагенетско-катагенетске секвенције формирања нафте којима одговарају вредности рефлексије витринита између R*o* = 0,70 % и R*o* = 0,80 %. Највероватиније су настале у изворним стенама терцијарне старости. Нафте са локалитета Брадарац-Маљуревац карактерише нешто нижи ниво органско-геохемијске хомогености него нафте са локалитета Сираково.

(Примљено 8. јануара 2001)

REFERENCES

1. M.Šaban, B. Jovančićević, S. Saračević, A. Hollerbach, D. Vitorović, *Org. Geochem.* **13** (1988) 325
2. M. Šaban, B. S. Jovančićević, T. Glumičić, N. Dogović, *Rapid Communications in Mass Spectrometry* **4** (1990) 505
3. B. Jovančićević, M. Šaban, T. Glumičić, E. Faber, D. Vitorović, *J. Serb. Chem. Soc.* **57** (1992) 391
4. B. Jovančićević, P. Polić, D. Vitorović, *J. Serb. Chem. Soc.* **63** (1998) 397
5. M. Ercegovac, A. Grubić, I. Djoković, B. Kuzeljević, M. Marović, D. Vitorović, M. Branković, S. Grkavac, A. Kostić, B. Prstojević, *Ann. Géol. Péninsule Balkanique* **57** (1993) 375
6. M. Ercegovac, A. Kostić, *J. Serb. Chem. Soc.* **61** (1996) 1063
7. M. Šaban, B. S. Jovančićević, T. Glumičić, S. Saračević, *Org. Geochem.* **16** (1990) 477
8. B. P. Tissot, D. H. Welte, *Petroleum Formation and Occurrence*, 2nd Ed., Springer-Verlag, Heidelberg 1984
9. D. Waples, *Geochemistry in Petroleum Exploration*, International Human Resources Development Corporation, Boston 1985
10. M. Schoell, *Org. Geochem.* **6** (1984) 645
11. W. K. Seifert, M. J. Moldowan, G. J. Demaison, *Org. Geochem.* **6** (1984) 633
12. Z. Sofer, J. E. Zumberge, L. Victor, *Org. Geochem.* **10** (1985) 377
13. J. K. Volkman, R. Alexander, R. I. Kagi, G. W. Woodhouse, *Geochim. Cosmochim. Acta* **47** (1983) 785
14. M. R. Mello, P. C. Gaglianone, S. C. Brassel, J. R. Maxwell, *Mar. Pet. Geol.* **3** (1988) 205
15. W. K. Seifert, J. M. Moldowan, *Geochim. Cosmochim. Acta* **45** (1981) 783
16. I. Rubinstein, O. Sieskind, P. Albrecht, *J. Chem. Soc., Perkin Trans. 1*(1975) 1833
17. K. E. Peters, J. M. Moldowan, *The Biomarker Guide, Interpreting Molecular Fossils in Petroleum and Ancient Sediments,* Prentice Hall, New Jersey 1993
18. W. K. Seifert, J. M. Moldowan, *Meth. Geochem. Geophys.* **24** (1986) 261
19. A. S. Mackenzie, R. L. Patience, J. R. Maxwell, M. Vandenbroucke, B. Durand, *Geochim. Cosmochim. Acta* **44** (1980) 1709
20. J. Rullkötter, R. Marzi, *Org. Geochem.* **13** (1988) 639
21. P. J. Grantham, *Org. Geochem.* **9** (1986) 293
22. A. Alajbeg, V. Britvić, S. Švel-Cerovečki, C. Cornford, A. Todorović, J. Rajković, G. Barić, A. Putniković, *Org. Geochem.* **16** (1990) 339.

J.Serb.Chem.Soc. 66(5)309–322(2001)
JSCS–2858

UDC 668.814.1
Original scientific paper

Photolysis of incorporated benzophenone derivatives inside compressed lipid monolayers

DEJAN Z. MARKOVIĆ

Faculty of Technology, YU-16000 Leskovac, Yugoslavia

(Received 4 July 2000)

The goal of this work was to study the possibility of the occurrence of radical-type lipid peroxidation of the lipid constituents on biomembranes, in compressed monolayers, having lipoidal benzophenone photosensitizers incorporated. The triplets of the photosensitizer abstract allylic and doubly-allylic hydrogen atoms from anti-conjugated moities of the lipid molecules. The results simultaneously confirmed the occurrence of H-abstraction (and so the initiation of the peroxidizing chain mechanism), and the absence of the formation of lipid peroxides. The reason lies in "cage effect": the highly restricted spacial area of compressed lipid monolayers limits the mobility of the created radicals (lipid radicals and ketyl radicals) and leads to their recombination, thus preventing the propagation step of the chain mechanism. With certain reservations it may be concluded that these results have a clear implication on real biomembranes: the structure of which is one of the main factors preventing the spread of the chain reaction, and the formation of lipid peroxides.

Keywords: free radicals, lipid peroxidation, photosensitizers, benzophenone, monolayers.

INTRODUCTION

Due to the enormous importance of biomembranes for the functioning of cells and tissues, lipid peroxidation studies have always attracted a lot of attention. According to a broader definition, the phenomenon of lipid peroxidation implies the oxidative destruction of polyunsaturated lipids,[1] which as a consequence leads to the production of numerous pathological effects. The primary consequences include lipo-protein and protein-protein crosslinking,[2] which may cause changes in the structure of enzymes and their activities.[3] The more specific consequences include: damage on subcellular organelles (such as the swelling of mitochondria; fast ribosomes leaking from the endoplasmtic reticulum; hemolysis of erythrocites), inhibition of proteins synthesis by peroxidation nus-products (such as malonaldehyde), and the inhibition of DNA and RNA synthesis in the liver and lungs, as a result of acrolein action.[4] On a macro-level, lipid peroxidation effects are included in number of widely spread diseases, from ath-

erosclerosis[5] to carcinogenesis.[6] Moreover, lipid peroxidation has been seen as "a common pathogenetic mechanism".[7]

Lipid peroxidation can be initiated photolitically through two different mechanisms. A photosensitizer in its excited state may transfer energy to ground state oxygen to produce reactive singlet oxygen ($^1O_2$), which in turn attacks lipids to generate peroxide species *via* a non-radical pathway (Type II). Alternatively, direct reaction between a photosensitizer and lipid may occur to generate reactive lipid free radicals (Type I).[8,9] The presence of polyunsaturated hydrophobic moieties in lipid constituents of biological membranes renders them particularly vulnerable to peroxidative degradation.[9] This vulnerability may be ascribed largely to the presence of double bonds in the hydrocarbon moieties, and the adjacent allylic and doubly-allylic sites from which hydrogen abstraction may be facilitated[10,11] (Fig. 1). While unsaturated sites may be directly attacked by singlet oxygen to produce lipid peroxides (Type II), more extensive damage occurs *via* the free-radical mechanism (Type I). The extent of such chain degradation depends on the concentration, packing and other parameters of the lipid environment.

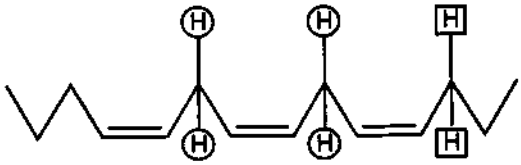

Fig. 1. Doubly-allylic (circled) and allylic (squared) hydrogen atoms in a typical anticonjugated structure of lipid hydrophobic moieties.

The Type II sensitized-reaction has been very widely studied and is relatively well understood. On the other hand, kinetic data of the radical-chain mechanism (Type I) are to a large extent absent.

While the chain peroxidation effects have been studied extensively *via* autooxidation,[12] quantitative characterization of the degradation requires *controlled* initiation of H-abstraction from the allylic and doubly-allylic sites. Several radiation chemical studies carried out using $^{\cdot}OH$ or $O^{2-\cdot}$ radicals as the H-abstraction agents suffered from non-selectivity as to the site of attack in the complex environments.[13–15] On the other hand, the use of benzophenone (BZP), already well known as a very efficient initiator of polymerization processes in which it reacts as a typical Type I photosensitizer,[16,17] permits very selective abstraction from allylic and doubly-allylic sites by its triplet excited state (^{3}BZP)[18] and so appeared to be a promising approach for further quantitative chain peroxidation studies.

There are two possible approaches to the study of the mechanisms of photosensitized peroxidation in biological membranes. The first one implies conducting experiments *in vivo*. The large number of related variables appears to be a very limiting factor for such approach. The second one includes experiments on membrane models, with increasing degree of molecular organization (micelles, compressed monolayers, vesicles), providing better control of the chain process inside. The latter approach was used in our previous studies.[18–20] The choice of benzophenone as the sensitizer is based on the well known organic photochemistry reaction, H-abstraction by longer-lived triplet

states of aromatic ketones.[21] To obtain basic data, significantly lacking, of the influence of the surrounding molecular organization, a series of BZP interactions with unsaturated lipoidal fatty acids was performed in benzene solution.[18] Then the same reaction was studied in micelles of sodium dodecyl sulphate (SDS),[20] and linoleic acid (LA)[19] to observe the influence of structure and molecular organization, by comparing the two sets of kinetic data from the two media. This report is a step forward, since it describes BZP-sensitized peroxidation in compressed lipid monolayers at the air-water interface, representing a more organized medium, even more imitative and similar to real biomembranes.

MATERIALS AND METHODS

Synthesis of benzophenone derivatives

Benzophenone-4-heptyl-4-undecanoic acid (BHUA) was synthesized according to the procedure described in a former report.[20] The second BZP-derivative, diphenyl-1-*o*-hexadecyl-2-*o*-(benzophenone-4-heptyl-4'-pentanoil)-*sn*-glycero-3-phosphate (DBP), was synthesized using a procedure described for the synthesis of very similar compounds.[22,23] The structures of BZP, BHUA and DBP are shown in Fig. 2.

The lipid used to create the monolayers, 1,2-dilinoleoyl-phosphatidyl-choline (1,2-DLPC) was purchased from Avanty Polar Lipids (Birmingham, AL).

Photolysis experiments on monolayers

The photolysis experiments on the lipid monolayers with incorporated BZP-derivatives as photosensitizers were performed using a specially constructed, self-made experimental set-up.

A teflon trough 15 cm 54 cm 3 mm (depth) was filled with water. An immovable rod was fixed parallel to the longer edge of the trough. The rod served as a support for two parallel teflon barriers 2–2.5 mm immersed in the water subphase. The two barriers, parallel to the shorter edge of the trough, glide along the rode and, on approaching each other, compress the lipid monolayer already created on the water surface. The compression speed of the monolayers, in the range of 0.016– 1.6 cm/min, was controlled by a four-phase Airpax stepper motor model K82954-MS (North American Phillips Controls Corp.). To prevent heating during operation the motor was cooled by water flowing through a copper tubing coiled around its cylindrical surface. A little box with the scales of a Cahn 2000 Electrobalance was fixed at the top of the experimental set-up. On the left arm of the scales, a nichrome wire was attached, with a 0.95 cm square filter paper plate at the end. The paper plate was immersed 1–2 mm into the water subphase, straight into the center of the trough. It served to register the changes in the surface pressure resulting from the monolayer compression. The right arm was fixed to the Cahn Electrobalance which transforms the stretching of the balance arms (caused by the surface pressure changes) into millivolts, mV. A calibration was performed prior to the experiments. The electrobalance is connected to a Hewlett Packard chart recorder, model 745A.

After creation of the lipid (1,2-DLPC) monolayer and the start of the compression, the surface pressure changes were registered on a chart. In this manner typical - isotherms were recorded, with the Y-axis ( ) giving the values of the surface pressure in mN/m, and the X-axis ( ) expressing the values of the molecular packing in $(Å)^2$/molecule. The values were easily calculated, knowing the exact valume and the concentration of the 1,2-DLPC solution (used for the monolayer creation), as well as the trough dimensions.

The monolayers samples were mixtures of the lipid (1,2-DLPC) and the photosensitizer (BHUA, DBP). The lipid/sensitizer ratios used in the experiments were 4:1 and 6:1. Usually, aliquots of 5 – 50 10^{-6} dm^{-3} were used with an approximate total (lipid + sensitizer) concentration of 1.5 mmol dm^{-3}.

Low pressure filament mercury lamps (manufactured by the Southern New England Ultraviolet Co., Hamden, CONN.) with phosphor coatings were used in the photolysis experiments. The lamps were packed into two separated sets, fixed about 15 cm above the water on a solid adjustable rack bearer. Each lamp housing contained 10 individually water-jacketed lamps, spaced 3.7 cm apart and in a position spanning beyond the entire monolayer area (each set covering approximately half of the area). To prevent the lamps heating (which can destroy the film), distilled water was circulated *via* tygon tubing coiled around the lamps. This provided an internal temperature control of °C. Before the photolysis experiments, the lamps were turned on and thermostated for about 10 min. The emission, directed towards the film, was blocked until the start of the experiments.

Since measurement of surface pressure is highly temperature dependent,[24,25] the entire trough and the lamp apparaturs was placed on a solid rectangular block haused inside a 92 cm 69 cm 61 cm plexiglass glove box. Since some experiments needed a particular atmosphere inside the plexiglass box (N_2, O_2, air), gas channels for the box interior were provided.

Post-photolysis procedure

At the end of the photolysis, the monolayers were aspirated by Pasteur pipette using a strong vacuum, into an especially designated cylindrical flask. A few cm^3 of the water phase was usually aspirated too, despite the efforts to dimenish the quantity. The collected water phase was then evaporated under vacuum in a small round-bottom flask. 1 cm^3 of CH_3CN was then added to dissolve the post-photolytical monolayer products. The solution was then analyzed by HPLC. The water subphase was also analyzed by this procedure periodically, to detect an eventual (undesirable) presence of post-photolytical monolayer products. About 30 % of the post-photolytical monolayer products were lost during the procedure from aspiration to HPLC analysis (estimated by a standard comparative method).

HPLC detection

A -bondapak C-18 column 8 mm 10 cm (especially designed to work under high pressures) and a 90 % aq. MeOH as the mobile phase were used for HPLC analysis (Waters Associates, Milford, MA) of the postphotolytical monolayer products, by analogy with report of Crawford and coworkers.[26] The total concentration was in the 10^{-5} mol dm^{-3} range. The peroxides were detected at 234 nm, at the maximal absorption ($A_{max.}$) of the created dienes structures.[27] The photosensitizers were detected in the 250–270 nm range.

RESULTS AND DISCUSSION

The triplet benzophenone chromophore, ^{3}BZP, reacts with olefinic structures *via* two competing mechanisms[28]:

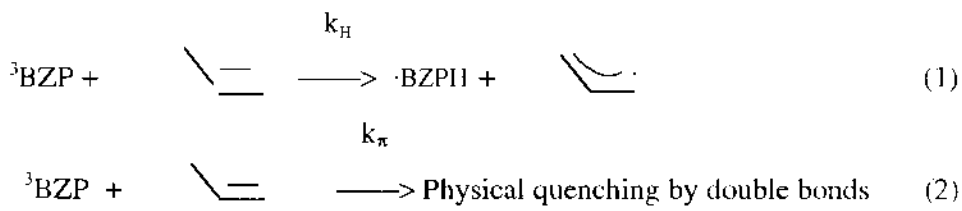

The first mechanism represents H-abstraction of the allylic, $H_{all.}$, and doubly allylic, $H_{dbl.all.}$, hydrogen atoms by ^{3}BZP with the consequential formation of two radicals: BZP ketyl-radical (·BZPH), and the lipid radical ( ). According to the second mechanism (2), BZP does not diminish as a chemical species (as it does by the first

mechanism): its triplet being physically quenched by the olefinic double bonds. Eventually, additional mechanisms are also included, depending on the employed medium: BZP interaction with solvent molecules in homogeneous solution,[29] the recombination of the created radical pairs in micelles.[30]

In an earlier report,[18] the fraction of the quenching events leading to ketyl-radical (·BZPH) generation, F_k, by H-abstraction from a series of olefinic compounds with increasing number of double bonds (unsaturated fatty acids and the two triglycerides): $k_H = F_k \quad k_r$, was calculated. k_H is the rate constant for H-abstraction, and k_r is the rate constant for the overall reactivity of ^{3}BZP toward the olefinic compounds. The calculated F_k values ranged from 0.36 (oleic acid) to 0.85 (arachidonic acid). If was very important to obtain these basic data, since only the related mechanism (1) – lipid radicals creation – is of relevance for the chain peroxidizing mechanism. In an other paper,[19] the behaviour of the created radical pairs (BZPH – lipid radicals) was studied in a very stericially restricted medium that mimics more closely real biomembranes. The use of BZP and its synthesized derivative, benzophenone-4-heptyl-4'-pentanoic acid (BHPA), as the photosensitizers in linoleic acid micelles (where LA plays the role of the lipid and of the medium simultaneously) resulted in F_k values of 0.41 (BZP) and 0.58 (BHPA). The somewhat higher F_k value found for BHPA was explained by the better alignment of the BZP-chromophore towards the main potential targets (H_{all} and $H_{dbl.all}$ atoms) caused by the better incorporation of the BHPA hydrophobic "tail". Furthermore, the study of BZP and BHPA interaction with LA in sodium dodecyl sulphate (SDS) micelles suggested a crucial role of the micellar "cage" in controlling the behaviour of the created radical pairs. They mostly undergo recombination inside the "cage", and only a small fraction (7–14 %) escapes to the surrounding aqueous phase.[20] These escaped lipid radicals are the only ones relevant for the peroxidation process, since they undergo the propagation step in the presence of O_2. The very small fraction (calculated in relation to initial number of radicals) suggested the significance of the "cage effect" on the efficiency of the whole process, and needed further supporting evidence. For this reason, a photolysis study using compressed lipid monolayers (with photosensitizers incorporated inside) emerged as a logical continuation of the previous work, since the molecular organization is even more spatially restricted and comparable to real biomembranes.

For these studies, 1,2-dilinoleoyl phosphatidylcholine (1,2-DLPC) was used as the lipid substrate spread in a monolayer at the air-water interface. The two choosen BZP-sensitizers were benzophenone-4-heptyl-4'-undecanoic acid (BHUA), and diphenyl-1-*o*-hexadecyl-2-*o*-(benzophenone-4-heptyl-4'-pentanoil)-*sn*-glycero-3-phosphate (DBP). The choice of the lipid and the sensitizers was not accidental. 1,2-DLPC is naturally present in certain types of biomembranes. The two double bonds located in the two hydrophobic "branches" (the two LA chromophores) should permit high reactivity with the incorporated photosensitizers, primarily by H-abstraction. On the other hand, BHUA and especially DBP (which is a lipoidal benzophenone – Fig. 2) should permit a more suitable incorporation inside the 1,2-DLPC monolayer, and the best possible alignment of the BZP-chromophore towards the main H-abstraction targets: the two doubly-allylic and 4 allylic H-atoms. The as-

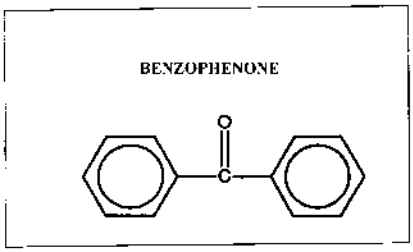

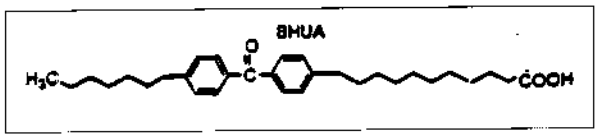

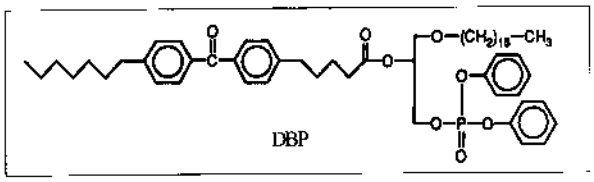

Fig. 2. Structure of benzophenone (top), as well as its synthesized derivatives: BHUA (middle), with hydrocarbon "tails", and DBP (bottom), representing actually a lipid with an incorporated benzophenone chromophore.

sumed optimal position of the BZP-chromophore inside the compressed 1,2-DLPC monolayer is shown in Fig. 3.

The idea of incorporating a sensitized chormophore into a lipid ("lipoidal chromophore") used for monolayers studies has already been exploited. Bohorquez and Patterson[31] used lipoidal pyrene for the study of monolayers by following the excimer fluorescence of the probe. Or, more recently and more relevant to this report, Maziere and coworkers[32] used diphenylhexatriene (DPH)-labeled lipids as a potential tool for studying lipid peroxidation in monolayer films; DPH was previously known as a fluorescent probe for monitoring lipoprotein peroxidation.[33] However, whereas DPH fluorescence served as a probe to follow lipid peroxidation started by another agent,[32] DBP used in this report itself initiates the peroxidation process.

However, before starting the photolysis experiments on the monolayers, it was necessary to consider "the blank" in solution: LA was used as the lipid substrate in solution and micelles,[18-20] not 1,2-DLPC itself. LA and 1,2-DLPC are not significantly different (1,2-DLPCmay be represented as two LA "branches" plus a polar phosphate head – Fig. 3). Still, the presence of the polar head (totally irrelevant for the peroxidation process) might cause (especially in the monolayer "cage") additional steric re-

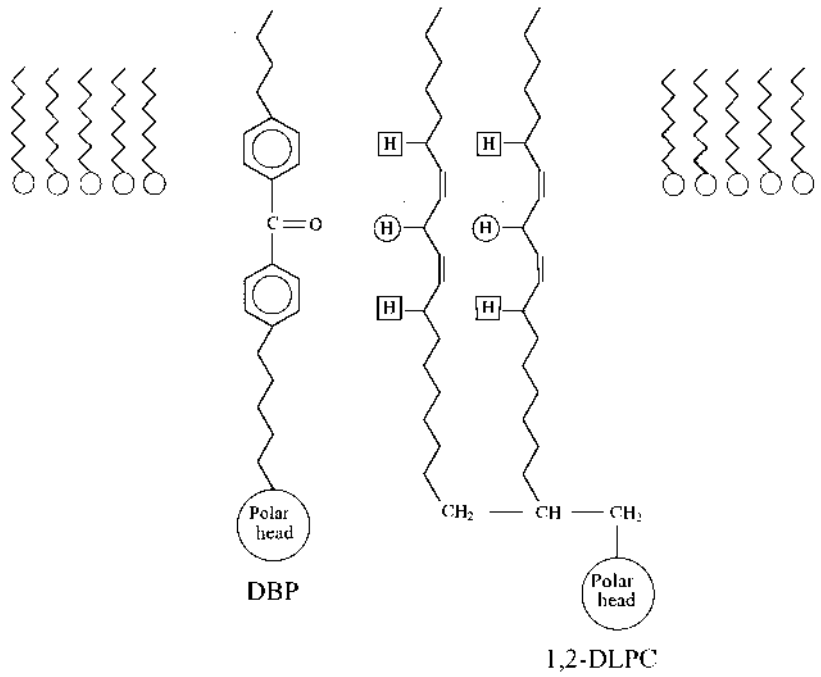

Fig. 3. The anticipated optimal position of the carbonyl chromophore of the benzophenone derivatives (BHUA and DBP) in compressed 1,2-DLPC monolayers, towards the main potential H-abstraction targets: allylic(squared) and doubly-allylic (circle) H-atoms.

strictions for the initiation of the process. The 1,2-DLPC peroxidation with BHUA as the sensitizer was performed in benzene with continuous photolysis. The result is shown in Fig. 4. The left part of the picture represents the HPLC chromatogram before photolysis (the photosensitizer peak only). The right part represents the HPLC chromatogram after two minutes of UV-irradiation: two peroxides peaks, and the photosensitizer peak in the middle can be seen, with the same absorption scale (to make comparison easier). The two peroxides peaks probably indicate incomplete peroxidation, otherwise only one peak is to be expected. The yield of BHUA photolysis has been calculated, based on chromatograms obtained for several irradiation periods. The calculated value of 0.1 is about 5 times smaller compared to the F_k value for the BZP-LA reaction in benzene. The difference is expected and can be attributed not only to the differences between the sensitizers (BZP and BHUA) and the substrates (LA and 1,2-DLPC), but to the presence of oxygen too: oxygen was depleted in the first (BZP + LA) case, but it is essential in the second (BHUA + 1,2-DLPC) for the production of peroxides. The rate constant for ^{3}BZP quenching with O_2 is very high, 2.3 ^{9} dm^3 mol^{-1} s^{-1},[34] and this is the main reason for the very low BHUA photolysis (*i.e.,* H-abstraction) yield. The choice of the UV-lamps with insignificant emission under 300 nm (A_{max} 350 nm – not shown) assured the prevention of the destruction of the formed peroxides, with A_{max} at 234 nm.[27] The same lamps were used in the monolayer photolysis experiments.

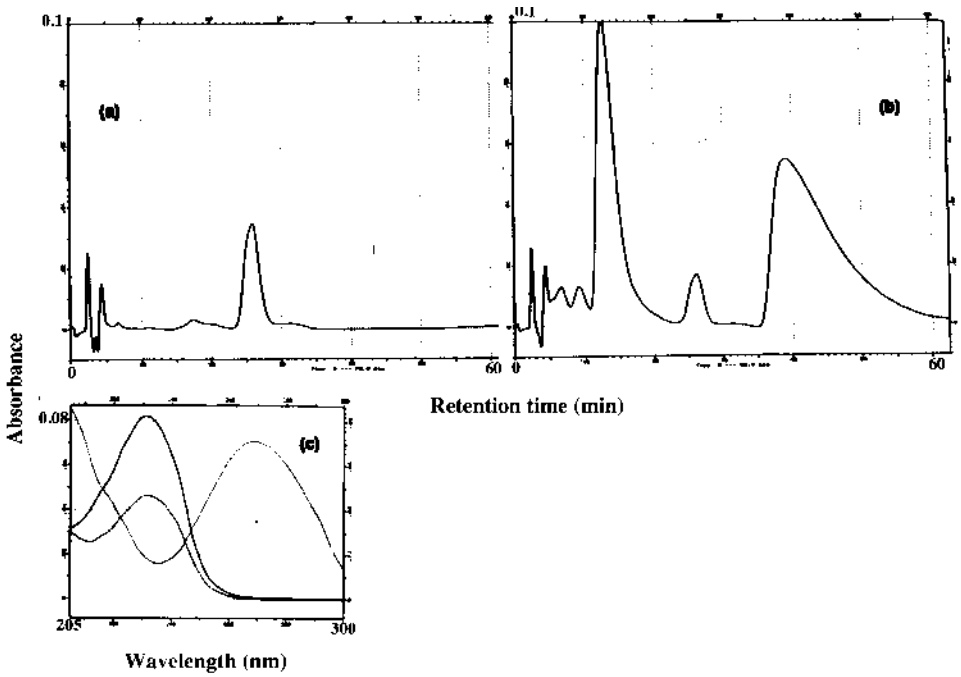

Fig. 4. (a) HPLC chromatogram, representing 1.26 mmol dm^{-3} 1,2-DLPC with 0.1 mmol dm^{-3} BHUA in benzene, before photolysis; (b) HPLC chromatogram of the same material, after two minutes of UV-irradiation, at the same absorption scale (for easier comparison); (c) Spectra of the separated compounds: (———) and (--------), 1,2-DLPC peroxides; (……..), BHUA.

Since the photosensitized peroxidation of 1,2-DLPC with BHUA is evidently possible (Fig. 4), the implication of the possibility of its occurrence in the compressed monolayers must be considered next: if the 1,2-DLPC peroxides do not appear in the HPLC chromatogram (under the same separation and detection conditions as those in Fig. 4) the reason could be, (1) in the prevention or at least significant suppression of initiation caused by steric limitations in the compressed monolayer "cage", or, (2) in the recombination of the formed radical pairs due to the "cage effect", logically expected to be even more pronounced, compared to SDS and LA micelles.

The photolysis experiments were performed with lipid (1,2-DLPC)/photosensitizers (BHUA, DBP) ratios of 4:1 and 6:1, over a broad range of surface ( ) pressures (5–30 *m*N/m), and for various irradiation periods (1–10 min). The ratios were not accidentally choosen. With the two ratios, the monolayers demonstrated complete stability before irradiation over the whole -range. This was necessary as a "blank" to be able to attribute the appearance of eventual (photolitically induced) changes to the lipid-sensitizer reaction itself, and to exclude any other factors. Furthermore, the relationships (4:1 and 6:1) prevented triplet self-quenching (or "fusion"), already detected in solution,[35] and so reasonably expected in the compressed monolayer "cages". The experiments were performed in a N_2 atmosphere (when the initiation step was in particular to be studied), and in O_2 or air atmosphere (when the accent was on the observance of eventual formation of lipid peroxides).

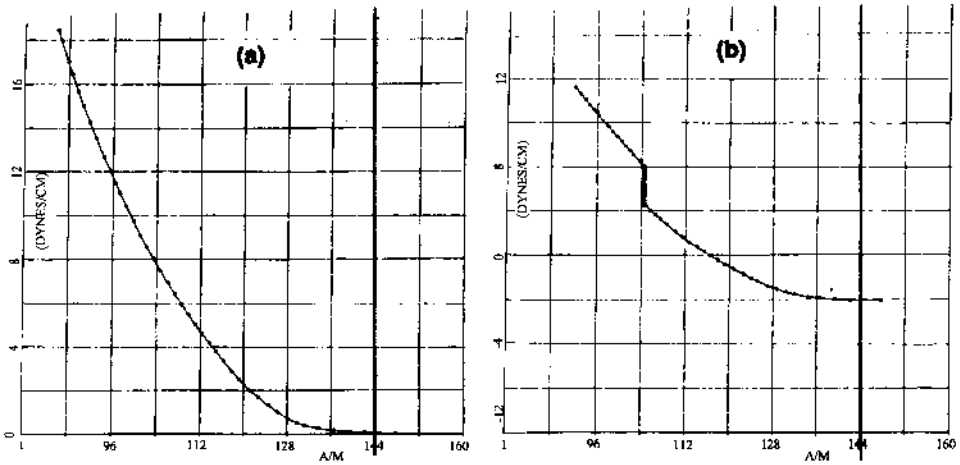

Fig. 5. isotherm of a (1,2-DLPC + BHUA, 4:1) monolayer, (a) before, and (b) after 10 min photolysis. The compressing teflon barriers were in a fixed position (*i.e.,* constant -value) during the photolysis. The -values (y-axes) are expressed in *m*N/m, and the -values (x-axes) show square angstroms, $(Å)^2$, per molecule.

Indirect evidence for the (lipid/sensitizer) reaction is obtained from Fig. 5, which shows isotherms of a (1,2-DLPC + BHUA, 4:1) monolayers, (a) before, and (b) after photolysis for 10 min. The isotherm itself has a shape typical for olefinic compounds, where the presence of double bonds prevents sharp (phase) changes during monolayer compression. A simple visual comparison of the isotherms given in Fig. 5(a,b) shows an increase of the surface pressure during the photolysis, performed at a constant value (the compressing teflon barriers were in a fixed position). However, more solid evidence for the occurrence of the lipid / sensitizer reaction is given in Fig. 6, which shows the decrease of the BHUA concentration in a (1,2-DLPC + BHUA, 6:1) monolayer during photolysis. The BHUA photolysis yield, calculated on the basis of an actinometer,[19] was 0.59, which is very close to the F_k value for BZP-LA interaction in benzene.[18] This is reliable evidence for ^{3}BHUA H-abstraction from 1,2-DLPC, since there are *no* other types of interaction between BHUA and 1,2-DLPC in the monolayers (and in a general sense) which would diminish the BHUA concentration (Fig. 6), *i.e.,* which would lead to its disappearance as a chemical species. Physical quenching by the 1,2-DLPC double bonds *does not* transform ^{3}BHUA into the corresponding ketyl-radical.

So, not surprisingly, the HPLC chromatogram recorded after photolysis (not shown) *did not show* traces of 1,2-DLPC peroxides. This was to be expected, based on results obtained in LA and SDS micelles.[19,20] The effect of radical pairs recombination is even more pronouced in the "cage" of the 1,2-DLPC compressed monolayer: the "escape event" is even less probable. Certainly, this last statement does not exclude, in an absolute sense, the possibility of lipid peroxide production in the investigated monolayers.

Certainly, it must not be forgotten that the detection of peroxides is limited by the HPLC conditions established for the "blank" (BHUA plus 1,2-DLPC, in benzene). So,

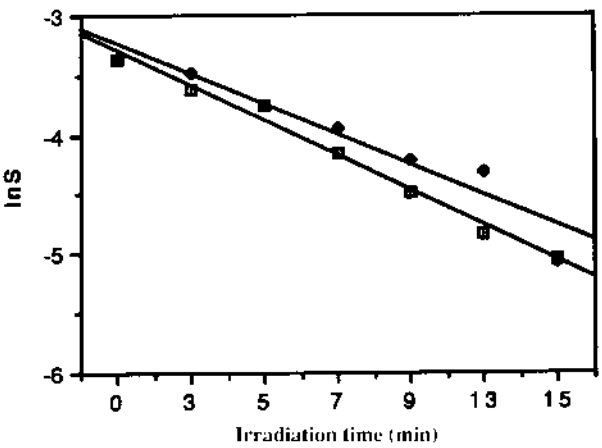

Fig. 6. Kinetics of BHUA reduction in a (1,2-DLPC + BHUA, 6:1) monolayers. The opened squares indicate the actinometer (BHUA in EtOH); S – HPLC integrated area of the BHUA peaks at 270 nm.

a limited peroxides production cannot be excluded as a possibility. To quantitatively establish the HPLC detection limit, the following procedure was employed. 1,2-DLPC peroxides were sythesized in benzene with BHUA, as for the "blank". After evaporation of benzene, $CHCl_3$ was added, and the peroxides concentration adjusted to be 1.3 mmol dm^{-3} (the concentration used for the formation of the monolayers). Aliquots of this solution, in the 5–50 10^{-3} cm^3 range, were spread over the water, thus forming surface, a set of monolayers containing known concentrations of peroxides. Then the post-photolytical procedure (described in the Materials and Methods) was applied. This time 1,2-DLPC peroxides *were detected* by HPLC. The chromatograms (not shown) contained only one peak, with a retention time close to the first peak in the chromatogram shown in Fig. 4.

The integrated peaks areas were used as the X-axis values. The second (Y-axis) set of data came from the same (5–50 10^{-3} cm^3) aliquots. The $CHCl_3$ was evaporated and the peroxides were then dissolved in 1 cm^3 CH_3CN (the same amount of the same solvent as was used for the final dissolution of the post- photolytical monolayer material - see the procedure in Materials and Methods). The samples absorbances were then measured on a UV-VIS spectrophotometer at 234 nm (the A_{max} value) to get the Y-axis values (it must be emphasized that at this wavelength the measured values reflect mostly the absorbance of the peroxides, and the absorbance of the unoxidized 1,2-DLPC molecules contributing only to a negligible amount).

The calibration plot is given in Fig. 7. From the smallest, but still detectable peak on the HPLC chromatogram (the lower detection limit), and the integrated area value, the corresponding absorbance was determined, and the concentration of the 1,2-DLPC peroxides calculated. This value was then expressed in %, calculated on the basis of the known concentration of the unoxidized 1,2-DLPC. The final result of 1–3 % defines the detection limit. If the post-photolytical peroxides concentration does not exceed 1–3 % of the total lipid (1,2-DLPC) monolayer material, they *will not be detected* under the given HPLC conditions. This small percentage value is very strong evidence in support of the

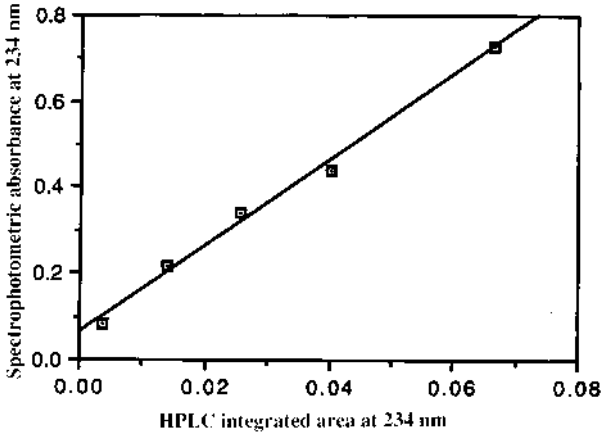

Fig. 7. Calibration diagram to determine the minimum detectable 1,2-DLPC peroxides concentration under the chosen HPLC conditions.

basic conclusion concerning the importance of the influence of the "cage" effect on the inhibition of the peroxidation process. It is reasonable to further conclude that the percentage of the photolitically induced 1,2-DLPC peroxides in the monolayers is probably less than 1 %: the presence of 1–3 % lipid peroxides in freshly isolated or synthesized unoxidized lipid material is considered normal, due to autooxidation.

Finally, additional proof in support of the absence of a significant extent of peroxidation in compressed lipid monolayers came from experiments performed at constant -pressures. This time the photolitically induced change was expressed in

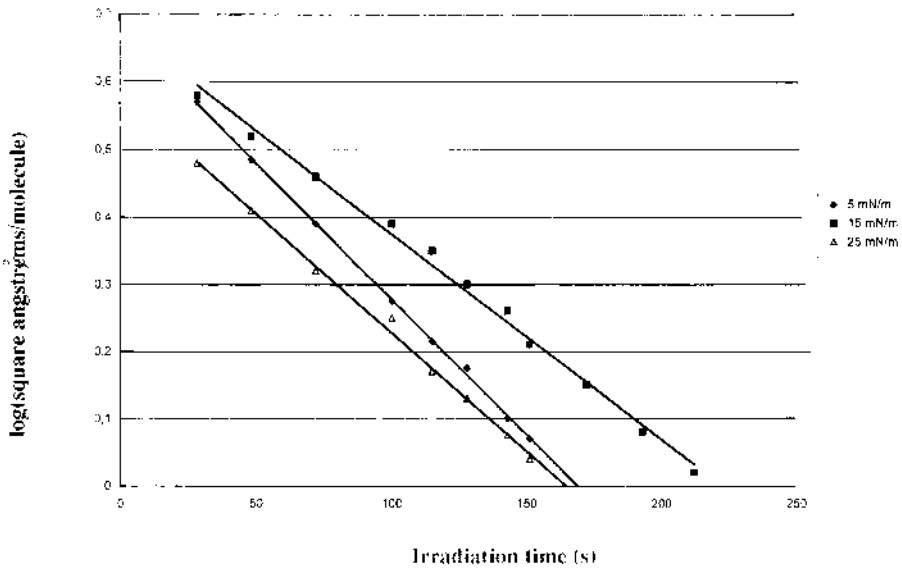

Fig. 8. Plots of temporal changes of molecular packing in (1,2-DLPC + DBP, 6:1) monolayers during photolysis (expressed in square angstroms per molecule), performed at various surface pressures.

terms of the number of square angstroms (Å)^2 per molecule. The calculation of these values was based on the knowledge of all the necessary data: the area encompassed by the compressing teflon barriers, the concentrations as well as the volumes of the aliquots used for the formation of the monolayers. The log plots representing temporal changes in the molecular packing of the (1,2-DLPC + DBP, 6:1) monolayers during photolysis are shown in Fig. 8, for three different -pressures.

Two clear facts may be seen from the plots. First, the ^{3}DBP –1,2-DLPC reaction is of pseudo-first order, reflecting the significantly smaller concentration of *triplet* sensitizer, compared to the lipid concentration: the reaction rate is dependent on the dynamics of the disappearance of the triplets only. Second, the calculated anti-log values (derived from the Y-axis in Fig. 8), giving the range of the molecular packing change during photolysis, do not exceed 5 (Å)^2/molecule, for all the experimental -pressures (5, 10, 15, 20, and 25 *m*N/m). For the lipid/senzitizer ratio of 6:1 used in the experiments, the maximum range change was about 30 (Å)^2/molecule. This last number is clear and additional proof of the absence of significant peroxidation in 1,2-DLPC compressed monolayers. Otherwise, the number would be much higher.

CONCLUSIONS

1. Production of peroxides in monolayers of 1,2-DLPC with the incorporated lipoidal photosensitizers was not detected up to 1–3 %, based on the total amount of lipid used for the formation of the monolayers. The result was obtained from experiments performed at different surface pressures. The reason is not because the photochemical reaction inside the monolayers does not occur; a clear decrease of the photosensitizer concentration with increasing irradiation time was found. Hence, H-abstraction inside the 1,2-DLPC monolayers (by ^{3}BHUA and ^{3}DBP) certainly occurs, but 1,2-DLPC peroxides were not formed because the radical pairs predominantly recombine inside the "cage" of compressed monolayers, in which their mobility is extremely limited. Additional proof for this statement lies in the proportionally small change of square angstroms per molecule in the investigated monolayers. The change would certainly be bigger if the lipid peroxidation chain reaction occurred to a significant extent.

2. Although compressed monolayers are only artificial models for biomembranes, the basic conclusion concerning the possibility of the occurrence of lipid peroxidation inside monolayers can be applied to biomembranes, with certain reservations. At least one of the factors which prevents the propagation of the lipid peroxidation chain mechanism inside biomembranes is their structure. It clearly appears that biomembranes, in the case of radical pair events, have some kind of self-protection mechanism on at least one part of the total peroxidation content. Certainly, this does not exclude the action of other factors preventing propagation of the chain mechanism (such as anitoxidants).

ABBREVIATIONS

BZP – benzophenone

BHUA – benzophenone-4-heptyl-4'-undecanoic acid

DBP – diphenyl-1-*o*-hexadecyl-2-*o*-(benzophenone-4-heptyl-4'-pentanoil)-*sn*-glycero-3-phosphate

1,2-DLPC – 1,2-dilinoleoyl-phosphatidyl-choline

BHPA – benzophenone-4-heptyl-4'-pentanoic acid

SDS – sodium dodecyl sulphate

LA – linoleic acid

И З В О Д

ФОТОЛИЗА ИНКОРПОРИСАНИХ ДЕРИВАТА БЕНЗОФЕНОНА У САБИЈЕНИМ МОНОМОЛЕКУЛСКИМ СЛОЈЕВИМА ЛИПИДА

ДЕЈАН З. МАРКОВИЋ

Технолошки факултет, 16000 Лесковац

Циљ рада је проучавање могућности одигравања липидне пероксидације слободно-радикалског типа на липидним конституентима биомембрана, у сабијеним мономолекулским слојевима, са инкорпорисаним липоидалним фотосензибилизаторима бензофенонског типа. Њихови триплети апстракују алилне и двоструко-алилне атоме водоника из антикоњугованих целина липидних молекула. Резултати истовремено потврђују одигравање апстракције водоникових атома (и према томе иницијацију ланчаног механизма пероксидације) и одсуство формирања липидних пероксида. Разлог је у "ефекту кавеза": ограничени простор сабијених липидних мономолекулских слојева ограничава покретљивост створених радикала (липидни и кетил-радикали) и води до њихове рекомбинације, спречавајући пропагациони корак ланчаног механизма. Са извесном апроксимацијом може се закључити да ови резултати имају јасну импликацију на реалне биомембране: сама њихова структура је један од главних фактора за спречавање ланчане реакције и формирање липидних пероксида.

(Примљено 4. јула 2000)

REFERENCES

1. B. Halliwell, J. M. C. Gutteridge, *Free Radicals in Biology and Medicine*, Clarendon Press (1985), p. 139
2. A. L. Tappel, *Fed. Proc.* **24** (1973) 1870
3. J. S. Bus, J. E. Gibson, *Reviews in Biochemical Toxicology* (1979) 125
4. M. U. Dianzini, G. Ugazio, *Biochemical Mechanisms of Liver Injury*, Academic Presss (1978), p. 669
5. U. P. Steinbrecher, H. Zhang, M. Lougheed, *Free Radic. Biol. Med.* **9** (1990) 155
6. B. D. Goldstein, G. Witz, *Free Radic. Res. Commun.* **11** (1990) 3
7. L. Dargel, *Exp. Toxic. Pathol.* **44** (1992) 169
8. C. S. Foot, *Free Radicals in Biology*, Academic Press (1976), Vol. II, p. 85
9. A. W. Girotti, *J. Free Radic. Biol. Med.* **1** (1985) 87
10. J. F. Mead, *Free Radicals in Biology*, Academic Press (1976), Vol. I, p. 51
11. R. D. Small, J. C. Scaiano, L. K. Patterson, *Photochem. Photobiol.* **29** (1979) 49
12. J. F. Mead, G. S. Wu, R. A. Stein, D. Gelmont, A. Sevanian, E. Sohlberg, R. N. McElhaney, *Lipid Peroxides in Biology and Medicine,* Academic Press (1982) 161

13. L. K. Patterson, *Oxygen and Oxy-radicals in Chemistry and Biology,* Academic Press (1981), p. 89
14. M. Erben-Russ, W. Bors, R. Winter, M. Saran, *Radiat. Phys. Chem.* **27** (1986) 419
15. M. G. J. Heijman, H. Nauta, Y. K. Levine, *Radiat. Phys. Chem.* **26** (1985) 73
16. J. P. Fouassier, D. J. Lougnot, *Polym. Photochem.* **3** (1983) 79
17. I. Mita, T. Tagaki, H. Kazuyki, Y. Shindo, *Macromolecules* **17** (1984) 2256
18. D. Z. Marković, L. K. Patterson, *Photochem. Photobiol.* **49** (1989) 531
19. D. Z. Marković, L. K. Patterson, *Photochem. Photobiol.* **58** (1993) 329
20. D. Z. Marković, T. Durand, L. K. Patterson, *Photochem. Photobiol.* **51** (1990) 389
21. J. C. Scaiano, *J. Photochem.* **2** (1973) 81
22. P. N. Guivisdalsky, R. Bittman, *J. Org. Chem.* **54** (1989a) 4637
23. P. N. Guivisdalsky, R. Bittman, *J. Org. Chem.* **54** (1989b) 4643
24. Z. Bilkadi, R. D. Neuman, *J. Colloid Int. Sci.* **82** (1981) 480
25. D. Vollhardt, L. Zastrow, P. Schwartz, *Colloid Plymer Sci.* **258** (1980) 1176
26. C. G. Crawford, R. D. Plattner, D. J. Sesa, J. J. Rackis, *Lipids* **15** (1980) 91
27. R. O. Recknagel, E. A. Glende Jr, *Methods in Enzymology*, Academic Press (1984), Vol. 105, p. 331
28. M. V. Encinas, J. C. Scaiano, *J. Am. Chem. Soc.* **103** (1981) 6393
29. L. J. Johnston, D. J. Lougnot, W. Wintgens, J. C. Scaiano, *J. Am. Chem. Soc.* **110** (1988) 518
30. J. C. Scaiano, E. B. Abuin, *Chem. Phys. Lett.* **81** (1981) 209
31. M. Bohorquez, L. K. Patterson, *Langmuir* **9** (1993) 2097
32. J. C. Maziere, J. D. Routier, C. Maziere, R. Santus, L. K. Patterson, *Free Radic. Biol. Med.* **22** (1997) 795
33. J. D. Routier, C. Maziere, F. Rose-Robert, M. Auclair, R. Santus, J. C. Maziere, *Free Rad. Res.* **23** (1995) 301
34. S. K. Chattopadhuyay, C. V. Kumar, P. K. Das, *J. Photochem.* **30** (1985) 81
35. D. I. Schuster, T. M. Weil, *J. Am. Chem. Soc.* **95** (1973) 4091.

J.Serb.Chem.Soc. *66*(5)323–330(2001)
JSCS–2859

UDC IgG hyman, 546.668
Original scientific paper

Two new murine monoclonal antibodies rised against human IgG

MARIJANA PETRIĆEVIĆ*, ALEKSANDRA INIĆ*, RATKO M. JANKOV**# and LJILJANA DIMITRIJEVIĆ*

**Institute for Immunology and Virology "Torlak", Vojvode Stepe 458, YU-11221 Belgrade and*
***Faculty of Chemistry, University of Belgrade, Studentski trg 16, YU-11000 Belgrade, Yugoslavia*

(Received 24 November 2000)

Many pathological conditions are accompanied with changes in the concentration of the total IgG or some of its fraction. For this reason there is great interest in the production of reagents specific for IgG. In this paper, the binding characteristics of two new murine monoclonal antibodies (MoAb), assigned MoAb 15 and MoAb 22, are reported. These MoAbs were produced by hybridoma technology. By performing ELISAs and Western blots analyzes, it was demonstrated that both MoAbs interact specifically with human IgG. Cross reactivity with other sera proteins was not observed. In order to precisely localize the epitopes recognized by MoAb 15 and MoAb 22, the Western blots interactions of these MoAbs with electrophoreticaly separated IgG-fragments, obtained by the action of proteolytic enzymes (papain, pepsin, trypsin), were analyzed. According to the results of these experiments, both MoAbs interacted with epitopes in the C 3 domain. The affinity constants, calculated from Scatchard plots of binding of MoAb 15 and MoAb 22 to human IgG, were $Ka_{15} = 1.71 \quad 10^6\ M^{-1}$ and $Ka_{22} = 2.15 \quad 10^9\ M^{-1}$. According to all these findings, MoAb 15 and MoAb 22 could be used in standard immunochemical techniques. However, the experiments showed that both MoAbs had bad immunoprecipitating properties. In solid phase techniques (ELISAs, Western blot, dot-blot, *etc.*), their application gave excellent results that highly recommended them for use in these types of analyzes.

Keywords: human IgG, affinity constant, murine monoclonal antibodies, immunochemical technique.

INTRODUCTION

Hybridoma technology, designed by G. Kohler and C. Milstain in 1975,[1] is the oldest way to produce monoclonal antibodies (MoAb) with the desired binding characteristics. This protocol enabled the production of, theoretically, unlimited variety source of homogenous amounts of MoAbs with "predefined" characteristics of binding (affinity and specificity). In spite of the development of new technologies based on methods of genetic engineering,[2] this procedure is still widely used.

Serbian Chemical Society active member.

After the appearance of hybridoma technology, MoAbs became the "reagents of choice" in research and diagnostic. The application of MoAbs made standard procedures more specific and more sensitive.[3] However, each application of MoAbs required its detailed characterization as a guarantee for the validity of the obtained results. So, expression "to produce MoAb-reagents" meant to obtain a MoAb and to fully characterize it.

Our goal was the production of MoAbs specific for human IgG (hIgG). Interest in the production of reagents specific for IgG can be explained by the fact that many pathological conditions are accompanied by changes in the concentration of the total IgG or some of its fractions.[4]

In this paper, investigations on the binding characteristics of two new murine MoAbs produced by hybridoma technology, assigned MoAb 15 and MoAb 22, are described. The investigations showed that they reacted specifically with hIgG, a fact that could make them usefull, primarily as diagnostic tools.

EXPERIMENTAL

Determination of affinity of MoAb 15 and MoAb 22 for hIgG by competitive ELISA

Affinity constants (*K*a) of MoAb 15 and MoAb 22 were calculated, according to Scatchard analyze, from the results obtained by competitive ELISA. In this experiment, a constant amount (1 g/ml *i.e.,* 6.4 nM) of MoAb labeled by biotin (MoAb-B) was incubated in the presence of different concentrations of hIgG for 2 h at 25 ºC. Determination of the concentrations of free MoAb (F) in these samples were based on binding to hIgG adsorbed on microtitar plate, while the concentrations of MoAb 15 and MoAb 22 bound to hIgG in solution (B) were equal to the differences between the total MoAb concentration and F.

For determination of F_{15} and F_{22}, hIgG was adsorbed on microtitar plates from hIgG/PBS solution at concentrations of 0.5 g/ml and 1 g/ml, respectively (50 l/well, at 4 ºC, over night). A solution of 1 % BSA (Sigma)/PBS was used for saturation (200 l/well, 2 h, at room temperature), preparation of samples and dilution of streptavidin-peroxidase (ICN) (50 l/well, 1 h, 25 ºC). Before each step, following saturation, the plates were washed with 0.05 % Tween 20 (Sigma)/PBS (4 200 l/well) and PBS (1 l/well). OPD (Sigma) (50 l/well) was used as substrate and its transformation by streptavidin-peroxidase was stopped by adding 2 M H_2SO_4 (50 l/well). The amount of MoAb-B bound to hIgG adsorbed on the plates was proportional to the absorbance read at 492 nm.

Fragmentation of hIgG by:

a) papain

Fragmentation of hIgG by papain was performed in 0.1 M Na-phosphate buffer, pH 6.5, in the presence of 50 mM Cys (Merck) and 1 mM EDTA (Fluka). The final ratio of masses of hIgG and papain (Gibco BRL) ($m_{hIgG} : m_{papain}$) was 100 : 1. The digestive mixture was incubated at 37 ºC for 16 h. The reaction was stopped by adding a solution of iodacetamide to a final concentration of 75 mM.

b) pepsin

Fragmentation of hIgG by pepsin was performed in 0.1 M acetic buffer, pH 3.5, at 37 ºC. The ratio of the amount of hIgG and pepsin (Sigma) in the digestion mixture was $m_{hIgG} : m_{pepsin} = 100 : 1$. The reaction was stopped in intervals of 1 h by raising the pH to 9.

c) trypsin

Fragmentation of the isolated Fc portion of hIgG (hFc) by trypsin was performed in 10 mM Tris / 0.1 M NaCl, pH 7.8, at 40 ºC for 1 h. Before the addition of trypsin, the pH of the hFc solution

was lowered to 2.5 by adding 2 M HCl. The solution was incubated for 5 min and the pH was returned to 7.8 by adding 1 M Tris. The ratio of hFc and trypsin in the reaction mixture was m_{hFc} : $m_{trypsin}$ = 100 : 2.

RESULTS AND DISCUSSION

Murine hybridoma 15 and 22, which secreted MoAb 15 and MoAb 22, respectively, were obtained by fusion of murine mieloma cells SP/02 mIL-6 and spleen cells of BALB/c mouse immunized with hIgG. Preliminary tests, performed with supernatant of clones 15 and 22, indicated that MoAb 15 and MoAb 22 interacted with hIgG. Further investigations, performed with MoAb 15 and MoAb 22 isolated from appropriate ascitic fluids, confirmed this observation.

Affinity of MoAb 15 and MoAb 22 for hIgG

The affinity of MoAb for its Ag is one of the most important properties determining its usefulness.[5] The affinities of MoAb 15 (Ka_{15}) and MoAb 22 (Ka_{22}) for hIgG were determined by competitive ELISA. In these experiments, the binding of MoAb 15 and MoAb 22 (both at constant concentration, 1 g/ml) to hIgG adsorbed on microtitar plate were inhibited by incubation with different amounts of hIgG. The obtained results

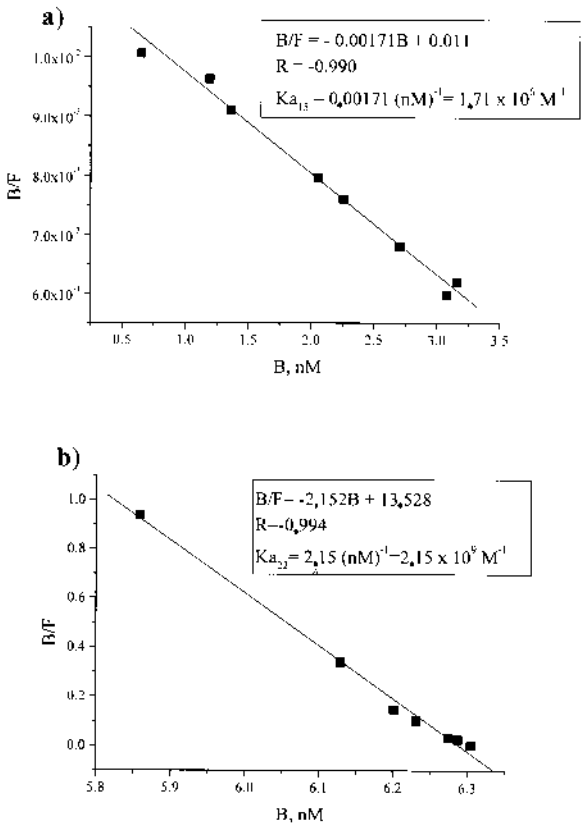

Fig. 1. Scatchard plots ($B/F = f(B)$) for the binding of MoAb 15 a) and MoAb 22 b) to hIgG; B – concentration of MoAb bound to hIgG, F – concentration of free MoAb.

were transformed according to the Scatchard equation and the value of *K*a was determined from Scatchard plot (Fig. 1). *K*a values of MoAb 15 and MoAb 22 for hIgG are: $Ka_{15} = 1.71 \quad 10^6\ M^{-1}$ and $Ka_{22} = 2.15 \quad 10^9\ M^{-1}$, respectively.

According to its affinity for hIgG, MoAb 22 might be used, after coupling to an inert matrix, for the isolation of hIgG by affinity chromatography, ELISA, Western blot, dot-blot, immunofluorescence and in different forms of immunoprecipitation.[5] However, MoAb 22, despite of high affinity, had bad immunoprecipitation characteristics and did not precipitate hIgG either in solution or in agarose gel. Steric hindrances or functional monovalency[6] that would prevent the formation of an immunoprecipitation lattice could be the explanations of this phenomenon.

The Ka_{15} value of MoAb 15 implied that it could be used in tests such as ELISA and Western blot, too.[5] However, it also showed bad immunoprecipitation properties, most probably, because of its low affinity for hIgG.

Localization of the epitopees recognized by MoAb 15 and MoAb 22

Western blot analyzes of electrophoreticaly separated human sera proteins, showed that both MoAbs reacted with the heavy chain of human immunoglobulins (Fig. 2). According to the results of these experiments, the reactivity of MoAb 15 and MoAb 22 with other, "non-IgG", sera proteins could also be excluded. The non-existence of cross-reactivity is very important if these MoAbs are to be used for the quantification of hIgG.

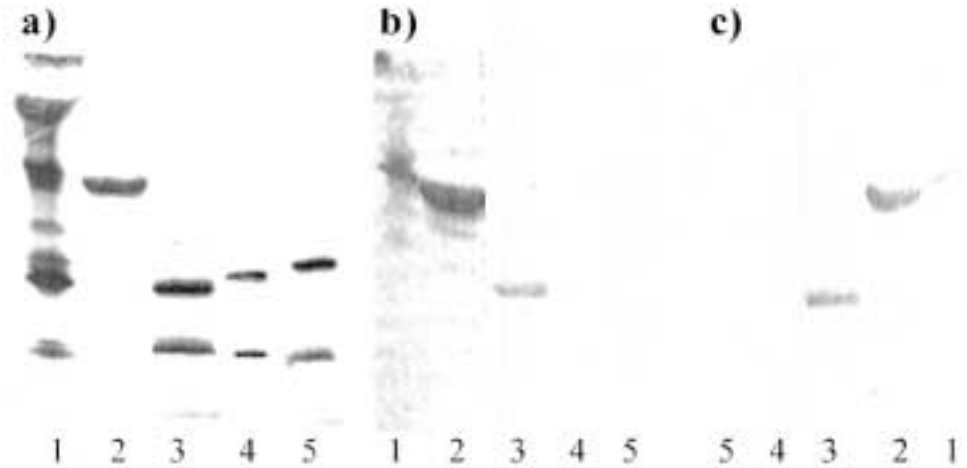

Fig. 2. SDS-PAGE in 4 – 15 % PAAG a) and Western blot analyzes of 1 – human sera, 2 – hIgG, 3 – hIgG reduced with -mercaptoethanol, 4 – hIgA reduced with -mercaptoethanol 5 – hIgM reduced with -mercaptoethanol; blots were developed in presence of MoAb 22 (b) and MoAb 15 (c).

The determination of the concentration of hIgG is usually performed by different types of ELISAs. We showed that both MoAbs could be used successively in these assays. Using MoAb 15 or MoAb 22, less than 1 g/ml of hIgG could be detected by

ELISA. The low value of the additivity index (*AI*)[7] for MoAb 15 and MoAb 22, $AI_{15,22}$ = 6.22, indicated that these MoAbs, because of steric hindrance for the simultaneous binding on hIgG, could not be used in sandwich ELISA which is more specific than others types of ELISAs. In "sandwich" ELISA they could be used in combination with MoAbs that recognize epitopes located far from those of MoAb 15 and MoAb 22. For example, they could be used with MoAb 44 (specific form human κ chain) for the determination of the concentration of IgGκ molecules.

In order to localize the epitopes recognized by MoAb 15 and MoAb 22 more precisely, the interactions of these MoAbs with fragments of hIgG, obtained by the action of papain, trypsin and pepsin, were analyzed.

The main products of papain digestion of hIgG were fragments of equal molecular size (50 kDa), Fab and Fc.[8] They could be separated by affinity chromatography on protein A.[9] The fragments obtained by papain digestion were analyzed by Western blot. According to the bands on blots of sample eluted from protein A, which appeared in the presence of both MoAbs (Fig. 3), it was concluded that the epitopes recognized by MoAb 15 and MoAb 22 were located in the Fc portion of hIgG.

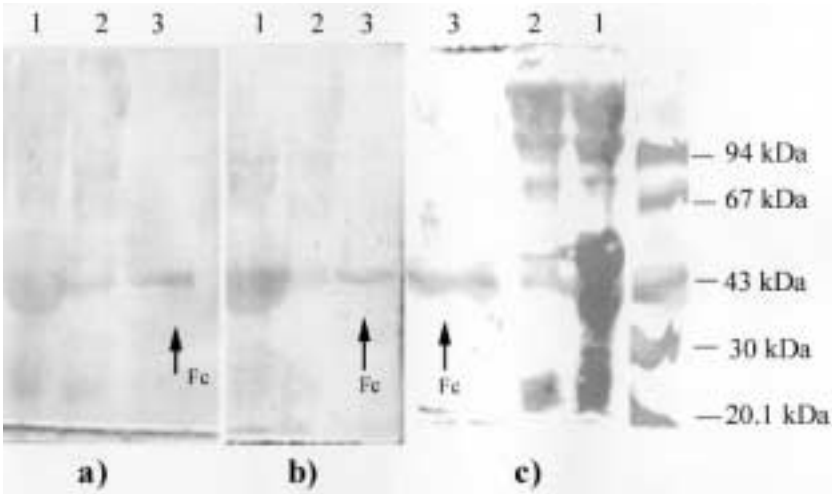

Fig. 3. SDS-PAGE (7.5 % PAAG) of hIgG fragments obtained by the action of papain (c) and Western blot analyses of the interaction of MoAb 15 (a) and MoAb 22 (b) with them; samples: 1 – digestive mixture of hIgG resulting from the action of papain, 2 – fraction of the digestive mixture of hIgG resulting from the action of papain which did not interact with protein A, 3 – fraction of digestive mixture of hIgG resulting from the action of papain which was eluted from protein A by 0.1 M citric buffer, pH 3.5.

It is well known that peptic digestion of hIgG yields $(Fab)_2$ (100 kDa) and pFc' as the main products. Beside these fragments, numerous intermediate products and peptides resulting from the enzymatic degradation of C 2 occur in the digestion mixture[10] (Fig. 4a). Four major bands appeared on blots developed in the presence of MoAb 15 (Fig. 4b) or MoAb 22 (Fig. 4a), after electrophoretical separation of the hIgG

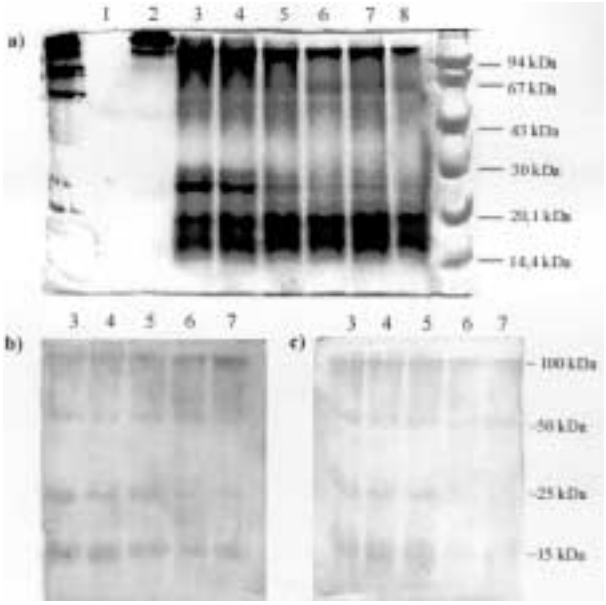

Fig. 4. SDS-PAGE (10 % PAAG) of hIgG fragmentized with pepsin (a) and Western blot analyzes of the interactions of MoAb 15 (b) and MoAb 22 (c) with the obtained fragments; samples: pepsin at concentration used for digestion (1), intact hIgG (2), mixtures of hIgG fragments obtained by the action of pepsin for 1 h (3), 2 h (4), 3 h (5), 4 h (6), 6 h (7) and 8 h (8).

fragments obtained by the action of pepsin. These bands, assigned according to corresponding molecular weights, were: “ 100 kDa”, “ 50 kDa”, “ 25 kDa” and “ 15 kDa”. The positions of molecular weights markers in the polyacrylamide gel (PAAG) indicated that, in this system, resolution of protein with “higher” (>100 kDa) molecular weight was not correct (Fig. 4a). So, it is possible that “ 100 kDa” bands on blots were the result of interaction of MoAb 15 or MoAb 22 with intact hIgG or its intermediates that possesed a partially degraded Fc portion. Regarding the fact that the major cleavage site of pepsin is in the lower hinge region, below interchain disulphide bonds,[10] the appearance of “ 50 kDa” in the PAAG was unexpected. It is possible that this band was the result of stochastic formation of disulphide bonds between free Cys residues of fragments produced by the action of pepsin. Interactions with proteins of band “ 25 kDa” (C 2-C 3) confirmed our finding that epitopes recognized by MoAb 15 and MoAb 22 were located in the Fc portion of hIgG.

Interactions of MoAb 15 and MoAb 22 with peptic bands of lower molecular weight indicated that epitopes recognized by these MoAbs could be located in the C 3 domain of the human chain. SDS-polyacrylamide gel electrophoresis (SDS-PAGE) and Western blot analyzes of fragments resulting from tryptic digestion of the hFc portion of Ig confirmed this hypothesis. HFc were obtained by papain digestion of hIgG, isolated by affinity chromatography on protein A and exposed to low pH (pH 2.5). Exposure to low pH rendered the region between C 2 and C 3 domains transiently susceptibile to trypsin upon return to neutral pH, allowing the splitting of Fc to those

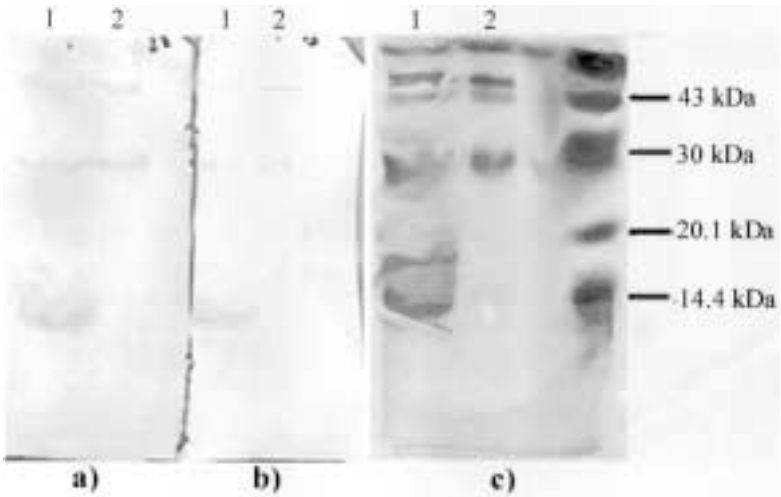

Fig. 5. SDS-PAGE (15 % PAAG) of hFc fragments obtained by the action of trypsin (c) and Western blots analyzes of the interaction of MoAb 15 (b) and MoAb 22 (a) with these fragments; 1 – hFc fragmentized by trypsin, 2 – hFc exposed to low pH.

two domains.[11] After SDS-PAGE of tryptic digestion mixture, there were 3 bands in PAAG: 25 kDa, 17 kDa and 12.5 kDa (Fig. 5a). Western blot analyzes showed that both MoAbs reacted with the " 25 kDa" band (unseparated between C 2-C 3) and the band of the lowest molecular weight (Fig. 5b, c) which, according to literature data, represents the C 3 domains.[12]

Precise localization of epitopes recognized by a MoAb could be useful data in functional studies, inhibition studies or in designing experiments that require simultaneous use of more MoAbs.

CONCLUSION

MoAb 15 and MoAb 22, obtained by hybridoma technology, were specific for hIgG. They specifically interacted with epitopes localized in the C 3 domain of the human chain. The affinity of the interaction of MoAb 22 was high ($Ka_{22} = 2.15 \quad 10^9$ M^{-1}), while MoAb 15 bound hIgG with low affinity ($Ka_{15} = 1.71 \quad 10^6$ M^{-1}). According to our results, MoAb 15 and MoAb 22 did not precipitate hIgG either in solution or in agarose gel. This inability to form precipitating complexes with hIgG reduce their applicability. Otherwise, both MoAbs, when used independently, demonstrated excellent properties in common diagnostic tests such as ELISA, blots, *etc*. However, in these assays advantage could be given to MoAb 22 because of its greater affinity that allows the detection of hIgG at lower concentrations.

И З В О Д

ДВА НОВА МИШЈА МОНОКЛОНСКА АНТИТЕЛА ДОБИЈЕНА ПРОТИВ ХУМАНОГ IgG-a

МАРИЈАНА ПЕТРИЋЕВИЋ[1], АЛЕКСАНДРА ИНИЋ[1], РАТКО М. ЈАНКОВ[2] и ЉИЉАНА ДИМИТРИЈЕВИЋ[1]

[1]Институт за имунологију и вирусологију "Торлак", Војводе Степе 458, 11221 Београд и [2]Хемијски факултет, Студентски трг 16, 11000 Београд

Многа патолошка стања су повезана са променама концентрације укупног IgG-a или неке од његових фракција. То је разлог великог интересовања за продукцију реагенаса специфичних за IgG. Ми смо у овом раду описали карактеристике везивања два нова мишја моноклонска антитела (MoAt), означена као MoAt 15 и MoAt 22. Ова MoAt су добијена хибридомском технологијом. Користећи ELISA-е и Western blot анализе, показали смо да оба MoAt специфично реагују са хуманим IgG-ом. Укрштена реактивност са другим серумским протеинима није уочена. Да би смо прецизно лоцирали епитопе које препознају MoAt 15 и MoAt 22, Western blot-ом смо анализирали интеракције ових MoAt са електрофоретски раздвојеним фрагментима IgG-a добијених дејством протеолитичких ензима (папаин, пепсин, трипсин). Према резултатима ових експеримената оба MoAt интерреагују са епитопима у C 3 домену. Константе афинитета, израчунате са Скачардових дијаграма везивања MoAt 15 и MoAt 22 за хумани IgG су $Ka_{15} = 1.71 \quad 10^6\ M^{-1}$ и $Ka_{22} = 2.15 \quad 10^9\ M^{-1}$. На основу свих ових чињеница, MoAt 15 и MoAt 22 би се могла користити у стандардним имунохемијским техникама. Међутим, наши експерименти су показали да оба MoAt имају лоше имунопреципитационе особине. Са друге стране, у техникама на чврстој фази (ELISA-е, Western blot, dot-blot, итд.) њихова примена је дала одличне резултате што их препоручује за употребу у овом типу анализа.

(Примљено 24. новембра 2000)

REFERENCES

1. G. Kohler, C. Milstein, *Nature* **256** (1975) 495
2. P. J. Hundson, *Current Opinion in Immunol.* **11** (1999) 548
3. C. K. Borrebaeck, *Imm. Today* **21** (2000) 379
4. A. K. Abbas, A. H. Lichtman, J. S. Pober, *Cellular and Molecular Immunology*, W. B. Saunders Co., 2nd ed. 1994
5. E. Harlow, D. Lane, *Antibodies - a Laboratory Manual*, Coald Spring Harbor Laboratory, 1988
6. R. A. Margni, R. A. Binaghi, *Ann. Rew. Immunol.* **6** (1988) 535
7. T. E. Creighton, *Protein Structure - a Practical Approach*, IRL Press, 1989
8. F. A. Nardella, D. C. Teller, *Mol. Immunol.* **22** (1985) 705
9. J. W. Goding, *J. Immunol. Methods* **20** (1978) 241
10. M. W. Turner, H. H. Bennich, J. B. Natvig, *Nature* **225** (1970) 853
11. C. Endersen, M. Heggeness, A. Grov, *Scand. J. Immunol.* **3** (1973) 261
12. J. R. Ellerson, D. Jasmeen, R. H. Painter, K. J. Dorrington, *J. Immunol.* **116** (1976) 510.

J.Serb.Chem.Soc. *66*(5)331–334(2001) UDC 546.668:669.794
JSCS–2860 *Short communication*

SHORT COMMUNICATION

Synthesis and characterization of a novel (glycinato-N,O) yttrium(III) complex

I. M. HODŽIĆ*# and S. R. NIKETIĆ#

Chemistry Department, Faculty of Science, University of Belgrade, Studentski trg 16, P.O. Box 158, YU-11001 Belgrade, Yugoslavia

(Received 20 November 2000, revised 7 February 2001)

A novel yttrium(III) complex with glycine has been synthesized starting from tris(ethanedioato-O,O)yttrium(III) by the substitution of the acetylacetonato chelate ligands with glycine. The reaction product was purified by ion-exchange chromatography and characterized on the basis of infrared spectroscopy. The structure of the product was tentatively established as tris(glycinato-N,O)yttrium(III) dihydrate.

Keywords: yttrium(III) complexes; glycinato-N,O chelates, IR spectroscopy.

INTRODUCTION

Coordination chemistry of tris(aminocarboxylato-N,O) complexes of trivalent transition metals has continually been in focus for many decades.[1] A number of complexes of the general formula $M^{III}(aa)_3$ (where aa = bidentate aminocarboxylato-N,O chelate) have been prepared, characterized by a variety of physical methods, and studied using chemical, kinetic, thermodynamic, photochemical and computational techniques.[2]

However, it is still possible to find gaps in the chemistry of $M(aa)_3$ complexes across the periodic table of elements. A notable example is the scarcity of data on lanthanide complexes with aminocarboxylato-N,O bidentate chelate rings. In this work an attempt to prepare a complex of a tris(bidentate) type of yttrium(III) with glycine is described. Yttrium chelates have attracted much attention lately due to their potential application as tumour-targeting contrast agents in magnetic resonance imaging,[3–5] and as luminescent bio-markers,[6] let alone their significance in basic coordination[7] and organometallic[8] chemistry. From this study we expect to gain some further insight into the nature of metal–ligand interaction between coordinated carboxylato oxygen (as a supposedly anisotropic ligator[9]) and Y(III). It will eventually provide a basis for the parametrization of a molecular mechanics force field for amino(poly)carboxylate complexes of lanthanides, which is one of our long-term goals.

Serbian Chemical Society active member.

EXPERIMENTAL

Tris(ethanedioato-O,O)yttrium(III) trihydrate was prepared according to the procedure of Sands et al.[10]

Tris(glycinato-N,O)yttrium(III) dihydrate. In 100 mL of ethanol (60 %) 6 g of tris(ethanedioato-O,O)yttrium(III) trihydrate was dissolved, and the solution was heated up to the boiling point in order to initiate the hydrolysis of the acetylacetonato complex. The solution was then cooled to ambient temperature and mixed with a previously prepared aqueous solution of glycine (4.6 g in 50 mL of water). The pH of the mixture was then adjusted to 5–6 and maintained at 30 ºC under constant stirring for a period of 12 hours. After subsequent removal of the solvent under reduced pressure, a yellowish-white precipitate was obtained, which was filtered off, washed with abs. ethanol, and dried at ambient temperature. In this way 3.6 g of a water-soluble solid was obtained. The solid was dissolved in a minimal amount of water and passed in turn through cationic and anionic Dowex ion-exchange columns eluted with water. The resultant solution was concentrated in a vacuum-evaporator and left overnight to crystallize. Anal.: Found: C, 20.63 %, H, 4.7 %, N, 12.55 %; calculated for $Y(Gly)_3$ $2H_2O$: C, 20.7 %, H, 5.43 %, N, 12.10 %.

Infrared spectra of reactants and the reaction product were measured on a Perkin-Elmer FTIR 172 instrument using the KBr pellet technique.

RESULTS AND DISCUSSION

The experimental procedure was conducted in an attempt to substitute acetylacetonato with glycinato ligands. Namely, the tris(ethanedioato-O,O) complexes of yttrium(III) as well as of other trivalent lanthanides are known to undergo facile hydrolysis in aqueous media yielding mixed hydroxo and ethanedioato species.[11] In the presence of excess glycine these hydrolysis products are expected to form chelate (glycinato-N,O) species. At pH 5–6 glycine is present predominantely in the zwitterionic form. Therefore, it can be easily coordinated to Y(III) *via* the carboxylate oxygen causing the ammonium to deprotonate (by elimination of H_2O molecule from Y(III)-hydroxo species). The latter step is favoured by the chelate effect of glycine.

A strong support for the proposed overall course of the substitution reactions stems from the fact that the same product was obtained using a range of different mole ratios of tris(ethanedioato-O,O)yttrium(III) to glycine. Even with glycine as the limiting reagent the identical product was obtained after removal of unreacted tris(ethanedioato O,O)yittrium(III).

The solid-state infrared spectrum of the glycinato complex of yttrium(III) in the region 2000–400 cm^{-1} is presented in Table I together with the assigned spectrum of crystalline glycine.[12] The differences in the positions of the infrared absorption maxima between the free glycine (zwitterion) and its yttrium(III) complex are small but consistent with our proposed structure of the complex having bidentately coordinated (glycinato-N,O) ligands. The characteristic features pertain to the vibrations associated with the COO group. They are indicated in bold in Table I. Thus, $_a$(COO) is shifted to a higher frequency (from 1616 to 1636 cm^{-1}) and the $_s$(COO) to a lower frequency (from 1413 to 1400 cm^{-1}); both wagging and rocking COO vibrations are shifted to higher frequencies (Table I) indicating a metal–oxygen coordination.[13]

Since our synthesis and ion-exchange chromatography yielded only one pure substance, we were not able at this stage to identify the geometrical configuration of the

product in terms of *fac* and *mer* isomerism characteristic for $M(Gly\text{-}N,O)_3$ species. In addition, our results do not exclude a possibility of the augmentation of the coordination sphere[14] with one of the H_2O molecules assumed to be lattice water. However, in either case it is highly unlikely that the glycinato ligands are not bidentately coordinated. Furhter structural investigations along these lines are in progress.

TABLE I. The observed infrared frequencies (cm^{-1}) for the crystalline glycine, and glycinato Y(III) complex, with tentative assignments

Glycine	$Y(Gly)_3$	Assignment
1630		shoulder
1616	**1632**	COO^- asym. stretching
1507	1500	
1468	-	
1445	1440	CH_2 bending
1413	**1400**	COO^- sym. stretching
1333	1332	CH_2 wagging
-	1300	
1132		NH_3^+ rocking
	1123	NH_2 rocking
1111		NH_3^+ rocking
	1100	NH_2 rocking
1033	1040	CN stretching
911	927	CH_2 rocking
893	893	CC stretching
699	700	COO^- bending
609	**620**	COO^- wagging
502	**520**	COO^- rocking
435		
419	421	

Acknowledgements: This work was supported by a grant from the Serbian Research Council (Contract No. 02E09).

И З В О Д

СИНТЕЗА И КАРАКТЕРИЗАЦИЈА НОВОГ (ГЛИЦИНАТО-N,O) ИТРИЈУМ(III) КОМПЛЕКСА

И. М. ХОЏИЋ и С. Р. НИКЕТИЋ

Хемијски факултет, Универзитет у Београду, Студентски трг 16, п. пр. 158, 11001 Београд

Супституцијом координованог ацетилацетоната глицином у трис-бидентатно координованом итријум(III) комплексу добијен је нов глицински комплекс итрјума(III),

који је после пречишћавања јоноизмењивачком хроматографијом окарактерисан на основу инфрацрвених спектара. На основу карактеристичних померања инфрацрвених трака за карбоксилатни фрагмент предложена је трис(глицинато-N,O) структура за ову супстанцу.

(Примљено 20. новембра 2000, ревидирано 7. фебруара 2001)

REFERENCES

1. The chemistry of tris(aminocarboxylato)metal(III) complexes spans a fascinating period of almost a century of research: from the first report by H. Ley and H. Winkler *Ber.* **42** (1909) 3894 to the present day see *e.g.,* Y. Yoshimura, *Bull. Chem. Soc. Japan* **73** (2000) 2739 . The most recent paper on the topic from THIS JOURNAL is: P. N. Radivojša, *J. Serb. Chem. Soc.* **62** (1997) 1045
2. B. Geisser, T. Skrivanek, U. Zimmermann, D. J. Stufkens, R. Alsfasser, *Eur. J. Inorg. Chem.* (2001) 439; J.-H. Choi, *J. Photosci.* **3** (1996) 43; M. S. El-Shahawi, *Spectrochim. Acta* **52A** (1996) 139; Y. Yoshimura*, Bull. Chem. Soc. Japan* **69** (1996) 2565; Y. Yoshimura, *Canad. J. Chem.* **76** (1998) 71
3. A. Heppeler, S. Froidevaux, H. R. Mäcke, E. Jermann, M. Béhé, P. Powell, M. Hennig, *Chem. Eur. J.* **5** (1999) 1974
4. A. Borel, L. Helm, A. E. Merbach, *Chem. Eur. J.* **7** (2001) 600
5. D. M. Corsi, L. Vander Elst, R. N. Muller, H. van Bekkum, J. A. Peters, *Chem. Eur. J.* **7** (2001) 64
6. A. M. Adeyiga, P. M. Harlow, L. M. Vallarino, R. C. Leif*, Proc. Intl. Soc. Anal. Cytology ISAC-96* (1996) Paper AC12
7. See, for example, the following recent papers and references cited therein: P. Lindquist-Reis, J. Näslund, I. Persson, M. Sandström*, J. Chem. Soc, Dalton Trans.* (2000) 2703; P. W. Roesky, *Chem. Ber* **130** (1997) 859; Z. Pikramenou, *Coord. Chem. Rev.* **172** (1998) 99
8. H. Schumann, K. Herrmann, J. Demtschuk, S. H. Muehle, *Z. anorg. allg. Chem.* **625** (1999) 1107; S. Arndt, T. P. Spaniol, J. Okuda*, Eur. J. Inorg. Chem.* (2001) 73
9. S. Zarić, S. R. Niketić, *Polyhedron* **16** (1997) 3565
10. M. F. Richardson, W. F. Wagner, D. E. Sands, *Inorg. Chem.* **7** (1968) 2497
11. R. M. Izatt, W. C. Fernelius, C. G. Hass, *J. Phys. Chem.* **59** (1955) 170
12. K. Machida, A. Kagayama, Y. Saito, Y. Kuroda, T. Uno*, Spectrochim. Acta* **33A** (1977) 569
13. K. Nakamoto, *Infrared and Raman Spectra of Inorganic and Coordination Compounds,* 3rd Edition, Wiley, New York, 1978
14. J. K. Przystal, W. G. Boss, I. B. Liss, *J. Inorg. Nucl. Chem.* **33** (1971) 679.

J.Serb.Chem.Soc. *66*(5)335–343(2001) UDC 661.862
JSCS–2861 *Original scientific paper*

Densification and crystallization behaviour of colloidal cordierite-type gels

RADA PETROVIĆ[1#], DJORDJE JANAĆKOVIĆ[1#], BRANISLAVA BOŽOVIĆ[1#], SLAVICA ZEC[2#] and LJILJANA KOSTIĆ-GVOZDENOVIĆ[1#]

[1]*Department of Inorganic Chemical Technology, Faculty of Technology and Metallurgy, University of Belgrade, Karnegijeva 4, YU-11001 Belgrade and* [2]*The Vinča Institute of Nuclear Sciences, P. O. Box 522, YU-11000 Belgrade, Yugoslavia*

(Received 26 October 2000, revised 31 January 2001)

Three cordierite-type gels were prepared from an aqueous solution of $Mg(NO_3)_2$, a boehmite sol and silica sols of very small particle sizes. The effect of varying the silica particle size on the crystallization and densification behaviour was studied. Phase development was examined by thermal analysis and X-ray diffraction, while the densification behaviour was characterized by measuring the linear shrinkage of pellets. The activation energy of densification by viscous flow was determined using the Franckel model for non-isothermal conditions and a constant heating rate. The results show that spinel crystallizes from the colloidal gels prior to cristobalite, and their reaction gives -cordierite, which is specific for three-phase gels. Decreasing the silica particles size lowers the cristobalite crystallization temperature and the -cordierite formation temperature. The activation energy of densification by viscous flow is lower and the densification more efficient, the smaller the silica particles are.

Keywords: cordierite, sol-gel, densification, crystallization, activation energy of densification.

INTRODUCTION

Cordierite ($Mg_2Al_4Si_5O_{18}$) as a ceramic material has a wide range of uses and applications stemming from its important properties of low thermal expansion and dielectric constant coupled with high chemical and thermal stability. Preparing dense cordierite ceramics has long been a problem because of the narrow sintering range near the incongruent melting point of the cordierite. Addition of a sintering aid[1,2] resulted in a decrease of the cordierite crystallization temperature and an increase of the density of the final product. On the other hand, these aids cause an increase in the thermal expansion coefficient and dielectric constant. The preparation of a homogeneous and fine cordierite powder that can be sintered without the addition of a sintering aid is, therefore, considered to be highly desirable.[3–6]

Serbian Chemical Society active member.

The sol-gel procedure has enabled the production of ceramic materials of high purity and with superior properties at lower temperatures than conventional methods.[7–9] Since alkoxide-derived powders offer potential for remarkable reductions in the crystallization temperatures, alkoxide methods have usually been applied to the preparation of cordierite powders.[10–19]

However, in multicomponent systems, such as cordierite ceramics, the difference in the hydrolysis rates of each alkoxide causes inhomogeneity in the resultant oxides. Moreover, gel-derived compacts often show the commencement of crystallization before complete densification, leaving large pores unremoved. This problem is most frequently encountered in the densification of multicomponent silica-containing gels that undergo viscous sintering. Since the densification rate is orders of magnitude faster when material transport occurs by viscous flow rather than by atomic diffusion, it is very difficult to remove the remaing pores after the commencement of crystallization. Therefore, in order to obtain dense sinter bodies it is important that the kinetics of viscous sintering are substantially faster than those of crystallization.

Recently, it has been reported that the heterogeneous distribution of the elements in the powders promotes densification in the sintering of some kinds of multicomponent systems. Colloidal processing[14,15,17,20–22] is considered an effective method for producing such controlled heterogeneity on a nanometer scale. A heterogeneous distribution of each element promotes the sintering of bodies by the genesis of a liquid phase of a lower melting temperature than that of a single phase.

Studies on the sol-gel synthesis of cordierite have confirmed that from colloidal, three-phase gels crystallization of spinel and cristobalite (or quarz) occurred, which react forming -cordierite. In this case, there is a wide temperature range in which densification without crystallization of the silica-containing component occurs. This means that full densification without crystallization can be reached by an appropriate choice of temperature and time.

The aims of this work were (1) to examine the crystallization and densification behaviour of colloidal cordierite-type gels, synthesized from an aqueous solution of $Mg(NO_3)_2$, a boehmite sol and silica sols of very small particle sizes and (2) to determine the influence of the silica particle size on the densification and crystallization behaviour of these gels.

EXPERIMENTAL

Three colloidal cordierite-type gels were prepared starting from silica sols of different particle size, a boehmite sol and an aqueous solution of $Mg(NO_3)_2 \cdot 6H_2O$.

The silica sols were obtained by the ion exchange method.[23] The characteristics of the silica sols are given in Table I.

The specific surface area of the solid phase was determined by the potentiometric titration method[24] – measuring the amount of OH^- ions adsorbed by the solid phase at pH 4–9. The mean particle diameter was calculated from the value of the specific surface area.

The boehmite sol (AlOOH) was obtained by peptization of freshly prepared $Al(OH)_3$, with nitric acid, under reflux.[25] It contained 2.2 mass % pseudoboehmite particles in an aqueous medium,

stabilized at pH 3.8. The specific surface area of the solid phase, determined by the BET method, was 267 m^2/g.

TABLE I. Characteristics of the silica sols

Silica sol	S5.5	S7.5	S9.5
Solid phase content/mass %	4.5	3.3	3.9
pH	9.3	9.8	9.2
$S_p/m^2\ g^{-1}$	490	367	284
d_{av}/nm	5.5	7.5	9.5

All three gels were synthesized in the following way: stoichiometric proportion of the boehmite sol and the silica sol were mixed and stirred for 2 h. Then, an saturated aqueous solution of $Mg(NO_3)_2{\cdot}6H_2O$ was added and the stirring continued for another two hours. The obtained multicomponent colloidal dispersion was coprecipitated and gelated by the addition of saturated aqueous solution of ammonium carbonate, which increased the pH to 9. The obtained gels were dried at 40 ºC for two days and then for 24 h at 110 ºC.

The relative linear shrinkage of the gel compacts was measured using a E.LEITZ thermomicroscope, at a heating rate of 10 ºC/min, up to 1300 ºC. The gels were pressed using a hand press, at about 20 MPa, into a compact with dimensions 3 3 3 mm.

The phase transformations occurring in the gels during heating were determined by DSC (NETZSCH Model 404) at heating rate of 10 ºC/min. The experiments were carried out in an air atmosphere, using Al_2O_3 as a reference. The sample mass was 50 0.5 mg.

The phase composition of powders obtained by gels calcination at 900, 1000, 1100, 1200 and 1250 ºC for 2 h were determined using a SIEMENS D500 diffractometer with CuK radiation in the 2 angle range from 5 to 60º or to 80º, with a 0.02 step.

RESULTS AND DISCUSSION

The results of differential scanning calorimetry for the synthesized gels are given in Fig. 1.

Two broad endothermal peaks in the temperature ranges from 20 ºC to 220 ºC and from 220 ºC to 500 ºC are noticeable on these curves. The second endothermal peak was formed from three overlapping individual peaks. The first endothermal peak corresponds to the desorption of physically bound water, while the second endothermal peak is ascribed to dehydroxylation, ammonia and CO_2 release, and decomposition of nitrates. At higher temperatures, two exothermal peaks are noticeable: a broad peak in the temperature range of about 900 ºC to about 1100 ºC and the other, relatively sharp peak, about 1190 ºC. As can be seen from Fig. 1, this peak is shifted towards higher temperatures with increasing size of the silica particles in the sol used for the gel synthesis. According to literature data,[14,15,17,20,21] it can be assumed that the first exothermal peak in the temperature range from 900 ºC to 1100 ºC, corresponds to the crystallization of either spinel, $MgAl_2O_4$, or cristobalite, or both. The second exothermal peak, at about 1190 ºC, corresponds to the formation of -cordierite, resulting from the reaction of spinel with cristobalite. In order to determine the nature of the processes or reactions

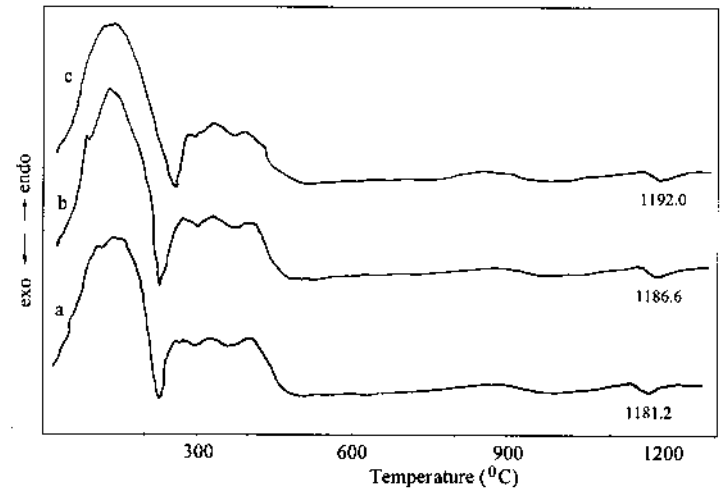

Fig. 1. DSC curves for the G5.5 (a), G7.5 (b) and G9.5 (c) gels (the numbers indicating the size of the SiO_2 particles in the sol used for the synthesis).

corresponding to the mentioned exothermal peaks, the gels were calcined at 900, 1000, 1100, 1200 and 1250 ºC, and the phase composition of powders obtained in this way were detrmined. The diffractograms of the powders obtained by calcination of the G7.5 gel at 900, 1000, 1100, 1200 and 1250 ºC are presented in Fig. 2.

In the diffractogram of the powder obtained by gel calcination at 900 ºC, weak and diffusive peaks, corresponding to spinel, are noticeable. At 1000 ºC, these peaks are slightly sharper and intense. Two other peaks at $d = 0.315$ nm and $d = 0.250$ nm, corresponding to cristobalite, are detectable, although the most intense peak for cristobalite at $d = 0.409$ nm was not detectable on this diffractogram. This peak is visible in the diffractogram of the powder obtained by gel calcination at 1100 ºC, together with the above mentioned peaks corresponding to cristobalite. The peaks corresponding to spinel become sharper and more intense. In the diffractogram of the powder obtained by gel calcination at 1200 ºC, peaks of low intensity, corresponding to -cordierite, are noticeable. The peaks corresponding to cristobalite and spinel are sharp and intense. At 1250 ºC, the peaks for spinel and cristobalite are less intense than the ones at 1200 ºC, while the peaks of -cordierite are sharp and intense. According to these results, it is evident that the first exothermal peak on the DSC gel curves corresponds to crystallization of spinel and cristobalite, while the second peak corresponds to the formation of -cordierite by the reaction between spinel and cristobalite. As previous investigations have shown,[26] formation of -cordierite by the reaction between spinel and cristobalite is a diffusion controlled process, proceeding with a constant number of nuclei and an average activation energy $E_a = 1242$ 66 kJ/mol.

The diffractograms of the powders obtained by calcination of the G5.5 and G9.5 gels at 900, 1000, 1100, 1200 and 1250 ºC differ from the corresponding diffractograms of the powders obtained by calcination fo the G7.5 gel only in the intensity of individual

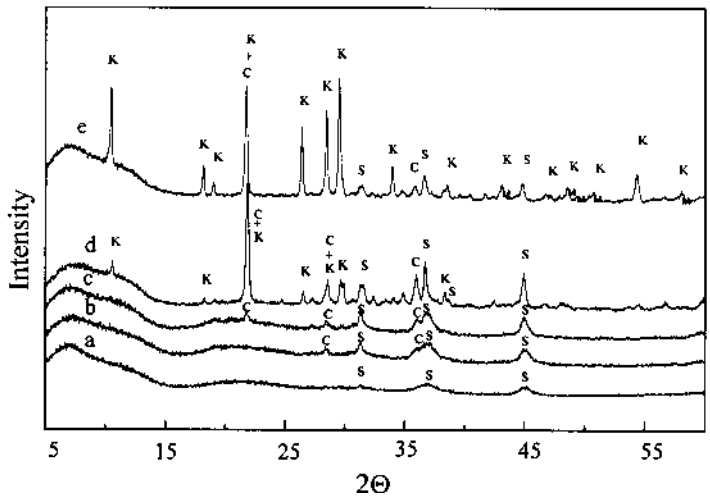

Fig. 2. Diffractograms of the powders obtained by calcination of the G7.5 gel at 900 ºC (a), 1000 ºC (b), 1100 ºC (c), 1200 ºC (d) and 1250 ºC (e) (S – spinel, C – cristobalite, K – -cordierite).

peaks. The diffractograms of the powders obtained by calcination of the G5.5, G7.5 and G.9.5 gels at 900 ºC and at 1100 ºC are presented in Fig. 3 and 4, respectively.

As can be seen from Figs. 3 and 4, there is no significant difference in the intensity of the peaks corresponding to spinel, at the same temperature for different powders. The intensity of the peaks corresponding to cristobalite decreases with increasing size of the silica particles in the sol used for the synthesis. This indicates that the temperature of the cristobalite crystallization decreases with decreasing size of the silica particles, but that the silica particle size has no effect on the spinel crystallization temperature. Considering also

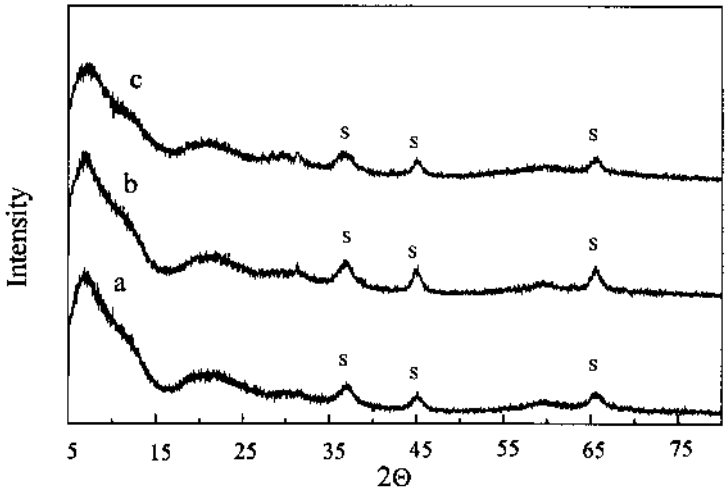

Fig. 3. Diffractograms of the powders obtained by calcination of the G5.5 (a), G7.5 (b) and G9.5 (c) gels at 900 ºC.

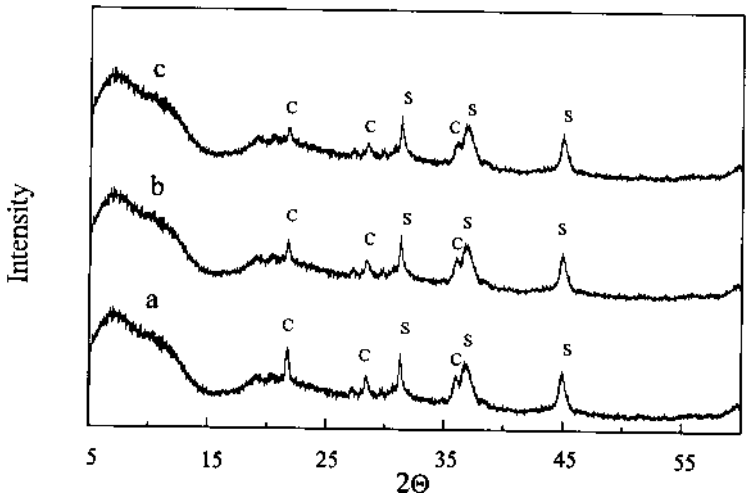

Fig. 4. Diffractograms of the powders obtained by calcination of the G5.5 (a), G7.5 (b) and G9.5 (c) gels at 1100 ºC.

the results of differential scanning calorimetry, it can be concluded that decreasing the size of the silica particles leads to a lowering of the cristobalite crystallization temperature, and consequently, a decrease of the -cordierite formation temperature.

The curves of the relative linear shrinkage during heating of the G5.5, G7.5 and G9.5 gels are shown in Fig. 5. It can be noticed that intense shrinkage occurs in the temperature range of 800–1000 ºC, ending at 1050 ºC.

Also from Fig. 5, it can be seen that the shrinkage increases with decreasing size of the silica particles, *i.e.,* densification of the gels prepared from sols of the smaller particle size is more efficient.

The activation energy of the sintering by viscous flow can be calculated using the Franckel model for non-isothermal conditions at a constant heating rate:[27]

$$L/L_0 = (\quad RT/2rA \quad E) \ \exp(-E/RT)$$

where: L/L_0 – the relative linear shrinkage, – the interfacial energy, T – the temperature, r – the particle size, A – a coefficient, – the heating rate, E – the activation energy and R – the gas constant. The dependence log (L/L_0T^2) on $1/T$ is linear, with a slope equal –0.43 E/R.

The dependancies of log (L/L_0T^2) on $1/T$ for the G5.5, G7.5 and G9.5 gels compact are shown in Fig. 6. The activation energies of densification by viscous flow were determined from the slope of these plots.

The value of the activation energy for densification by viscous flow decreases with a decreasing in size of the silica particles, which is evident from the following results: for the G9.5 gel – E = 218 12 kJ/mol, for the G7.5 gel – E = 200 9 kJ/mol and for the G5.5 gel – E = 178 14 kJ/mol.

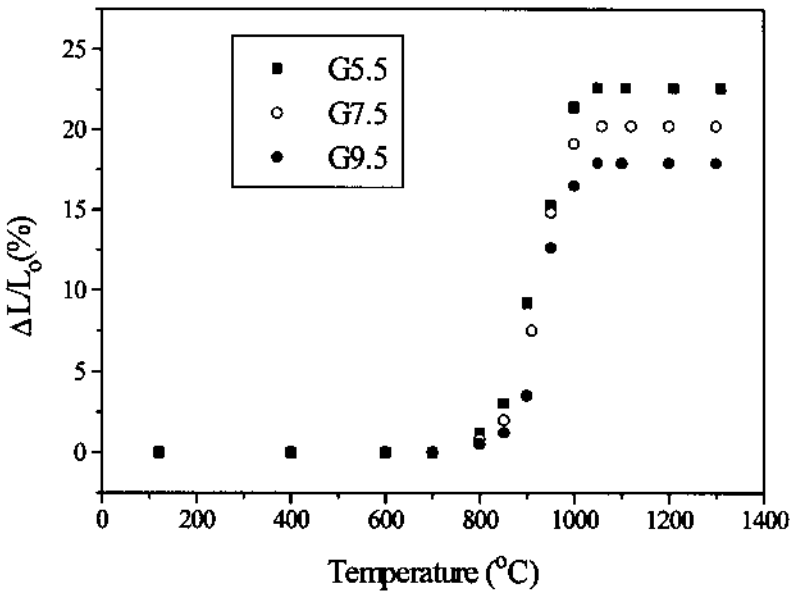

Fig. 5. Relative linear shrinkage during heating of the G5.5, G7.5 and G9.5 gel compacts.

The results of the X-ray analysis show that spinel is the first to crystallize from the three-phase gels at about 900 °C, followed by cristobalite, crystallizing at temperatures between 1000 and 1100 °C. In this temperature range, shrinkage of the compacted gels was completed (Fig. 5). It is evident that densification was not affected by the crystalli-

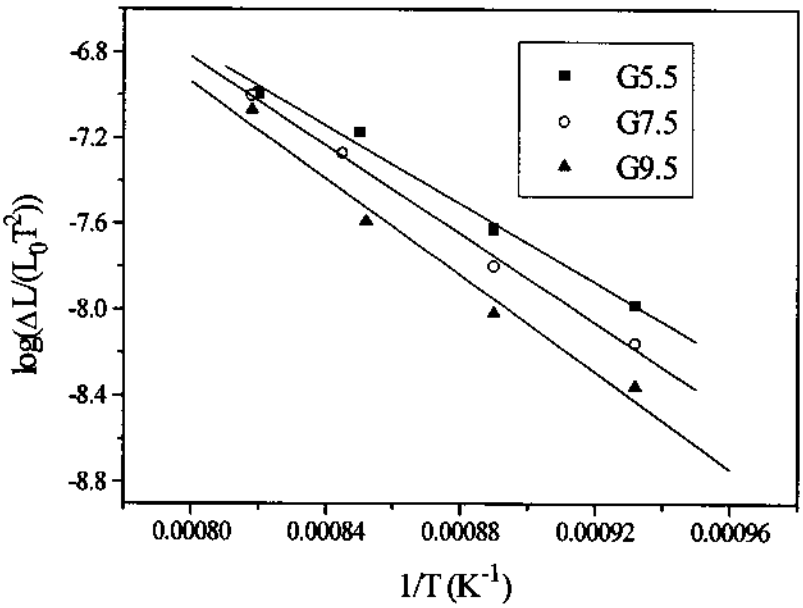

Fig. 6. Dependence log (L/L_0T^2) on $1/T$ for the G5.5, G7.5 and G9.5 gels.

zation of spinel, *i.e.,* intense shrinkage of the calcinated gel compact continues irrespective of spinel crystallization. In the temperature range 1000–1100 ºC, both completion of shrinkage and the onset of cristobalite crystallization occur. The temperature of cristobalite crystallization decreases with decreasing in size of the silica particles. Due to the decrease of the cristobalite crystallization temperature, the temperature of -cordierite formation by the reaction between spinel and cristobalite also decreases with a decreasing size of the silica particles. The size of the silica particles has a great influence on densification because the activation energy of densification by viscous flow decreases with decreasing particle size.

CONCLUSION

Three colloidal cordierite-type gels were prepared from a boehmite sol, an aqueous solution of $Mg(NO_3)_2$ and silica sols of very small particle size. Despite the fact that the size of the silica particles is very small, spinel and cristobalite crystallizing from the gels react with each other forming -cordierite, which is specific for three-phase cordierite gels. However, decreasing the size of the silica particles leads to a decrease of the cristobalite crystallization temperature and, consequently, to a decrease of the -cordierite formation temperature. The size of the silica particles has a great influence on densification because the activation energy of densification by viscous flow decreases with decreasing particle size.

И З В О Д

ДЕНЗИФИКАЦИЈА И КРИСТАЛИЗАЦИЈА КОЛОИДНИХ ГЕЛОВА КОРДИЈЕРИТНОГ САСТАВА

РАДА ПЕТРОВИЋ[1], ЂОРЂЕ ЈАНАЋКОВИЋ[1], БРАНИСЛАВА БОЖОВИЋ[1], СЛАВИЦА ЗЕЦ[2] и ЉИЉАНА КОСТИЋ-ГВОЗДЕНОВИЋ[1]

[1]*Технолошко-металуршки факултет, Катедра за неорганску хемијску технологију, Карнегијева 4, 11000 Београд и* [2]*Институт за нукеларне науке "Винча", п. пр. 522, 11000 Београд*

Припремљена су три гела кордијеритног састава полазећи од воденог раствора $Mg(NO_3)_2$, бемит сола и солова SiO_2, веома малих величина честица. Варирана је величина честица сола SiO_2 да би се испитао утицај величине честица сола SiO_2 на дензификацију и кристализацију гелова. Диференцијално скенирајућом калориметријом и рендгенском анализом утврђене су промене које се одигравају при топлотној обради гелова, док је дензификација испитивана мерењем линеарног скупљања компакта гелова. Енергија активације дензификације вискозним током је одређена применом Френкеловог модела за неизотермске услове са константном брзином загревања. Резултати показују да из колоидних гелова кордијеритног састава прво кристалише спинел, затим кристобалит, који реагују и дају -кордијерит, што је карактеристично за трофазне гелове. Са смањењем величине честица SiO_2 снижава се температура кристализације кристобалита, што доводи до снижења температуре формирања -кордијерита. Енергија активације дензификације вискозним током је мања, а дензификација ефективнија што су честице SiO_2 мање.

(Примљено 26. октобра 2000, ревидирано 31. јануара 2001)

REFERENCES

1. Lj. Kostić-Gvozdenović, T. Janaćković, M. Tecilazić-Stevanović, Dj. Janaćković, in *Electroceramics and Ceramics for Special Applications (Proc. II Euro. Ceram. Soc. Conf.),* G. Ziegler and H. Hausner Eds. (Deutsche keramische Gesellschaft e. V., Frankfurkt, 1993), vol. III, p. 2431
2. R. W. Dupon, R. L. McConville, D. J. Musolf, A. C. Tanous, M. S. Thompson, *J. Am. Ceram. Soc.* **73** (1990) 335
3. R. Ćirjaković, S. Milonjić, Lj. Kostić-Gvozdenović, in *Processing of Ceramics (Proc. III Euro. Ceram. Soc. Conf.),* P. Duran and J. F. Fernandez Eds., Faenza Editrice Iberica, S. L., 1993, vol I, p. 273
4. Dj. Janaćković, V. Jokanović, Lj. Živković, Lj. Kostić-Gvozdenović, D. Uskoković, in *Ceramics: Charting the Future, Advances in Science and Technology (Proc. VIII Cimtec Conf.),* P. Vincenzini Ed., Techna, Faenca, 1995, p. 1229
5. S. Milonjić, Lj. Čerović, R. Ćirjaković, O. Milošević, D. Uskoković*, EMRS 1993 Fall Meeting, 4th European East-West Conference & Exhibition on Materials and Process,* St. Petersburg, Russia, Oktober 17–21, 1993, Abstract B-VII.2
6. Dj. Janaćković, V. Jokanović, Lj. Kostić-Gvozdenović, S. Zec, D. Uskoković*, J. Mater. Sci.* **32** (1997) 163
7. B. J. J. Zelinski, D. R. Uhlmann, *J. Phys. Chem. Solids* **45** (1984) 1069
8. Ph. Colomban, *Ceramics International* **15** (1989) 23
9. C. W. Turner, *Ceramic Bulletin* **70** (1991) 1487
10. J. C. Barnier, *Powder Metallurgy International* **18** (1986) 165
11. H. Suzuki, K. Ota, H. Saito, *Yogyo-Kyokai-Shi* **95** (1987) 163
12. H. Suzuki, K. Ota, H. Saito, *Yogyo-Kyokai-Shi* **95** (1987) 170
13. K. Maeda, F. Mizukami, S. Miyashita, S. Niwa, M. Toba*, J. Chem. Soc., Chem. Commun.* **18** (1990) 1268
14. A. M. Kazakos, S. Komarneni, R. Roy, *J. Mater. Res.* **5** (1990) 1095
15. B. C. Lim, H. M. Jang*, J. Mater. Res.* **6** (1991) 2427
16. M. Okuyama, T. Fukui, C. Sakurai, *J. Am. Ceram. Soc.* **75** (1992) 153
17. H. M. Jang, B. C. Lim, *J. Mater. Res.* **9** (1994) 2627
18. S. K. Saha, P. Pramanik, *J. Mater. Sci.* **30** (1995) 2855
19. D. Pal, A. K. Chakraborty, S. Sen, S. K. Sen, *J. Mater. Sci.* **31** (1996) 3995
20. M. Awano, H. Takagi, Y. Kuwahara, *J. Am. Ceram. Soc.* **75** (1992) 2535
21. M. Awano, H. Takagi, *J. Mater. Sci.* **29** (1994) 412
22. S. J. Lee, W. M. Kriven*, J. Am. Ceram. Soc.* **81** (1998) 2605
23. S. K. Milonjić, *PhD Thesis*, University of Belgrade, Belgrade, 1981
24. G. W. Sears Jr., *Anal. Chem.* **28** (1981) 1956
25. R. Petrović, S. Milonjić, V. Jokanović, Lj. Kostić-Gvozdenović, I. Petrović-Prelević, Dj. Janaćković, *Powd. Tech.* (sibmitted)
26. R. Petrović, Dj. Janaćković, S. Zec, S. Drmanić, Lj. Kostić-Gvozdenović, *J. Mater. Res.* **16** (2001) 451
27. M. Prassas, J. Phalippou, J. Zarzycki, *Science of Ceramic Chemical Processing,* L. L. Hench and D. R. Ulrich, Eds., Wiley – Interscience Publication, New York, 1986, p. 156.

J.Serb.Chem.Soc. *66*(5)345–357(2001)
JSCS–2862

UDC 66.065:546.48:
Original scientific paper

Underpotential deposition of cadmium onto Cu(111) and Cu(110) from chloride containing solutions

V. D. JOVIĆ[1#] and B. M. JOVIĆ[2#]

Materials Engineering Department, Drexel University, Philadelphia, PA 19104, USA

(Received 26 December 2000)

Underpotential deposition (UPD) of Cd onto the (111) and (110) faces of copper in chloride containing electrolyte has been investigated by cyclic voltammetry and the potentiostatic pulse technique. It was shown that the UPD of Cd onto the (111) face of copper is characterized by two pairs of peaks, one pair corresponding to the formation of the $(\sqrt{19}\ \sqrt{19})$R23.4º structure of Cd and the other one, taking place close to the reversible potential of Cd deposition, corresponding to the alloying of Cu with Cd. Deposition of $(\sqrt{19}\ \sqrt{19})$R23.4º structure of Cd was found to take place by the mechanism of replacement of the adsorbed structure of chloride, without chloride desorption (the chloride stays adsorbed on top of the Cd layer). Similar behaviour was found for the (110) face of copper, with more pronounced alloying which provokes an irreversible change of the original (110) surface of copper.

Keywords: Cu(111), Cu(110), $(\sqrt{19}\ \sqrt{19})$R23.4º structure of Cd, alloying.

INTRODUCTION

Although underpotential deposition (UPD) of different metals onto Ag, Pt and Au single crystal surfaces has been widely investigated,[1] a limited number of fundamental studies of UPD has been performed onto Cu single crystal surfaces,[2–6] all of them examining the UPD of lead. On the other hand, chloride adsorption onto copper single crystals has been extensively examined by cyclic voltammetry, *ex situ* LEED and AES techniques,[7–11] as well as *in situ* by the STM technique.[12–14] In the papers of Brisard *et al.*[5,6] it was shown that the presence of chloride ions in the supporting electrolyte (0.01 M $HClO_4$) has a strong effect on the potential region where deposition/stripping of a Pb monolayer occurs, as well as on the reversibility of this reaction.

UPD of cadmium onto Cu(111) has been the subject of only two papers. Ge and Gewirth[15] investigated the UPD of Cd onto Cu(111) in perchlorate medium by AFM

1 On leave of absence from the Center for Multidisciplinary Studies University of Belgrade, P.O. Box 33, 11030 Belgrade, Yugoslavia.

2 On leave of absence from the Institute of Technical Sciences SASA, P.O. Box 745, 11001 Belgrade, Yugoslavia.

Serbian Chemical Society active member.

and cyclic voltammetry. They found that UPD of Cd takes place in the potential region between 0.0 V and – 0.2 V *vs*. SHE and that Cd forms (4 4) stucture with atomic spacing 0.343 nm, while overpotential deposition (OPD) of Cd commences at about – 0.4 V *vs*. SHE with the resulting crystalline structure being Cd(0001) hcp.

Stuhlmann *et al.*[16] investigated UPD of Cd onto Cu(111) in pure chloride containing solution (0.01 M HCl with addition of 0.0001 M or 0.001 M $CdCl_2$) by cyclic voltammetry and UHV based spectroscopies. By LEED, they detected an UPD layer of Cd of the structure $(\sqrt{19}\ \sqrt{19})$R23.4º with a coverage of 9/19 monolayers (= 0.474) with respect to Cu(111) and a Cd–Cd distance within the layer of 0.371 nm, which is much larger than in bulk Cd but close to that of $CdCl_2$ (0.384 nm), suggesting that the adsorbed chloride may stabilize the structure. According to their low energy scattering spectrum, a Cd layer is sandwiched between a Cl layer and the Cu substrate. They also detected the $(\sqrt{3}\ \sqrt{3})$R30º structure at more positive potentials than the potential of Cd UPD, which was ascribed to the layer of adsorbed chloride atoms. The authors claim that Cl is completely discharged on the clean Cu(111) surface as well as on the Cd covered surface and that the adsorbed Cl does not contribute to the charge transfer during the formation of the Cd layer.

In this paper an attempt was made to investigate the UPD of Cd onto Cu(111) and Cu(110) in pure chloride solution of higher concentrations of cadmium ions. It was shown that on the (111) face of copper this process is characterized by two pairs of sharp peaks, one taking place at the potential of chloride adsorption/desorption and the other one at a potential close to the reversible potential of bulk deposition of Cd. On the (110) face of copper, the UPD of Cd is characterized by three pairs of peaks.

EXPERIMENTAL

All experiments were carried out in a two-compartment electrochemical cell at 25 1 ºC in an atmosphere of purified nitrogen. The single crystal electrodes (d = 2.54 cm) were sealed in epoxy resin (resin EPON 828 + hardener TETA) in such a way that only the (111), or (110) disc surface was exposed to the solution. The surface area of the electrode exposed to the electrolyte was 5.05 cm^2. The counter electrode was a platinum sheet which was placed parallel to the working electrode. The reference electrode was a saturated calomel electrode (SCE), or Cd wire (99.999 %) immersed in the solution of Cd^{2+} ions, which was placed in a separate compartment and connected to the working compartment by means of a Luggin capillary. The potential values are referenced to SCE or to the Cd^{2+}/Cd electrode. All solutions were made from supra pure (99.999 %) chemicals (Aldrich) and EASY pure UV water (Barnstead).

Copper single cyrstals (Monocrystals Comp.) were mechanically polished on fine grade emery papers (1200, 2400 and 4000) with subsequent polishing on polishing clothes impregnated with a suspension of polishing alumina with particles dimension of 1 m, 0.3 m and 0.05 m. After chemical polishing, the copper single crystals were electrochemically polished in a solution of 85 % phosphoric acid at a constant voltage of 1.7 V (*vs*. Pt counter electrode) until the current density dropped to a value of about 18 mA cm^{-2}. The electrode was then thoroughly rinsed with pure water (Barnstead - EASY pure UV) and transferred to the electrochemical cell.

Cyclic voltammetry experiments were performed using a universal programmer PAR M-175, a potentiostat PAR M-173 and an *X–Y* recorder (Houston Instrument 2000R). Potentiostatic *j–t* transients were recorded on a digital oscilloscope (Nicolet 4094 A) and transferred to the *X–Y* recorder.

RESULTS

To avoid IR drop effects, a solution of 0.1 M NaCl + 0.001 M HCl, of pH 3 was used as the supporting electrolyte in all measurements. Two concentrations of $CdCl_2$ were investigated. In the case of the low concentration (0.005 M), $CdCl_2$ was added to a solution of 0.1 M NaCl + 0.001 M HCl after the voltammogram of Cu(111) has been recorded in the supporting electrolyte. In this case the potential was referenced to SCE. For the high concentration of $CdCl_2$ (0.1 M), the solution was made as a mixture of 0.1 M NaCl + 0.001 M HCl + 0.1 $CdCl_2$, Cd wire (99.999 %) was used as the reference electrode and, accordingly, the potential was referenced to the reversible potential of Cd in 0.1 M $CdCl_2$ solution (Cd^{2+}/Cd). In this solution, the potential of the Cd wire was –0.704 V *vs*. SCE.

(111) Face of copper

Cyclic voltammograms of Cu(111) recorded in the supporting electrolyte at three different sweep rates are shown in Fig. 1a. As can be seen a sharp anodic peak appears on all three voltammograms, indicating chloride ions adsorption, while in the cathodic going direction one shoulder and one broad peak represent the desorption of chloride ions and the hydrogen evolution reaction.[7–14] These voltammograms are in good agreement with the results of other authors. [7–14]

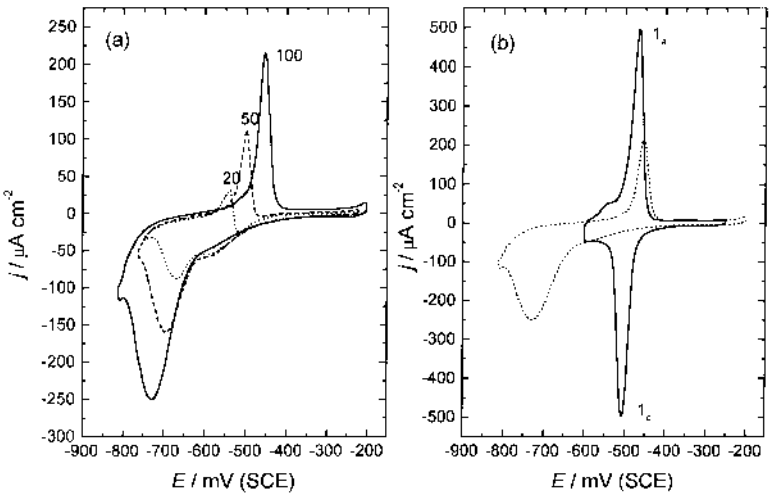

Fig. 1. (a) Cyclic voltammograms recorded at different sweep rates (marked in the figure in mV s^{-1}) onto the (111) face of copper in a solution of 0.1 M Na Cl + 0.001 M HCl. (b) Cyclic voltammograms recorded at sweep rate of 100 mV s-1 onto the (111) copper in a solution of 0.1 M NaCl + 0.001 M HCl (dotted line) and in a solution of 0.1 M Na Cl + 0.001 M HCl + 0.005 M $CdCl_2$

After addition of 0.005 M $CdCl_2$ to the supporting electrolyte, the voltammogram shown in Fig. 1b (full line) was obtained. Well defined sharp peaks (1_c and 1_a) of the UPD of Cd onto Cu(111) at about –500 mV *vs*. SCE appear on the voltammogram. At a sweep rate of 100 mV s^{-1}, these peaks look like a single voltammetric peak, but they are actually composed of two peaks, as was shown for high $CdCl_2$ concentration.

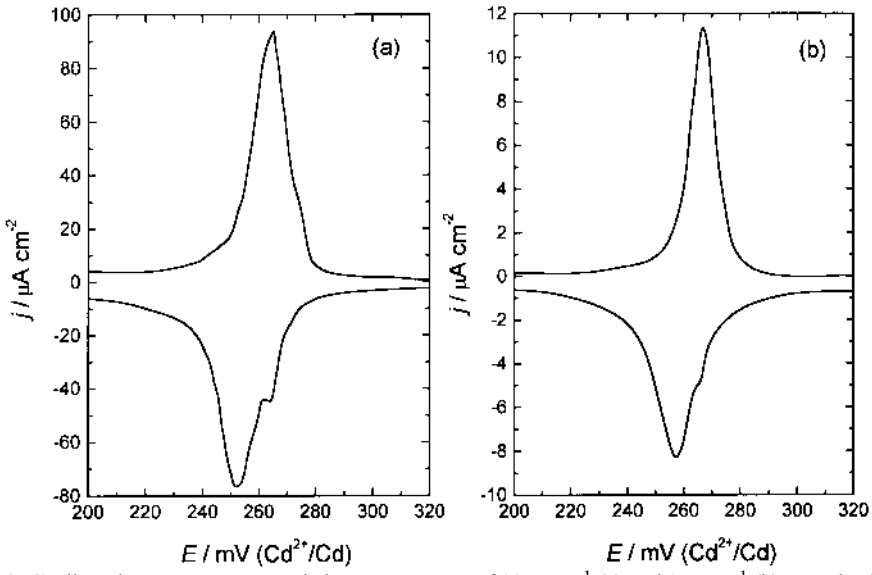

Fig. 2. Cyclic voltammograms recorded at a sweep rate of 10 mV s^{-1} (a) and 1 mV s^{-1} (b) onto the (111) face of copper in a solution of 0.1 M NaCl + 0.001 M HCl + 0.1 M $CdCl_2$.

The fine structure of these peaks can only be detected at sweep rates lower than 20 mV s^{-1}. Cyclic voltammograms recorded in a solution of 0.1 M $CdCl_2$ + 0.1 M NaCl + 0.001 M HCl at a sweep rate of 10 mV s^{-1} (a) and 1 mV s^{-1} (b), shown in Fig. 2, clearly indicates the presence of two peaks in the cathodic branch of the voltammogram, most probably corresponding to two processes taking place simultaneously. The charge under the cathodic (as well as under the anodic) peak recorded at a sweep rate of 10 mV s^{-1} amounts to about 220 C cm^{-2}.

By using a computer program (PeakFit) for fitting experimentally recorded voltammograms it is possible to obtain much better insight into the processes taking place under the cathodic (1_c) and anodic (1_a) peaks. The results of such analysis are shown in Fig. 3. As can be seen in Fig. 3a, the best fitting of the cathodic peak was obtained with three peaks, two of them being very sharp, while the best fitting of the anodic peak is obtained using two sharp peaks (Fig. 3b). Hence, neither the cathodic nor the anodic peak is a simple voltammetric peak, indicating the simultaneous occurrence of two or more processes.

In the presence of 0.005 M $CdCl_2$ in the supporting elecrolyte, the peak of hydrogen evolution is suppressed and at about –720 mV *vs*. SCE another pair of peaks appears on the voltammogram, as can be seen in Fig. 4a. Because of the commencement of bulk Cd deposition, these peaks cannot be resolved at sweep rates higher than 5 mV s^{-1}, but they are clearly seen on the voltammogram recorded at 1 mV s^{-1} (see Fig. 4a). It is interesting to note that the charges under the anodic and cathodic part of this voltammogram amounts to about 500 C cm^{-2} and 560 C cm^{-2}, respectively, which are higher than the charge needed for a Cd monolayer deposition (Q_{mon} = 412 C cm^{-2}).

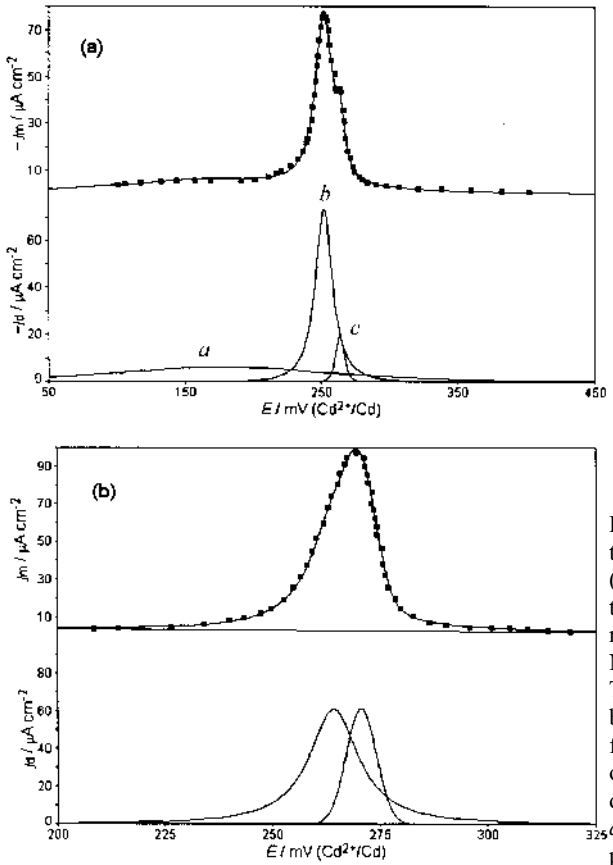

Fig. 3. Results of the deconvolution of the experimentally recorded cathodic (a) and anodic (b) peak recorded on the (111) face of copper at a sweep rate of 10 mV s^{-1} in a solution of 0.1 M NaCl + 0.001 M HCl + 0.1 M $CdCl_2$. The experimental points are presented by squares ($j_m - E$ dependence), the fitted curve is presented by the full line on the same dependence, while the deconvoluted peaks are marked with *a*, *b* and *c* and presented by $j_d - E$ dependence.

In the solution containing a much higher concentration of $CdCl_2$ (0.1 M), the peaks appearing at potential close to the reversible potential of Cd deposition are much bigger at the same sweep rate of 1 mV s^{-1}, as can be seen in Fig. 4b. As in the previous case, these peaks can only be detected at sweep rates lower than 5 mV s^{-1}. Since in this case a Cd wire was used as the reference electrode, it can be seen that a second cathodic UPD peak (2_c) appears at a potential of about 5 mV *vs*. Cd^{2+}/Cd, while the OPD process (peak 3_c) starts immediately after reaching the reversible potential of Cd deposition. The anodic peak of bulk dissolution of Cd (3_a), appearing at about 2 mV *vs*. Cd^{2+}/Cd, is very sharp, while the second anodic UPD peak (peak 2_a – corresponding to the dissolution of Cd deposited under the cathodic peak 2_c) appears at about 25 mV *vs*. Cd^{2+}/Cd. Hence, it is obvious that just before the commencement of the OPD of Cd, the appearance of a second pair of UPD peaks (2_c and 2_a) characterizes the process of UPD of Cd onto Cu(111). In this case the anodic and cathodic charge under the voltammogram are also higher than the charge needed for the deposition of a Cd monolayer, amounting to 591 C cm^{-2} and 1500 C cm^{-2}, respectively.

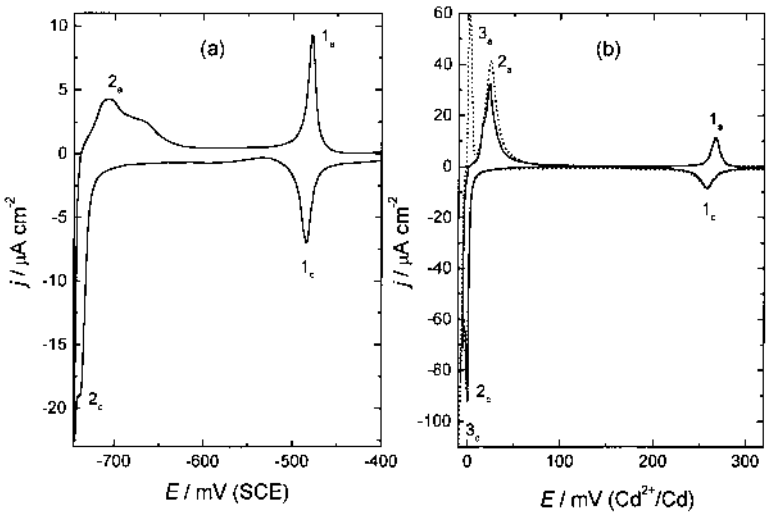

Fig. 4. Cyclic voltammograms recorded at a sweep rate of 10 mV s^{-1} onto the (111) face of copper in a solution of 0.1 M NaCl + 0.001 M HCl + 0.005 M $CdCl_2$ (a) and 0.1 M NaCl + 0.001 M HCl + 0.01 M $CdCl_2$ (b) .

Since the second UPD peak can be detected only at sweep rates lower than 5 mV s^{-1} and this peak cannot be resolved from the increase in the cathodic current corresponding to the OPD of Cd at a sweep rate of 10 mV s^{-1}, a holding experiment at the commencement of this process (potential of E_h = 0 mV *vs*. Cd^{2+}/Cd) was performed (at the potential of 0 mV *vs*. Cd^{2+}/Cd, the cathodic current density recorded at 10 mV s^{-1} just starts to increase and there is no corresponding anodic peak on the voltammogram re-

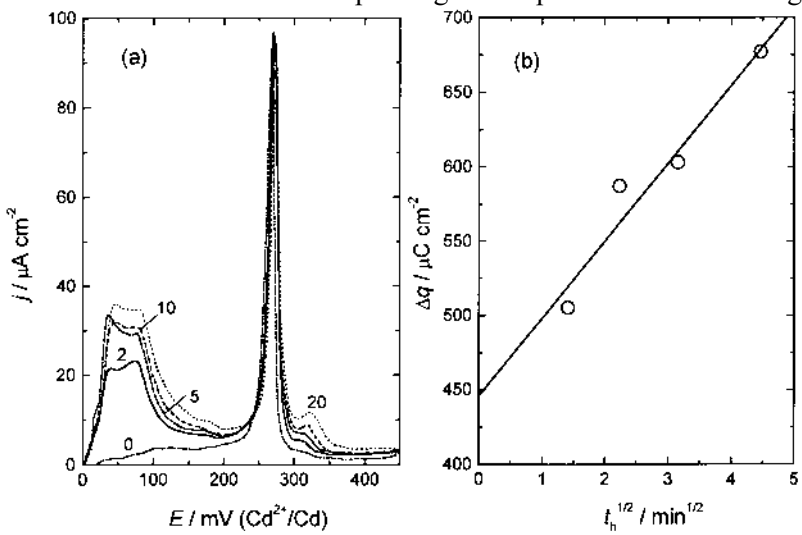

Fig. 5. (a) Anodic voltammograms recorded at a sweep rate of 10 mV s^{-1} after holding the (111) face of copper at a potential of E_h = 0 mV *vs*. Cd^{2+}/Cd for different times (marked in the Figure in minutes) in a solution of 0.1 M NaCl + 0.001 M HCl + 0.1 M $CdCl_2$. (b) Corresponding $q - t_h^{1/2}$ dependences.

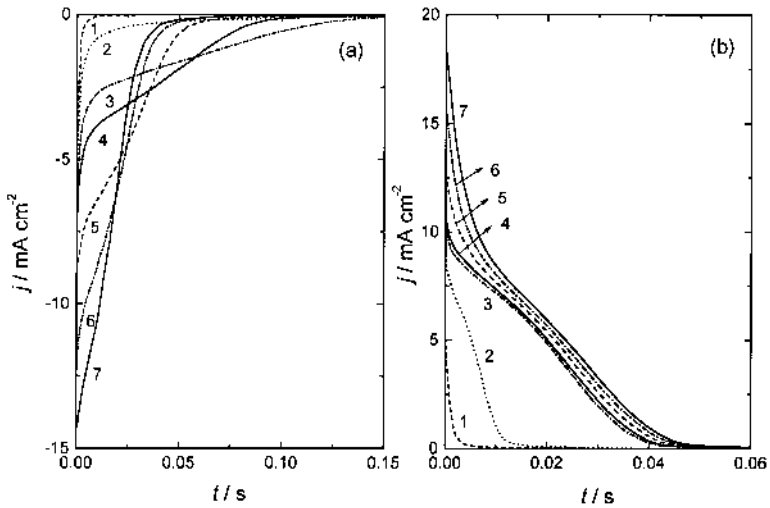

Fig. 6. Catodic potentiostatic *j–t* transients recorded onto the (1110 face of copper in a solution of 0.1 M NaCl + 0.001 M HCl + 0.1 M $CdCl_2$ by pulsing from E_{in} =400 mV *vs*. Cd^{2+}/Cd to the following potentials (given in mV *vs*. Cd^{2+}/Cd): 1.300; 2.260; 3.220; 4.200; 5.150; 6.100; 7.50. (b) Anodic *j–t* transients recorded by pulsing back to E_{in}.

corded by repetitive cycling – see voltammogram marked with 0 in Fig. 5a). The results of such an experiment are shown in Fig. 5. As can be seen in Fig. 5a, the shape of the voltammogram changes with holding time, *i.e.,* anodic peaks recorded in the potential region between 0 mV and 100 mV *vs*. Cd^{2+}/Cd, as well as a small peak appearing at a potential of about 325 mV *vs*. Cd^{2+}/Cd, increase with time of holding the elctrode at E_h = 0 mV *vs*. Cd^{2+}/Cd. The linear $q - t_h^{1/2}$ dependence shown in Fig. 5b indicates the occurrence of solid state diffusion and alloying of Cu with Cd.[17–21]

The results of potentiostatic pulse experiments, performed in the potential region positive to peak 2_c are shown in Fig. 6. As can be seen, cathodic and anodic *j–t* transients typical for UPD are obtained.[22] By integration of the charge under the cathodic *j–t* transients, the $Q_m - E$ dependence, shown in Fig 7a is obtained. Assuming that the charge recorded in the potential region between 400 mV and 300 mV *vs*. Cd^{2+}/Cd corresponds to the double layer charge, it is possible to correct the measured charge (Q_m) for the double layer charge (Q_{dl}) in order to obtain the charge needed for the UPD process (Q_{UPD}). As can be seen on the $Q_{UPD} - E$ curve a sharp increase in charge (from 5 C cm^{-2} to 180 C cm^{-2}) is recorded in the potential region between 280 mV and 240 mV *vs*. Cd^{2+}/Cd. As can be seen in Fig. 7b, an almost identical $Q_{UPD} - E$ dependence is obtained by integration of anodic *j–t* transients.

(110) Face of copper

As in the case of Cu(111), the fine structure of the UPD process can only be detected at sweep rates lower than 20 mV s^{-1}. The voltammograms recorded in a solution of 0.1 M $CdCl_2$ + 0.1 M NaCl + 0.001 M HCl at a sweep rate of 5 mV s^{-1} (a) and 10 mV s^{-1} (b) are shown in Fig. 8. As can be seen, the cathodic and anodic parts of the voltammograms differ

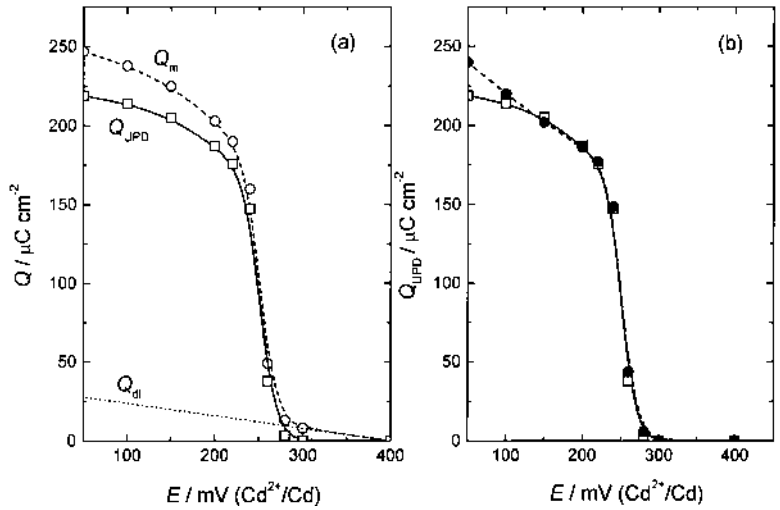

Fig. 7. (a) *Q–E* dependences obtained by the integration of the cathodic *j–t* transients shown in Fig. 6. (b) Cathodic (full line – □) and anodic (dashed line – ●) QUPD – E dependences obtained by integration of the cathodic and anodic *j–t* transients shown in Fig. 6.

significantly in the potential region of the first pair of peaks (1_c, $1_{c'}$ and 1_a, $1_{a'}$). It is interesting to note that the anodic and cathodic charges recorded for peaks 1 and 2 amount to 520 C cm^{-2} and 694 C cm^{-2}, respectively, indicating that more than a monolayer of Cd had already been deposited at the potential of 100 mV *vs*. Cd^{2+}/Cd. Hence, peak 3_c can be ascribed to the process of surface alloying of Cu with Cd.

To confirm this statement, a holding experiment was performed at the potential of

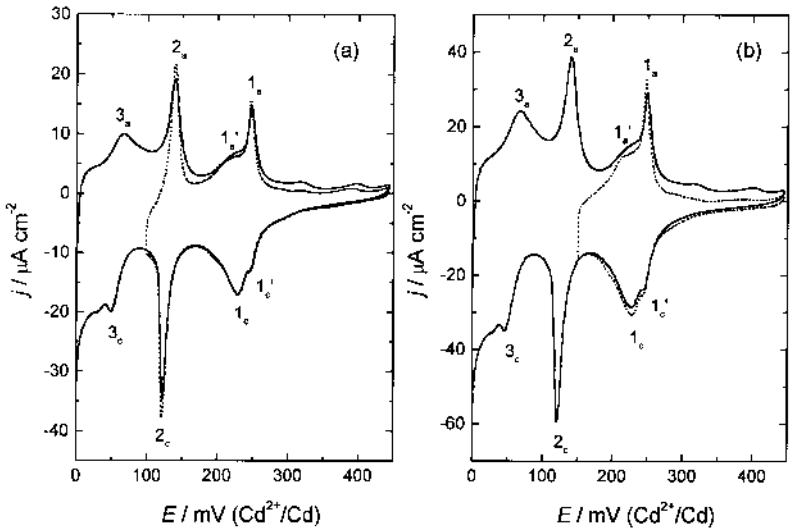

Fig. 8. Cyclic voltammograms recorded at a sweep rate of 5 mV s^{-1} (a) and 10 mV s^{-1} (b) onto the (110) face of copper in a solution of 0.1 M NaCl + 0.001 M HCl + 0.01 M $CdCl_2$.

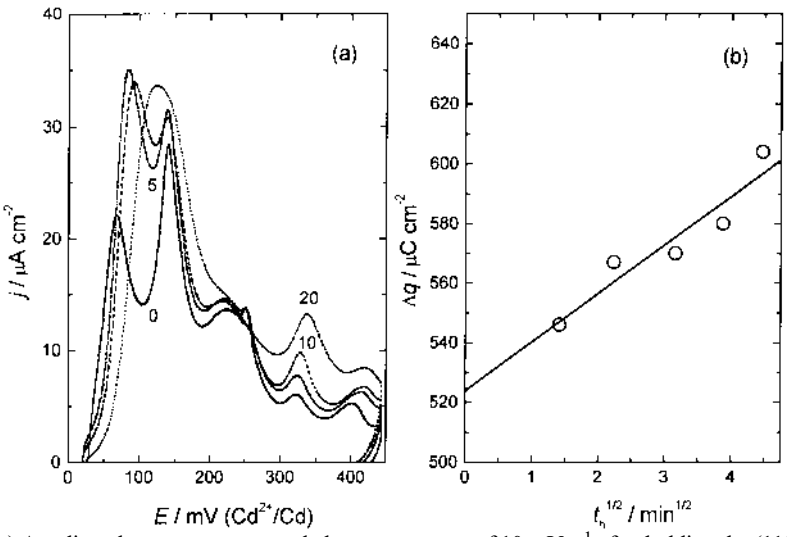

Fig. 9. (a) Anodic voltammograms recorded at a sweep rate of 10 mV s^{-1} after holding the (110) face of copper at a potential of E_h = 20 mV *vs*. Cd^{2+}/Cd for different times (marked in the Figure in minutes) in a solution of 0.1 M NaCl + 0.001 M HCl + 0.1 M $CdCl_2$. (b) Corresponding $q - t_h^{1/2}$ dependences.

20 mV *vs*. Cd^{2+}/Cd. The obtained results are shown in Fig. 9. As can be seen almost all the anodic peaks increase with holding time (Fig. 9a). A linear $q - t_h^{1/2}$ dependence shown in Fig. 9b indicates, as in the case of Cu (111), the occurrence of solid state diffusion and alloying of Cu with Cd.[17–21]

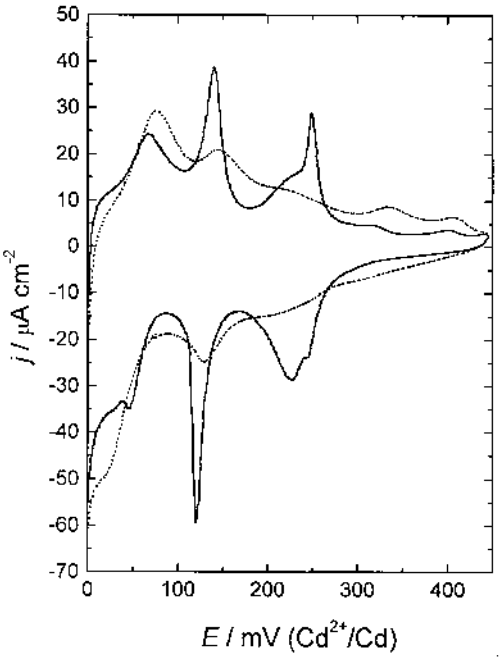

Fig. 10. Cyclic voltammograms recorded at a sweep rate of 10 mV s^{-1} onto the (110) face of copper in a solution of 0.1 M NaCl + 0.001 M HCl + 0.1 M $CdCl_2$ before (full line) and after alloying of Cu(110) with Cd (dotted line).

The voltammograms recorded in a solution of 0.1 M $CdCl_2$ + 0.1 M NaCl + 0.001 M HCl at a sweep rate of 10 mV s^{-1} before (full line) and after performing the holding experiment (dotted line) are shown in Fig. 10. As can be seen the (110) face of copper is irreversible changed after alloying with Cd.

DISCUSSION

(111) Face of copper

Since there is only one paper concerning Cd UPD in chloride containing solution,[16] our results can only be compared with the results presented in this paper. According to the results of Stuhlmann *et al.*[16] UPD of Cd is chracterized by the presence of only one peak of a complex nature, recorded in the potential region between – 0.8 V and – 0.85 V *vs.* saturated sulphate electrode (SSE) (for $CdCl_2$ concentration of 0.001 M), while the cyclic voltammogram of the same process in a solution of 0.0001 M $CdCl_2$ is characterized by one spike at about – 0.82 V *vs.* SSE and a broad peak situated between – 0.82 V and – 0.90 V *vs.* SSE (Figs. 1 and 2 of Ref. 16). It is quite interesting that for a solution of 0.0001 M $CdCl_2$ the XPS intensity for Cd starts to increase sharply at about – 0.85 V *vs*. SSE, in the region of the broad peak on the voltammogram (Fig. 2 of Ref. 16), while the intensity for Cl also slightly increasses in the potential region between – 0.85 V and – 1.15 V *vs*. SSE. Although the authors did not explain this voltammogram, it seems that the spike appearing at the potential of about – 0.82 V *vs*. SSE is not connected with the process of Cd UPD and might be the consequence of a phase transformation of ordered $(\sqrt{3}\ \sqrt{3})R30^{o}$ chloride structure into a randomly adsorbed layer of chloride as the first step in the process of UPD of Cd, since it is hard to believe that the formation of some ordered structure (such as structure $(\sqrt{19}\ \sqrt{19})R23.4^{o}$ found for Cd) can start with a spike, which is characteristic of a phase transformation process, on the cyclic voltammograms. It is also interesting to note that, although ordered $(\sqrt{3}\ \sqrt{3})R30^{o}$ chloride structure has been evidenced by LEED and STM on Cu(111) in pure chloride solution,[7–14] the voltammogram of its formation is not characterized by the presence of a spike neither in the cathodic nor anodic region.[7–14] Under the second, broad peak, (Fig. 1c of Ref. 16), on commencement of UPD of Cd the randomly adsorbed chloride layer is replaced with ordered Cd structure $(\sqrt{19}\ \sqrt{19})R23.4^{o}$, while the chlorides do not desorb but remain adsorbed on top of the Cd layer. According to the change of XPS intensity with potential for chloride (slight increase in the potential region between – 0.85 V and –1.15 V *vs*. SSE) it seems that during the formation of the $(\sqrt{19}\ \sqrt{19})R23.4^{o}$ structure of Cd, additional chloride ions adsorbs on top of the Cd layer.

Concerning the appearance of peak 1 there is relatively good agreement between the results presented in our paper with those published by Stuhlmann *et al.*.[16] It can be seen that at low[16] and high (our paper) concentration of cadmium ions this peak is composed of at least two peaks, indicating the simultaneous occurrence of two processes. Taking into account the charge under this peak and Q_{UPD}–E dependence (Fig. 7), it is obvious that the Cd structure detected by Stuhlmann *et al.*[16] is formed and that the desorption of the complete ordered $(\sqrt{3}\ \sqrt{3})R30^{o}$ chloride structure does not occur. The contribution of chloride

desorption is very small and can be attributed to a phase transformation of this ordered structure into a randomly adsorbed one, while the corresponding peak should be peak *a*, obtained by the deconvolution of peak 1_c and presented in Fig. 3a. By transforming peak *a* into a $-E$ dependence and fitting this dependence by Frumkin adsorption isotherm, the interaction factor $f_a = -6.64$ 0.42 is obtained, indicating strong attraction between the adsorbed atoms, as is to be expected for an ordered 2D structure (in this case $(\sqrt{3}\ \sqrt{3})$R30º chloride structure). Once this structure is transformed into randomly adsrobed chloride, cadmium starts to replace chloride atoms forming the $(\sqrt{19}\ \sqrt{19})$R23.4º structure of Cd, the process being characterized by peak *b* (Fig. 3a), while the chloride remains adsorbed on top of this Cd structure. By fitting peak *b* in the same way as peak *a*, the interaction factor $f_b = -3.76$ 0.07 is obtained, again indicating strong attraction between the adsorbed atoms. It is interesting to note that different results are obtained by the deconvolution of the anodic peak 1_a, as can be seen in Fig. 3b. The best fit of the experimentally recorded peak 1_a are obtained by two peaks, *a* and *b*. Again, by fitting these peaks with Frumkin adsorption isotherm, the interaction factor $f_a = -6.61$ 0.43 (in this case the phase transformation of the randomly adsorbed chloride layer into the $(\sqrt{3}\ \sqrt{3})$R30º chloride structure) and $f_b = -4.41$ 0.18, desorption of the $(\sqrt{19}\ \sqrt{19})$R23.4º structure of Cd. As can be seen, the values of the anodic and cathodic f_a parameters are almost identical, while the f_b parameters differ, which is most probably the consequence of the different number of peaks resulting from the deconvolution procedure. The additional peak *c* obtained by deconvolution of the experimentally recorded cathodic peak (Fig. 4a) might represent a contribution of the hydrogen evolution reaction, which is assumed to occur during desorption of chloride anions.[7–14]

The main difference between our results and results of Stuhlmann *et al.*[16] is the appearance of a second pair of peaks, 2_c and 2_a, close to the reversible potential of Cd deposition, as seen in Fig. 4. Although there is an indication of the appearance of a second pair of peaks in the paper of Stuhlmann *et al.*[16] (Fig. 2 of Ref. 16), the authors paid no attention to these peaks. As can be seen in Fig. 4, with increasing concentration of cadmium ions these peaks become sharper and the charge under the peaks increases. It is also important to note that the process taking place under these peaks is slow and these peaks can be detected only at very low sweep rates (< 5 mV s^{-1}). Since the corresponding anodic charge for the whole voltammogram exceeds the charge (about 500 C cm^{-2} for 0.005 M $CdCl_2$ and 591 C cm^{-2} 0.1 M $CdCl_2$) needed for the deposition of a Cd monolayer ($Q_{mon} = 412$ C cm^{-2}), it is obvious that these peaks represent the process of alloying of Cu with Cd. This is confirmed by the results presented in Fig. 5. The linear $q - t_h^{1/2}$ dependence shown in Fig. 5b is typical for solid state diffusion and alloying of Cu with Cd.[17–21]

(110) Face of copper

The results obtained on the (110) face of copper cannot be compared to any other results, since there are no data in the literature about UPD of Cd onto this surface. From the voltammograms shown in Fig. 8 it seems that an ordered, open structure Cd layer is adsorbed under peaks 1_c' and 1_c and desorbed under peaks 1_a' and 1_a. Again, as in the case of the (111) face of copper, these peaks are significantly different (dashed line in

Fig. 8b). This difference is most probably the consequence of the same factors as were assumed for the (111) face of copper. The sharp peaks 2_c and 2_a might represent phase transformation of this open structure into a monolayer of Cd, but the charge under the voltammogram recorded at the cathodic potential limit of 100 mV *vs*. Cd^{2+}/Cd (dashed line in Fig. 8a) is significantly higher than that needed for a full monolayer of Cd. Such a behaviour could be the consequence of two processes: alloying of Cu with Cd might commence already at the potential of these two peaks, or a significant amount of additional chloride ions is adsorbed on top of the Cd monolayer. This statement needs to be confirmed by additional holding experiments performed at the potential of peak 2_c. This is going to be the subject of further investigations. Alloying of Cu with Cd is confirmed for the peak 3_c in Fig. 9 by the well defined linear dependence $q - t_h^{1/2}$, typical for solid state diffusion and alloying.[17–21] For a more open surface, as is the (110) face compared to the (111) face, more pronounced alloying might be expected, as is the case, since the original (110) surface is destroyed after alloying of Cu with Cd (Fig. 10).

CONCLUSIONS

Considering the presented results, it can be concluded that in chloride containing electrolyte UPD of Cd onto the (111) face of copper is characterized by two pairs of peaks, one pair corresponding to the formation of the $(\sqrt{19}\ \sqrt{19})R23.4^o$ structure of Cd and the other one, taking place close to the reversible potential of Cd deposition, corresponding to alloying of Cu with Cd. Deposition of the $(\sqrt{19}\ \sqrt{19})R23.4^o$ structure of Cd occurs by replacement of the adsorbed structure of chloride, without chloride desorption (the chloride stays adsorbed on top of the Cd layer). A similar behaviour was found for the (110) face of cooper, with more pronounced alloying which provokes irreversible changes of the original (110) surface of copper.

ИЗВОД

ТАЛОЖЕЊЕ КАДМИЈУМА ИЗ РАСТВОРА ХЛОРИДА НА Cu(111) И Cu(110) ПРИ ПОТЕНЦИЦАЛИМА ПОЗИТИВНИЈИМ ОД РАВНОТЕЖНОГ

В. Д. ЈОВИЋ и Б. М. ЈОВИЋ

Дрексел Универзитет, Филаделфија, Пенсилванија 19104, САД

Методама цикличне волтаметрије и потенциостатског пулса испитиван је процес таложења кадмијума из раствора хлорида на монокристалима бакра оријентација (111) и (110) при потенцијалима позитивнијим од равнотежног. Показано је да се на оба монокристала прво формира уређена, али не густо пакована структура адсорбованог кадмијума. На основу количине наелектрисања испод цикличног волтамограма и потенциостатских *j–t* одговора установљено је да се на Cu(111) формира структура типа $(\sqrt{19}\ \sqrt{19})R23.4^o$, која је детектована у раду Stuhlmann *et al.*[16] помоћу LEED технике и да се ова структура таложи на тај начин што се слој адсорбованих хлорида истискује са површине Cu(111). При томе се хлориди не десорбују, већ остају адсорбовани на слоју адсорбованог кадмијума. При негативнијим потенцијалима, близу равнотежног потенцијала таложења кадмијума, на оба монокристала долази до леги-

рања бакра са кадмијумом, при чему је овај процес израженији на Cu(110) и изазива трајну деформацију оригиналне површине монокристала бакра.

(Примљено 26. децембра 2000)

REFERENCES

1. D. M. Kolb, *Advances in Electrochemistry and Electrochemical Engineering*, H. Gerischer and C. W. Tobias Eds., Vol. 11, Wiley, 1978, p. 125
2. H. Siegenthaler, K. Juttner, *J. Electroanal. Chem.* **163** (1984) 327
3. J. R. Vilche, K. Juttner, *Electrochim. Acta* **32** (1987) 1567
4. A. Bewick, J. Jovićević, B. Thomas, *Faraday Symp. Chem. Soc.* **12** (1977) 24
5. G. M. Brisard, E. Zenati, H. A. Gasteiger, N. M. Marković, P. N. Ross Jr., *Langmuir* **11** (1995) 2221
6. G. M. Brisard, E. Zenati, H. A. Gasteiger, N. M. Marković, P. N. Ross Jr., *Langmuir* **13** (1977) 2390
7. J. L. Stickney, I. Villegas, C. B. Ehlers, *J. Am. Chem. Soc.* **111** (1989) 6473
8. C. B. Ehlers, I. Villegas, J. L. Stickney, *J. Electroanal. Chem.* **284** (1990) 403
9. I. Villegas, C. B. Ehlers, J. L. Stickney, *J. Electrochem. Soc.* **137** (1990) 3143
10. J. L. Stickney, C. B. Ehlers, *J. Vac. Sci. Technol. A* **7** (1989) 1801
11. J. L. Stickney, C. B. Ehlers, B. N. Gregory, *ACS Symp. Ser.,* No. **378** (1988) 99
12. Li-Jun Wan, K. Itaya, *J. Electroanal. Chem.* **473** (1999) 10
13. T. P. Moffat, *J. Phys. Chem. B* **102** (1998) 10020
14. T. P. Moffat, *Mat. Res. Soc. Symp. Proc.* **451** (1997) 75
15. M. Ge, A. A. Gewirth, *Surface Science* **324** (1995) 140
16. C. Stuhlmann, Z. Park, C. Bach, K. Wandelt, *Electrochim. Acta* **44** (1998) 993
17. H. Bort, K. Juttner, W. J. Lorenz, G. Staikov, *Electrochim. Acta* **28** (1983) 993
18. E. Schmidt, M. Christen, P. Beyeler, *J. Electroanal. Chem.* **42** (1973) 275
19. G. Schwitzgebel, *Z. phys. Chem. NF* **95** (1975) 15
20. G. Schwitzgebel, P. Michael, Y. Zohdi, *Acta metall* **23** (1975) 1551
21. M. E. Martins, A. Hernandez-Creus, R. C. Salvarezza, A. J. Arvia, *J. Electroanal. Chem.* **375** (1994) 141
22. V. D. Jović, J. N. Jovićević, A. R. Despić, *Electrochim. Acta* **30** (1985) 1455.